Simulation of a Polystyrene Silica Nanocomposite

TECHNISCHE UNIVERSITÄT DARMSTADT

Vom Fachbereich Chemie
der Technischen Universität Darmstadt

zur Erlangung des akademischen Grades eines
Doktor rerum naturalium (Dr. rer. nat.)

genehmigte
Dissertation

vorgelegt von

Tinashe Victor Mandishonha Ndoro, M.Sc. (Chemical Engineering)

aus Harare, Zimbabwe

Referent: Prof. Dr. Florian Müller-Plathe
Korreferent: Prof. Dr. Nico van der Vegt
Tag der Einreichung: 12. September 2011
Tag der mündlichen Prüfung: 24. Oktober 2011

Darmstadt 2011
D17

To my family which is always supportive

and my fiancée, Sebenzile Myeni, who is my inspiration and partner in everything that I do.

Acknowledgments

I am indebted to my supervisor, Prof. Dr. Florian Müller-Plathe, for allowing me the privilege to work with him and learn from his ingenious approach to understanding and imparting scientific knowledge. Thank you Prof. Dr. Michael C. Böhm for your kindness, constructive criticism, and willingness to always help regardless of whatever else was happening or your other time commitments.

To my PhD committee consisting of Prof. Dr. Florian Müller-Plathe, Prof. Dr. Nico van der Vegt, Prof. Dr. Robert Berger, and Prof. Markus Biesalski: thank you for reading my dissertation and taking time to make my thesis defense possible.

I am grateful to all past and current colleagues in both work groups of Prof. Dr. Florian Müller-Plathe and Prof. Dr. Nico van der Vegt for productive and fun times spent. The same I extend to Christian Krekeler, Evangelos Voyiatzis, and Volker Weiss. To Dr.-Ing. Hans-Jürgen Bär, thank you for your help in my teaching duties as your enthusiasm made the whole experience exciting. To Karim Farah and Thomas Müller, my colleagues and friends, I will miss our times together in the office, our many discussions be they scientific, fun, or solving administrative computer cluster problems. I wish you the best in everything. Thank you Jessica Ahluwalia for your friendship and encouragement. I am very appreciative to you Kristin Adolph for helping me with the German part of this dissertation and its overall finalization as you have been a true friend and encourager in helping me complete this work.

I am thankful to all my friends for the moments and laughter that we have shared during this journey.

To my beloved family, I am very grateful for your love, encouragement, and support. My gratitude goes beyond words to my parents, Susan and Prosper Mandishonha Ndoro, who have taught me all the virtues that I aspire to have. To my brothers, Prosper and Tapiwarufaro, thank you for the laughter and diversions especially when the going was tough. There is nothing like family and I am very thankful as well to my future family-in-law (Sibongile, John, Zwakele, Wenzile, and Phathiswa) for their belief in me and support.

Last but for sure not least, I am very thankful for everything to my fiancée, Sebenzile Myeni, my love and companion who always believes and brings out the best in me.

1. Summary and Introduction / Zusammenfassung und Einleitung

1.1 Structural and Dynamical Properties of Atactic Polystyrene in the Interface and Interphase Region Surrounding Grafted and Ungrafted Silica Nanoparticles

The composite industry has long achieved enhanced material properties by mixing micro sized inorganic filler particles with a polymer matrix[1,2]. This is because the combination of two or more different materials can have a synergistic effect on the overall composite material properties imparting advantages that are absent in the individual constituents. A well-known example is that of adding carbon black as reinforcing material to increase tire strength, toughness, and resistance to tear and abrasion[3,4]. To achieve improved materials performance, the design of conventional composites has typically focused on reducing the dimensions of the filler particles. This is done in order to increase the filler surface area to enable greater interaction with the polymer matrix. Consequently, these efforts have received a significant boost with the dawn of the 'nano era'. Wherein experimental methods and tools are now used to synthesize, characterize, and investigate matter at the nano-scale level [10^{-9} m] which is close to molecular and atomic dimensions. The advent of such methods is exciting as it suddenly offers new possibilities of creating novel materials that can be tailored at very small dimensions. This expectation has been derived from the notion that the behavior of materials at their nanoscale level directly influences their microscopic properties and consequently their bulk macroscopic characteristics. As is typical in any emerging field, the challenge is to understand the fundamental aspects that control the final observable properties of these composite materials.

In contrast to the behavior of materials in conventional composites, recent experimental observations of polymer nanocomposites have demonstrated multifunctional changes in their properties. Examples include - but are not limited to - the decrease in the polymer viscosity[5], shifts in the polymer glass transition temperature[6,7], and changes in the composite material's thermo-mechanical[8,9] properties. However, what is still lacking and remains unclear are the fundamental explanations for the differences in the behavior between conventional composites and nanocomposites. In order to address questions pertaining to these differences, this PhD work was part of a large European Union consortium of universities and industrial partners, NanoModel. The aim of the group was to develop a unified scientific understanding from both experimentalists and theoreticians on the behavior of polymers in the presence of a surface. Such understanding of the important controlling parameters would ultimately support the design of industrial polymer nanocomposite materials. Therefore, both

the structural and dynamical investigations always sought to address some of several important open questions that necessitated this work. These questions include among other things: (1) Does a nanoparticle influence the behavior of the surrounding polymer? (2) Since the dispersion state of the nanoparticles is known to control the resulting nanocomposite properties, which controlling parameters are important in obtaining a well-mixed polymer nanocomposite? (3) What role does the size/dimension of the nanoparticle play? (4) Is it necessary to graft or attach polymers to the filler particles, in other words, functionalizing the nanoparticles to facilitate their dispersion in the polymer melt? (5) How long should the grafted polymer chains be relative to the bulk polymer and which grafting density is optimal to achieve a good dispersion state? (6) To what extent are the polymer properties in the interface (next to the surface) and interphase (where grafted and bulk free polymer chains mix) region changed if they are at all? (7) Which parameters influence the width or extent of both the interface and interphase region? (8) Can we observe the same phenomena or changes by employing both experimental and theoretical approaches?

Therefore, the contribution of this PhD thesis within the NanoModel framework was to investigate the structural and dynamical properties of atactic polystyrene in the vicinity of a silica nanoparticle as a model system for polymer nanocomposites at the atomistic level (see Figure 1.1 for a simulation snapshot). This model system was chosen because of its importance to the NanoModel partners since bulk polystyrene is an important, largely used, and well characterized polymer while silica is a typical traditional filler particle. Naturally, consortium partners like BASF would find it invaluable to produce new tailored plastics with superior properties to the traditional ones. At the same time, partners like BOSCH and CRP-FIAT would benefit from knowing the nanoparticle effect on the mechanical properties and the processing of the nanocomposite which directly impacts their injection molding processes for example. On the experimental front, Fribourg University, Juelich, and Epidoris were involved in nanocomposite sample preparation and characterization. These experimental results validated those obtained from computational studies from TU Darmstadt, National University of Athens, Trieste University, and BASF. Therefore, the influence of the nanoparticles of various diameters (3.0, 4.0, and 5.0 nm) and grafting states (0.0, 0.5, and 1.0 chains/nm^2) on atactic polystyrene was studied. To perform this work, a computer molecular dynamics (MD) simulation tool, YASP[10], was employed. This tool numerically solves Newton's equations of motion for a system of interacting atoms to generate a trajectory of their movements. Following this, the resulting trajectories can be analyzed for different properties that characterize the structure, dynamics, and thermodynamics of the system.

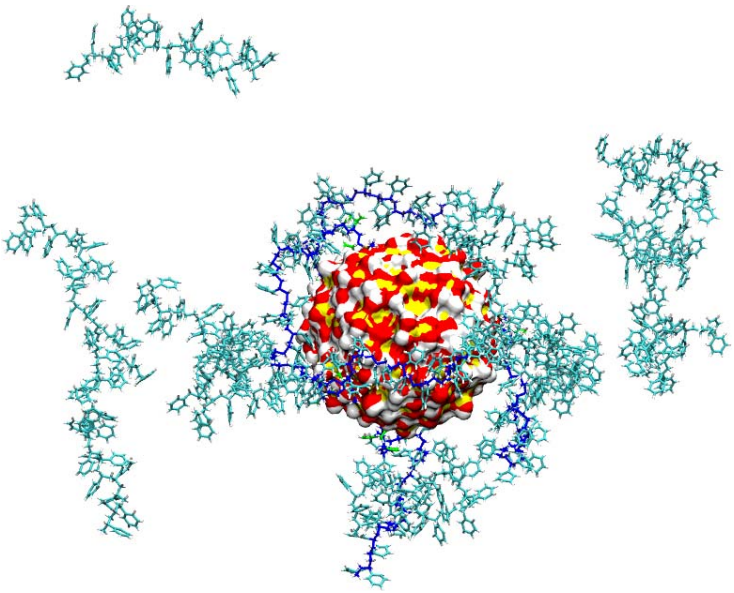

Figure 1.1. Schematic representation of the spherical silica nanoparticle, grafted (shown by the blue backbone carbon atoms) and free (all in cyan) atactic polystyrene chains. Note: There are more grafted and free chains in the simulation which are not shown to improve the clarity of the figure.

The use of atomistic MD simulations has the advantage of being able to investigate both static and dynamic properties of a system in fine detail. The ensuing results have the benefit of being related to experimental observations such as those probed by nuclear magnetic resonance[11] (NMR) and dielectric spectroscopy[12] (DS) studies. Additionally, other experimental techniques like neutron, x-ray, and light scattering now allow the determination of the atomistic structure of a material. Thus, computer modeling techniques interface with and complement experimental methods in understanding the link between structural and dynamical properties of polymers. While many experimental[5,6,9,13-20] investigations have been performed to study the behavior of polymers at surfaces, very few atomistic[21-25] computer modeling studies have been done. This necessitates the development a unified theoretical and experimental understanding of the polymer static and dynamic modifications in the presence of a surface. This is important because such changes determine in part the overall material properties. Examples of these material properties include their mechanical strength, appearance, how well they can be processed, and the duration of the polymer aging process. Additionally, this work sets a foundation for coarse-grained simulations, which investigate longer polymer chains and bigger systems.

Static and dynamic properties of polymers determine whether nanoparticles form clusters or are well dispersed in a polymer melt. This is a pivotal challenge in experimental techniques because it is difficult to control the dispersion of nanoparticles, which finally determines the resulting material

properties. Parameters that influence the static, dynamic, and nanoparticle dispersion state include - but are not limited to - the nanoparticle size, grafting density, the ratio of the length of grafted to free chains, and surface-polymer interactions. Therefore, developing an understanding of how these parameters interplay with each other will aid in the control and tailoring of the final nanoparticle dispersion state.

The first half of this cumulative PhD thesis, chapter 2, presents results of the atactic polystyrene structure around the nanoparticle. The quantities of interest were the polymer density, radius of gyration, and its orientation relative to the nanoparticle surface. The analysis of the computer simulation output trajectory files resolved these polymer properties as a function of distance from the nanoparticle surface to quantify the surface effect. Varying both the polymer grafting density and the nanoparticle surface curvature enabled the understanding of how these two parameters interplay and influence the polymer's structural properties. For instance, the extents of the polymer density modifications under the influence of the nanoparticle surface indicate the wettability of the surface by the polymer. This is important in mitigating adhesive failure and mechanical stress distribution in the nanocomposite material. At the same time, the density changes directly influence the polymer dynamical properties like the glass transition temperature and polymer aging processes. Therefore, understanding and being able to control these changes is vital since polymer properties like the elastic modulus and conductivity amongst many other physical properties change significantly around the polymer glass transition. These observations underscore not only the importance of the polymer in the interface region but also the width of the interphase region. The latter is influenced by the nanoparticle grafting state and the nanoparticle curvature as investigated in this work but also on the length ratio between the grafted and free polymer chains. While changes in the polymer radius of gyration give a measure of how stretched a polymer coil is, this has the effect of directly influencing the packing of polymer chains and their orientation. Additionally, the induced orientation of the polymer and its segments is important in processes that depend on transport properties such as electrical and thermal conductivity. Therefore, the different polymer structural properties are interlinked and understanding their cause-and-effect gives tuning parameters in the design of polymer nanocomposites.

Complementary to structural properties discussed in chapter 2, chapter 3 forms the second half of this thesis and discusses the dynamical properties of the polymer. These included the mean-squared displacement (MSD) of the polymer chain center-of-mass and reorientational dynamics of intramolecular segment vectors. These quantities were also calculated under different nanoparticle grafting states and surface curvature. Changes in the polymer chain MSD and the reorientation of its end-to-end vector have given a measure of the global polymer mobility. To understand the local

dynamics at the monomer level, the reorientation of a three-monomer and the C_α-C_{para} segment vector as well as the backbone C_α-H bond vector was investigated (see Figure 1.2). The advantage of obtaining such a local resolution is that it allows for comparison with experimental NMR and DS studies which probe the C-H bond vector and the C_α-C_{para} segment vectors, respectively. To develop a unified understanding, explanations of the dynamical property changes were linked to the previously observed structural properties either in the interface or interphase region, see chapter 2.

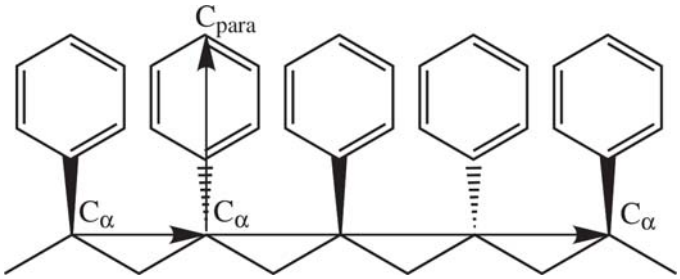

Figure 1.2. This schematic diagram is of a 5 monomer polystyrene chain to show the one monomer (C_α-C_α), three monomers (C_α ... C_α), and C_α-C_{para} segment vectors considered in the study of chain segmental dynamics.

The objectives to this thesis were to use the molecular dynamics simulation tool (YASP), setup the model system under investigation, perform the simulations, and write analysis programs to determine the different polymer properties. Therefore, I interpreted, understood, and explained my results in light of their interconnectedness as well as results from other simulations and experimental work on polymer nanocomposite systems. Finally, this work ends with chapter four which encompasses the conclusions and an outlook for further investigations.

1.2 Struktur und Dynamik von ataktischem Polystyrol an der Grenzfläche und Interphase zu gepfropften und ungepfropften Silica-Nanoteilchen

Der Verbundwerkstoff-Industrie gelingt es seit längerer Zeit, Materialeigenschaften von Polymeren durch Beimischung anorganischer Füllstoffe zu verbessern.[1,2] Verursacht wird dies durch Synergien bei der Kombination von zwei oder mehr Komponenten. Die resultierenden Verbundwerkstoffe können Eigenschaften aufweisen, die in den Komponenten nicht vorhanden sind. Ein bekanntes Beispiel ist die Beimischung von Ruß zu einer Polymermatrix, um das Ermüdungsverhalten, die Zähigkeit sowie den Widerstand gegenüber Bruch und Abrieb zu verbessern[3,4]. Bei der Optimierung konventioneller Verbundwerkstoffe hat man versucht, dies durch eine Reduktion in der Dimension der Füllstoffe zu realisieren. Dies führt zu einer Vergrößerung der Oberfläche der Füllstoffe und damit zu einer stärkeren Wechselwirkung mit dem Polymer. Mit dem Aufkommen von Nanomaterialien haben diese Versuche einen rasanten Aufschwung genommen. Experimentelle Methoden zur Synthese und Charakterisierung können mittlerweile im Nano-Maßstab (10^{-9} m), also in atomaren und molekularen Größenordnungen, durchgeführt werden. Mit diesen neuen Methoden ist es plötzlich möglich, Materialien zu entwickeln, die innerhalb sehr kleiner Dimensionen modifiziert werden können. Änderungen im Nanobereich führen zu veränderten mikroskopischen Eigenschaften und somit auch zu Änderungen in makroskopischen Dimensionen. Wie immer, wenn wissenschaftliches Neuland betreten wird, ist es eine Herausforderung, fundamentale Einflussgrößen zu detektieren, die die Systemeigenschaften bestimmen.

Im Unterschied zum Verhalten konventioneller Verbundwerkstoffe, haben neuere Experimente an Polymer-Nano-Verbundwerkstoffen multifunktionale Änderungen in ihren Eigenschaften gezeigt. Beispiele für dieses Verhalten sind die Abnahme in der Viskosität von Polymeren[5], Änderungen in der Temperatur für den Glasübergang[6,7] oder Änderungen im thermochemischen Verhalten[8,9]. Diese Liste ist in keiner Weise vollständig. Unverstanden sind bisher die Ursachen für das unterschiedliche Verhalten von konventionellen und Nanowerkstoffen. Um solche Fragen zu beantworten wurde die vorliegende Dissertation in einem Forschungsprojekt der Europäischen Union „NanoModel" durchgeführt, an dem Gruppen aus Universitäten und der Industrie beteiligt waren. Ziel des Programms war die experimentelle und theoretische Beschreibung des Polymerverhaltens in der Nähe einer Oberfläche. Ein möglichst vollständiges Verständnis aller Einflussgrößen auf die Materialeigenschaften würde die Charakterisierung neuer Polymer-Nano-Verbundwerkstoffe enorm erleichtern. Sowohl die strukturellen als auch dynamischen Untersuchungen der vorliegenden Arbeit

haben offene Fragen berührt, die dieses EU Projekt initiiert haben: (1) Beeinflusst ein Nanoteilchen die Eigenschaft der Polymerphase? (2) Da die Dispersion von Nanoteilchen die Eigenschaften eines Verbundwerkstoffes kontrolliert, ergibt sich die Frage, welche Faktoren eine gute Dispersion in der Polymerphase ermöglichen? (3) Welchen Einfluss hat die Größe des Nanoteilchens? (4) Ist es notwendig, Polymerketten auf Nanoteilchen aufzupfropfen? Führt eine Funktionalisierung der Nanoteilchen zu einer besseren Dispersion in der Polymerschmelze? (5) Welche Länge sollten diese aufgepfropften Ketten relativ zur Länge der freien Polymerketten haben? Welche Pfropfungsdichte führt zu einer optimalen Dispersion? (6) In welchem Maß werden die Polymereigenschaften an der Polymer-Nano-Oberfläche und in der Interphase (Gebiet der gepfropften Ketten) - wenn überhaupt - geändert? (7) Welche Parameter beeinflussen die Ausdehnung der Oberfläche und Interphase? (8) Führen experimentelle Beobachtungen und Computersimulationen zu ähnlichen Ergebnissen oder Vorhersagen bezüglich der Materialeigenschaften? Aufgrund dieser Fragen wurden in der vorliegenden Dissertation die strukturellen und dynamischen Eigenschaften von ataktischem Polystyrol in Nachbarschaft von Silica (Quarz)-Nanoteilchen als Modellsystem für Polymer-Verbundwerkstoffe in atomarer Auflösung untersucht. Abbildung 1.1 zeigt eine Momentaufnahme aus einer Computersimulation eines solchen Systems. Dieses Modellsystem wurde gewählt, da es auch für die Partnergruppen im NanoModel-Projekt sehr wichtig ist. Polystyrol ist ein häufig verwendetes, gut charakterisiertes Polymer und Silica (Quarz), ein typisches Füllmaterial. Es liegt im Interesse der Konsortiumspartner wie der BASF, der Bosch GmbH oder CRP Fiat, neue Nanomaterialien mit verbesserten Eigenschaften zu entwickeln. Dies könnte erfolgreicher gelingen, wenn der Einfluss des Nanoeffektes auf die mechanischen Eigenschaften und die Herstellungsbedingungen für solche Polymere besser bekannt wäre. Im Detail wurde der Einfluss der Dimension des Nanoteilchens (Durchmesser von 3.0, 4.0 und 5.0 nm) sowie der Pfropfungsdichte (0.0, 0.5 und 1.0 Polymerketten/nm²) analysiert. Als numerisches Werkzeug wurde ein Molekulardynamik (MD)-Programm (YASP[10]) verwendet, das auf den Gesetzen der Newtonschen Mechanik beruht. Die numerische Lösung der Newtonschen Bewegungsgleichungen für wechselwirkende Atome führt zu Trajektorien für die Teilchenbewegungen. Die Auswertung dieser Trajektorien erlaubt die Berechnung verschiedener Eigenschaften des Systems, die seine Struktur, Dynamik und Thermodynamik charakterisieren.

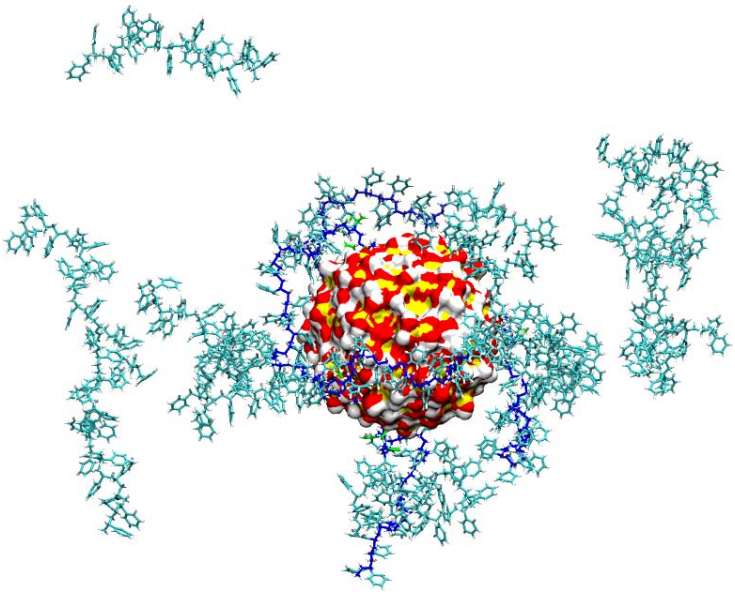

Abbildung 1.1. Schematische Darstellung eines sphärischen Silica-Nanoteilchens sowie aufgepfropfter (symbolisiert durch die blauen Kohlenstoff-Atome der Polymerkette) und freier (türkis) Polystyrol-Ketten. Anmerkung: Um die Darstellung überschaubarer zu machen, wurden nicht alle Polymerketten der zu Simulation gezeigt.

MD-Simulationen in atomarer Auflösung haben den Vorteil, dass sowohl statische als auch dynamische Eigenschaften mit hoher Genauigkeit untersucht werden können. Die Ergebnisse der Simulationen lassen sich mit einer Reihe experimenteller Daten korrelieren, z.B. mit magnetischer Kernresonanz[11] (NMR) oder mit dielektrischer Spektroskopie[12] (DS). Strukturelle Parameter können mithilfe der Neutronen- oder Röntgenbeugung sowie der Lichtstreuung ermittelt werden. Mithilfe von Computersimulationen können diese Experimente ergänzt bzw. erst sinnvoll interpretiert werden. Außerdem erlauben sie, Beziehungen zwischen strukturellen und dynamischen Eigenschaften herzustellen. Während das Verhalten von Polymeren in der Interphase/Grenzfläche in vielen Experimenten untersucht wurde,[5,6,9,13-20] ist die Zahl der atomar aufgelösten Computersimulationen recht überschaubar.[21-25] Auch dies zeigt die Notwendigkeit, die Änderungen von Polymer-Eigenschaften in der Grenzfläche mithilfe experimenteller und theoretischer Ansätze zu verstehen. Dies ist deshalb so wichtig, da solche Änderungen die Eigenschaften des Polymers bestimmen. Beispiele für solche Eigenschaften sind die Massenverteilung, die äußere Erscheinung, Probleme bei der Bearbeitung und Alterungsprozesse. Die atomaren MD-Simulationen in der vorliegenden Arbeit können ebenfalls als Vorlage bei der Durchführung vergröberter MD-Rechnungen, so genannter CG-Verfahren, benutzt werden. In einer CG-Auflösung lassen sich längere Ketten in komplexeren Systemen mit MD simulieren, die in einer atomaren Auflösung nicht mehr zugänglich sind.

Die statischen und dynamischen Eigenschaften von Polymeren bestimmen auch, ob Nanoteilchen in der Polymerlösung zu Clusterbildung neigen oder ob sie gut dispergiert sind. Da die Dispersion der Nanoteilchen experimentell nur wenig beeinflusst werden kann, ist das Verstehen dieses Verhaltens von zentraler Bedeutung. Die Einflussparameter für die statischen und dynamischen Eigenschaften sowie für den Dispersionsgrad der Nanoteilchen umfassen unter anderem die Größe der Nanoteilchen, die Pfropfungsdichte, das Längenverhältnis aufgepfropfter und freier Polymerketten sowie die Wechselwirkung zwischen Polymer und Oberfläche. Die Entwicklung von Polymer-Verbundwerkstoffen mit genau definierten Eigenschaften macht es deshalb notwendig, die gegenseitige Beeinflussung dieser Parameter zu verstehen.

In der ersten Hälfte dieser kumulativen Dissertation, Kapitel 2, werden strukturelle Eigenschaften von ataktischem Polystyrol diskutiert. Interpretiert werden die Massendichte des Polymers, der so genannte Gyrationsradius und die Polymer-Orientierung relativ zur Oberfläche des Nanoteilchens. Diese Eigenschaften werden als Funktion des Abstands zum Nanoteilchen analysiert, um die Reichweite von Oberflächeneffekten zu beschreiben. Die Variation der Pfropfungsdichte und der Krümmung des Silica-Teilchens hat es ermöglicht, das Wechselspiel beider Einflussgrößen zu untersuchen und ihren Einfluss auf strukturelle Eigenschaften zu erläutern. So bestimmt z.B. die Ausdehnung von Dichteunterschieden unter dem Einfluss der Nanoteilchen die Benetzbarkeit der Oberfläche durch das Polymer. Dieser Effekt ist wichtig, um den Bruch bei der Adhäsion oder die mechanische Belastung im Verbundwerkstoff zu reduzieren. Dichteänderungen haben ebenfalls einen direkten Einfluss auf dynamische Eigenschaften wie dem Glasübergang oder der Alterung eines Polymers. Das Verständnis und die Kontrolle dieser Änderungen sind deshalb von Bedeutung, da sich Polymereigenschaften wie elastische Konstanten oder die Leitfähigkeit in der Nähe des Glasübergangs dramatisch ändern. Diese Abhängigkeit betont noch einmal die Bedeutung der Polymereigenschaften in der Interphase. Die Ausdehnung dieser Region wird durch Aufpfropfen verändert, ebenfalls durch die Krümmung des Nanoteilchens. Beide Einflussgrößen werden in dieser Arbeit untersucht. Ebenfalls ein wichtiger Einflussparameter ist das Längenverhältnis von aufgepfropften und freien Polymerketten. Berechnete Gyrationsradien lassen zum Beispiel Aussagen darüber zu, wie stark gestreckt die Polymer-Ketten der Probe sind. Dies bestimmt dann die Packung der Ketten, ihre Orientierung und schließlich die Polymerdichte. Die durch das Nanoteilchen induzierte Orientierung der Ketten sowie kleinerer Segmente ist für Prozesse relevant, in denen es auf die thermische oder elektrische Leitfähigkeit ankommt. Generell sind verschiedene strukturelle Eigenschaften miteinander verknüpft. Das Auffinden von Struktur-Wirkungs-Prinzipien liefert dann „Stellschrauben" im Design von Polymer-Nano-Verbundwerkstoffen.

Komplementär zu Kapitel 2, werden in Kapitel 3 dieser Dissertation dynamische Polymereigenschaften vorgestellt. Diese Daten sind in der zweiten Hälfte der Arbeit zu finden. Analysiert werden die mittlere quadratische Auslenkung (MSD) des Polymer-Schwerpunktes sowie die Reorientierungsdynamik intramolekularer Fragmente. Diese Größen werden ebenfalls für verschiedene Pfropfungsdichten und Krümmungen des Nanoteilchens diskutiert. Berechnete MSD-Parameter sowie Reorientierungszeiten des End-zu-End-Vektors sind ein Maß für die Polymer-Beweglichkeit. Um die lokale Dynamik auf Basis der monomeren Bausteine zu verstehen, wurde die Reorientierung folgender Fragment-Vektoren untersucht (siehe Abbildung 1.2): Vektor über drei Monomere, C_α-C_{para}-Vektor sowie der C_α-H-Bindungsvektor. Der Vorteil solcher Simulationen liegt in der möglichen Korrelation mit NMR- oder DS-Messungen, die die Dynamik der C_α-H-Bindung sowie des C_α-C_{para}-Segmentvektors widerspiegeln. Zum besseren Verständnis wurden die Ergebnisse der „dynamischen" Eigenschaften mit den in Kapitel 2 diskutierten strukturellen Eigenschaften in Verbindung gesetzt.

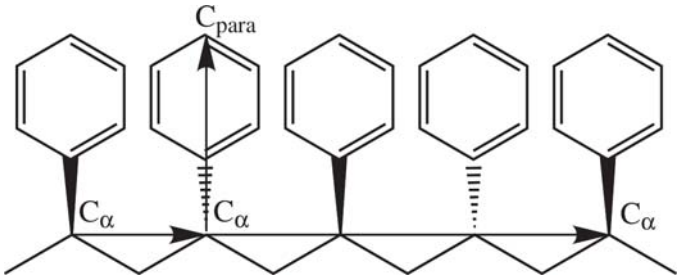

Abbildung 1.2. In dem schematischen Diagramm wird ein Ausschnitt von fünf Polystyrol-Monomeren gezeigt. Definiert werden dabei der C_α-C_α-Monomer-Vektor, der Drei-Monomer (C_α... C_α)-Vektor sowie der C_α-C_{para}-Segment-Vektor, die für die Analyse der Segment-Dynamik herangezogen wurden.

Aufgabe der vorliegenden Dissertation war die Verwendung eines Molekulardynamik-Programms, YASP, die Definition geeigneter Modellsysteme, die Durchführung der Simulationen sowie das Schreiben von Analyse-Programmen, um verschiedene Polymer-Eigenschaften zu bestimmen. Zusammenfassend habe ich meine Ergebnisse unter Berücksichtigung interner Konsistenz sowie anderer experimenteller und Simulationsergebnisse interpretiert. Die Arbeit wird mit Kapitel 4 abgeschlossen, in dem die erhaltenen Ergebnisse noch einmal zusammengefasst werden und ein Ausblick auf zukünftige Untersuchungen gegeben wird.

1.3. References / Literaturverzeichnis

(1) Kraus, G. *Reinforcement of elastomers*; NY: Interscience Publishers: New York, 1965.
(2) Kraus, G. *Angew. Makromol. Chem.* **1977**, *60*, 215-248.
(3) Koenig, J. L. *Accounts Chem. Res.* **1999**, *32*, 1-8.
(4) Zhang, Y.; Ge, S.; Tang, B.; Koga, T.; Rafailovich, M. H.; Sokolov, J. C.; Peiffer, D. G.; Li, Z.; Dias, A. J.; McElrath, K. O.; Lin, M. Y.; Satija, S. K.; Urquhart, S. G.; Ade, H.; Nguyen, D. *Macromolecules* **2001**, *34*, 7056-7065.
(5) Mackay, M. E.; Dao, T. T.; Tuteja, A.; Ho, D. L.; Van Horn, B.; Kim, H.-C.; Hawker, C. J. *Nature Mater.* **2003**, *2*, 762-766.
(6) Tsagaropoulos, G.; Eisenburg, A. *Macromolecules* **1995**, *28*, 396-398.
(7) Tsagaropoulos, G.; Eisenburg, A. *Macromolecules* **1995**, *28*, 6067-6077.
(8) Whittington, A. P.; Nguyen, S. T.; Kim, J.-H. *Nanoscape* **2009**, *6*, 26-30.
(9) Mahfuz, H.; Hasan, M.; Dhanak, V.; Beamson, G.; Stewart, J.; Rangari, V.; Wei, X.; Khabashesku, V.; Jeelani, S. *Nanotechnology* **2008**, *19*, 445702.
(10) Müller-Plathe, F. *Comput. Phys. Commun.* **1993**, *78*, 77-94.
(11) He, Y.; Lutz, T. R.; Ediger, M. D.; Ayyagari, C.; Bedrov, D.; Smith, G. D. *Macromolecules* **2004**, *37*, 5032-5039.
(12) Harmandaris, V. A.; Floudas, G.; Kremer, K. *Macromolecules* **2011**, *44*, 393-402.
(13) Bansal, A.; Yang, H.; Benicewicz, B.; Kumar, S. K.; Schadler, L. S. *J. Polym. Sci. Pol. Phys.* **2006**, *44*, 2944-2950.
(14) Harton, S. E.; Kumar, S. K.; Yang, H.; Koga, T.; Hicks, K.; Lee, H.; Mijovic, J.; Liu, M.; Vallery, R. S.; Gidley, D. W. *Macromolecules* **2010**, *43*, 3415-3421.
(15) Kalb, J.; Dukes, D.; Kumar, S. K.; Hoy, R. S.; Grest, G. S. *Soft Matter* **2010**, *7*, 1418-1425.
(16) Chevigny, C.; Dalmas, F.; Di Cola, E.; Gigmes, D.; Bertin, D.; Boue, F.; Jestin, J. *Macromolecules* **2011**, *44*, 122-133.
(17) Dukes, D.; Li, Y.; Lewis, S.; Benicewicz, B. C.; Schadler, L. S.; Kumar, S. K. *Macromolecules* **2010**, *43*, 1564-1570.
(18) Oh, H.; Green, P. F. *Nat. Mater.* **2009**, *8*, 139-143.
(19) Priestly, R. D.; Ellison, C. J.; Broadbelt, L. J.; Torkelson, J. M. *Science* **2005**, *309*, 456-459.
(20) Akcora, P.; Kumar, S. K.; Sakai, V. G.; Li, Y.; Benicewicz, B.; Schadler, L. S. *Macromolecules* **2010**, *43*, 8275-8281.
(21) Brown, D.; Mélé, P.; Marceau, S.; Albérola, N. D. *Macromolecules* **2003**, *36*, 1395-1406.
(22) Barbier, D.; Brown, D.; Grillet, A.-C.; Neyertz, S. *Macromolecules* **2004**, *37*, 4695-4710.
(23) Yelash, L.; Virnau, P.; Binder, K.; Paul, W. *Phys. Rev. E* **2010**, *82*, 50801-50804.
(24) Cordeiro, R. M.; Zschunke, F.; Müller-Plathe, F. *Macromolecules* **2010**, *43*, 1583-1591.
(25) Eslami, H.; Müller-Plathe, F. *J. Phys. Chem. B* **2009**, *113*, 5568-5581.

2. Interface of Grafted and Ungrafted Silica Nanoparticles with a Polystyrene Matrix: Atomistic Molecular Dynamics Simulations

ABSTRACT: Atomistic molecular dynamics simulations of a composite consisting of an ungrafted or a grafted spherical silica nanoparticle embedded in a melt of 20-monomer atactic polystyrene chains have been performed. The structural properties of the polymer in the vicinity of a nanoparticle have been studied. The nanoparticle modifies the polymer structure in its neighbourhood. These changes increase for higher grafting densities and larger particle diameters. Mass and number density profiles show layering of the polymer chains around the nanoparticle, which extends to about 2 nm. In contrast, the increase of the polymer's radius of gyration and other induced ordering (alignment of the chains parallel to the surface, orientation of shorter backbone segments) are shorter-ranged. The infiltration of free polystyrene chains into the grafted chains region is reduced with increasing grafting density. Thus, the interpenetration of grafted and free chains at high grafting densities, which is responsible for the mechanical anchoring of nanoparticles in the polystyrene matrix, is less than what would be desirable for a well-reinforced composite. (Macromolecules **2011**, 44, 2316-2327)

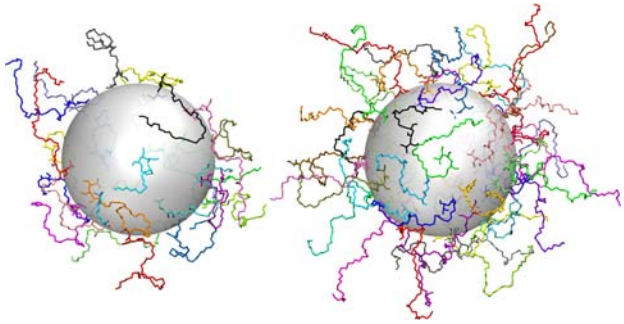

2.1. Introduction

Composites of inorganic particles embedded in a polymer matrix have attracted scientific and technological attention for a variety of reasons. For example, the rubber industry widely employs carbon black and silica particles of a wide size distribution as reinforcing fillers[1,2]. Carbon black increases tire strength and toughness while also improving the rubber's resistance to tearing, abrasion, and flex fatigue[3,4]. Consequently, the traction of rubber and its durability are increased. It is therefore possible and advantageous to combine the properties of different materials, e.g. elastomers or rubber with carbon black or silica, to make functional materials where one component provides the function

and the other the mechanical strength. The usage of nanoparticles as additives to modify polymer properties has greatly increased with many different possibilities being explored[5,6]. In most cases, a regular dispersion of the nanoparticles in the polymer is desired to prevent particle aggregation[6,7]. This can be achieved by compatibilising the nanoparticle and polymer, for example, by coating the nanoparticle or grafting it with a polymer[8]. Such polymer brushes are also used for other physicochemical applications such as colloid stabilization[9] and dispersion[10], or improved lubrication[11,12]. It has been observed by Mackay *et al.*[13] that the addition of nanoparticles to polymer melts can lead to a non-Einstein-like decrease of the viscosity. This can be employed to lower the viscosity of polymers for processes such as extrusion and injection-molding without compromising the mechanical strength of the final object.

An important part of a composite is the interface between the polymer and inorganic filler. The mere existence of the interface modifies the polymer structure[14]. The structural perturbation can extend to more than just the first molecular layer and can cause the formation of an interphase were the polymer does not (yet) show bulk-like behavior. This phenomenon is particularly pronounced for nanocomposites. In the nanometer-size interstices between nanoparticles, the polymer will not always reach its bulk behavior. Structural modifications are expected for both bare and grafted nanoparticles, but they will be different. As a result of their unusual properties, polymer interfaces formed near solid surfaces have attracted considerable interest from both academic and industrial communities. For example, Tsagaropoulos *et al.*[15] observed that many polymer properties such as viscosity, diffusion coefficient, or the T_2 relaxation time in NMR measurements dramatically change in the interfacial region. These differences are attributed to restrictions on the mobility of polymer chains in the vicinity of a surface. The reduced mobility has, in turn, been explained by the reduction of the configurational entropy due to crowding and/or ordering at the interface.

The polymer nanocomposites studied in this work consist of either an ungrafted or a grafted spherical silica nanoparticle of varying diameters and surrounded by a polystyrene matrix. The interaction between grafted and free chains on one hand, and with the surface on the other, determines the dispersion state of the nanoparticles and whether reinforcement is improved or not. Recent experimental work by Chevigny *et al.*[16,17] has shown that these interactions are one of the key factors in controlling the dispersion of nanoparticles. Dispersion of nanoparticles into polymeric matrices remains an outstanding problem as highlighted in the recent review article of Kumar and Krishnamoorti[18]. To control polymer dispersion, understanding of the factors involved in the interaction between grafted and free chains is vital. The free energy of swelling polymer brushes consists of a mixing entropy term between the grafted and ungrafted chains, and an elastic deformation

term for the grafted chains. Entropic effects drive the chain interpenetration and scale inversely with the molecular weight. Borukhov *et al.*[19] also introduced an enthalpic interaction term to explain the mixing of large solvent molecules with polymer brushes.

Following this short overview of experimental activities, we will now comment on simulation studies performed on polymeric nanocomposites. There are many studies of ungrafted nanoparticles in polymers, at various levels of theory. Frischknecht *et al.*[20] employed a coarse-grained (CG) variant of the self-consistent polymer reference interaction site model (SC/PRISM) to study the effect of well dispersed nanoparticles on the equilibrium chain configurations. They observed an expansion in the polymer radius of gyration, R_g, when the nanoparticle radius was below R_g. This effect was further enhanced with increasing nanoparticle volume fraction. Chain expansion was suggested to be a result of both the excluded volume taken up by the nanoparticles and the attractive interaction between the monomers and the nanoparticles. Both phenomena make the nanoparticles behave like a good solvent. Polymer chains formed bound layers around multiple nanoparticles and their packing changed over a length scale up to three nanoparticle diameters.

Also employing the PRISM theory, Hooper and Schweizer[21,22] sought to identify "design rules" for the thermodynamic stability and miscibility of fillers in dense polymer melts. In their work, they reported that the particle-particle potential of mean force can show contact aggregation, steric stabilization, local bridging attraction, and longer range "tele-bridging" attraction. This behavior depends on the strength and spatial range of intermolecular attractions. The observed steric stabilization of the spherical particles is attributed to the thermodynamic stability of distinct bound polymer layers. This knowledge can assist in the rational design to achieve good particle dispersion and thus homogeneous mixtures.

Using Monte Carlo (MC) simulations of a coarse grained model, Vogiatzis *et al.*[23] investigated the structure of a polystyrene matrix filled with an ungrafted nanoparticle, made up of internally tightly cross-linked polystyrene. Their work shows an increased polymer density near the nanoparticle surface. The calculated density profiles were only weakly dependent on the chain length. The authors furthermore reported that interfacial chains orient with their longest dimension tangentially to the nanoparticle surface. Similar observations were seen for local chain segments.

Fully atomistic molecular dynamics (MD) simulations of an ungrafted spherical silica nanoparticle embedded in a poly(ethylene oxide) (PEO) matrix by Barbier *et al.*[24] revealed dense packing of flattened PEO backbones arranged in ordered shells around the nanoparticle. Interactions between PEO and silica further stabilized the densely packed shells. Analogous to the work of Vogiatzis *et al.*[23], they observed two distinct density maxima near the nanoparticle surface. This well-defined

layering effect is typical of strongly attractive polymer-surface interactions. The predicted alignment of the PEO backbones parallel to the silica surface was strongest in the first layer. Note that these results are similar to observations of a generic polymer in the vicinity of a surface[25]. The increase in the polymer density near the surface was also reported by Borodin *et al.*[26], who studied the interface between poly(ethylene oxide) and a planar crystalline TiO_2 surface.

Computer simulation work of polymer composites containing ungrafted surfaces has also been carried out in our group. In these studies, however, the surfaces were flat, i.e. they are representative of large filler particles (particle curvature radius is large compared to the polymer radius of gyration). Eslami and Müller-Plathe[27] performed atomistic MD simulations of polyamide-6,6 trimers confined between graphite surfaces. They observed a layering/structuring effect of the oligomers parallel to the surface. Recent work on the structural properties of polyamide-6,6 tetramers around one and two embedded carbon nanotubes (CNT) also reveals dense chain packing around the CNT surface[28].

There is also a considerable body of simulation work on polymer-grafted surfaces and nanoparticles. Grest[29] pioneered computer simulations of a polymer brush in a polymer melt. Previous work had only simulated polymer brushes in solvents. The challenge of simulating a polymer melt is that most of the computer time is spent on calculating the melt and not the brush. Both MD and MC studies of a system of chains attached to a flat surface demonstrated that the brush height at low coverage is nearly independent of the grafting density (ρ_{gr}, chains per surface area, i.e. chains/nm^2). At higher surface coverage, it increases as $(\rho_{gr})^{1/3}$. Layering of monomers close to the surface was evident in both the overall number density and the brush monomer number density. The number of free chains that were excluded from the brush volume increased with increasing chain length due to entropic interactions and excluded volume effects, showing a crossover from a wet to a dry brush.

Lo Verso *et al.*[30] compared MD and density functional theory (DFT) to study a coarse grained model of fully flexible polymers end-grafted to repulsive spherical nanoparticles under good solvent conditions. In their systems, R_g is similar to the size of the nanoparticle. The density profiles for both methods show a tightly bound monolayer close to the surface that is followed by a clearly visible second layer. They report a local stretching of the grafted chains and a decrease in the tangential orientation to the surface with increasing ρ_{gr}. However, their DFT method overestimated chain stretching with increasing surface curvature.

In the entanglement regime, Kalb *et al.*[31] analyzed the effect of surface coverage and curvature of spherical grafted nanoparticles on the autophobic dewetting of the melt from the brush. Using MD, they employed a coarse grained bead-spring model with a truncated and shifted Lennard-Jones potential for brush and melt monomers. These authors integrated this potential over the nanoparticle

sphere to obtain the interaction between the nanoparticle and the brush as well as the melt monomers. Their work shows that the solvent quality of the melt becomes progressively poorer with increasing ρ_{gr}. It becomes increasingly more difficult to compensate for the entropic loss upon brush infiltration of the matrix chains. In addition, polymer brush chains attached to small nanoparticles of higher curvature can explore more space. The opposite is true for chains attached to a planar surface. Consequently this results in a greater entropic loss for matrix chains wanting to infiltrate. The radial brush monomer density profiles changed from concave for small nanoparticles (behavior similar to star polymers) to parabolic for large particles.

Lattice MC simulations on a system of linear chains end-grafted to a spherical surface were performed by Klos and Pakula[32-34] using the cooperative motion algorithm. The monomer concentration profiles under good solvent conditions are reported to change from concave to convex with increasing nanoparticle radius. For small surface coverage, a depletion layer is observed for the latter. In the case of small ρ_{gr} (surface coverage) and particularly for smaller nanoparticles with a high curvature, chain centers of mass were found inside the particle, indicating that the polymers can wrap around it. Similar observations have been reported by Vogiatzis *et al.*[23]. Chains near the surface were tangentially oriented to it whereas distant chains had stronger radial orientations.

Cordeiro *et al*.[35] investigated the mutual repulsion of two PEO-grafted surfaces by a combination of atomistic and coarse-grained models. Repulsive surfaces made chains to attain more extended conformations while chains adsorbed onto attractive surfaces. They observed that the chain length had a larger influence on the particle stability when comparing particles of similar grafting density but different chain molecular weight.

Trombly and Ganesan[36] have employed the polymer mean-field theory to study curvature effects of polymer-grafted nanoparticles immersed in a chemically identical polymer melt. The interpenetration width between grafted and free chains was quantified as a function of surface curvature, grafting density, and the relative molecular weights of the grafted and free chains. The stretching cost of the grafted chains associated with the penetration of free chains was found to reduce with increasing surface curvature thereby enhancing the tendency for interpenetration of free chains into the grafted chains regime.

To understand better the structural properties of a chemically realistic polymeric matrix around spherical nanoparticles, we have used MD simulations to study an atactic polystyrene (a-PS) matrix surrounding either an ungrafted or a grafted spherical silica nanoparticle. We have performed these simulations as a function of the nanoparticle curvature, i.e. its diameter. This investigation has been performed at the atomistic level and we employed the YASP[37] MD code. All simulations were carried

out at a pressure of 101.3 kPa and a temperature of 590 K. The temperature is above the glass transition temperature of polystyrene of 368 K. These simulation conditions enabled us to understand the structural properties of a polymer melt in the vicinity of an inorganic silica spherical surface. The important topic of the polymer dynamics in the vicinity of the surface is intended to be a part of our forthcoming work. The nanoparticle is either ungrafted (bare) or grafted with a-PS chains of the same length as the matrix chains. Two grafting densities have been chosen. All polymer chains consist of 20 monomers. The grafted chains are covalently attached to the spherical silica nanoparticle by an anionic linker unit. Our investigation intends to give insight into the effect of surface curvature and grafting densities on the structure of the surrounding polymer, the possible formation of an interphase, and the interpenetration of grafted and free polystyrene chains. This information will serve as input to the rational design of well dispersed nanoparticles since this determines the nanocomposite material properties[38]. A second purpose of this work is to provide reference data for the generation of a coarse-grained model of polystyrene/silica nanocomposites, which will allow for the simulation of larger systems containing longer polymer chains.

2.2. Model and Simulation Details

Molecular dynamics (MD) simulations were performed of a-PS (-[C_8H_8]-$_n$) either in contact with an ungrafted or an a-PS-grafted spherical silica (SiO_2) nanoparticle. Nanoparticle diameters of 3, 4, and 5 nm as well as grafting densities of 0.0 (bare, ungrafted), 0.5, and 1.0 chains/nm^2 were simulated. Due to the large computational demand to equilibrate long polymer chains, both free and grafted a-PS chains in our model system have been restricted to n = 20 monomers. All polymer chains have been terminated by a methyl group (-CH_3). Grafted a-PS chains were attached to the silica surface oxygen atoms via an anionic linker unit/molecule (-[$H_2C(H(C_2H_3)C]_3(CH_3)_2Si$-) as used in experiments[39]. A picture of this molecule is shown in the Appendix 1 (A1), Fig. A1.18.

The systems studied by atomistic MD simulations are summarized in Table 2.1. The total number of grafted and free chains was at least 202. Despite an increasing mass (or volume) fraction of the silica nanoparticle with increasing diameter, the obtained results can be systematically deduced across the different systems. The basis for comparison amongst the different systems containing different nanoparticle sizes is the grafting density, ρ_{gr}. The bulk mass density of a-PS was 910.86±1.52 kg/m^3 at 590 K and 101.3 kPa (experimental[40] density = 904.02±0.10 kg/m^3). The average mass density of the silica nanoparticle was 2770.60±7.56 kg/m^3 (density of natural quartz[41] = 2635 – 2660 kg/m^3).

Table 2.1: Studied Nanocomposite Systems (T = 590 K, P = 101.3 kPa)

Number of grafted a-PS chains	Number of free a-PS chains	ρ_{gr} /chains/nm^2	Mass density /kg/m^3	SiO_2 core /mass%	Grafted a-PS chains /mass%	Free a-PS chains /mass%	Simulation time /ns	Box length /nm
			Nanoparticle diameter ∅ = 3 nm					
0	202	0.0	940.11±0.87	5.3	0.0	94.7	73.1	9.23±0.01
14	188	0.5	948.00±0.83	5.3	7.2	87.5	68.1	9.23±0.01
28	174	1.0	944.71±0.56	5.3	14.2	80.5	66.0	9.26±0.01
			Nanoparticle diameter ∅ = 4 nm					
0	202	0.0	980.91±0.90	11.7	0.0	88.3	64.0	9.31±0.01
25	202	0.5	976.52±1.09	11.7	9.5	78.8	57.0	9.69±0.01
50	177	1.0	978.10±0.87	11.7	20.0	68.3	47.6	9.71±0.01
			Nanoparticle diameter ∅ = 5 nm					
0	202	0.0	1042.70±0.35	20.5	0.0	79.5	63.1	9.46±0.01
40	162	0.5	1046.80±1.32	20.5	16.8	62.7	50.7	9.49±0.01
80	122	1.0	1047.46±1.27	20.5	33.0	46.5	50.0	9.54±0.01

Tables 2.1 – 2.5 provide a summary of the potential energy parameters. Force field parameters (containing the Lennard-Jones and Coulombic terms) for a-PS have been designed to describe mixtures of a-PS with benzene[42] and ethylbenzene[43]. They are based on the OPLS-AA force field[44] for hydrocarbon systems. The same force field parameters were used for the anionic linker molecule. Harmonic dihedral angles were employed for the carbon-carbon double bonds in the linker molecule and the phenyl rings to maintain planarity. Carbon and hydrogen atoms of the phenyl ring have small partial charges to reproduce the electric quadrupole moment. Silica Lennard-Jones and Coulombic interaction parameters were obtained from a model that describes bulk crystalline silica[45]. In this force field, silicon and oxygen atoms have partial charges. Surface silica oxygen atoms were saturated with hydrogen atoms. No torsional potentials are necessary inside the spherical silica core.

Table 2.2: Nonbonded Force Field Parameters for atactic-Polystyrene and Silica[(a)]

Nonbonded interactions	$V(r_{ij}) = 4\varepsilon[(\sigma/r_{ij})^{12}-(\sigma/r_{ij})^{6}] + (q_i q_j/4\pi\varepsilon_0 r_{ij})[r_{ij}^{-1}+((\varepsilon_{RF}-1)(2\varepsilon_{RF}+1))(r_{ij}^{2}/r_{cutoff}^{3})]$		
	ε / kJ mol^{-1}	σ / nm	q / e
Polystyrene			
Csp^3	0.3519	0.3207	0.000
Hsp^3	0.3180	0.2318	0.000
Csp^2	0.2940	0.3550	-0.115
Hsp^2	0.1260	0.2420	0.115
Anionic linker molecule			
Csp^3	0.3519	0.3207	0.000
Hsp^3	0.3180	0.2318	0.000
C2sp^2	0.3180	0.3550	-0.230
C1sp^2	0.3180	0.3550	-0.115
Hsp^2	0.1260	0.2420	0.115
[(b)]Si	2.5104	0.3920	0.255
Silica nanoparticle			
[(b)]Si	2.5104	0.3920	1.020
[(b)]O	0.6368	0.3154	-0.510
[(b)]H	0.0920	0.2352	0.255

(a) Nonbonded interactions are considered between all atom pairs that are more than two bonds apart, that is, pairs whose distance is not fixed by connectivity. The first part of the nonbonded potential, $V(r_{ij})$, is a Lennard-Jones potential determined by the interaction energy ε and the contact distance σ. The second part is a Coulomb potential between two charges q_i and q_j. The vacuum permittivity is denoted as ε_0. The effect of a reaction field with a dielectric constant ε_{RF} beyond the cutoff is modeled by a Kirkwood approximation. Lennard-Jones parameters for mixed interactions are obtained from the Lorentz-Berthelot mixing rules[46]. For the Lennard-Jones part of the potential, a long-range correction to the virial is applied. The labels sp^2 and sp^3 denote carbon atoms with 3 and 4 covalent bonds, respectively. Hydrogen atoms covalently attached to sp^3 hybridized carbon atoms are also labeled with the abbreviation sp^3, i.e. Hsp^3. C1sp^2 and C2sp^2 are the first and second carbon atoms in the vinyl group that branches from the backbone of the anionic linker molecule.

(b) Silica core parameters were obtained from ref. 45. The rest of the parameters are based on the OPLS-AA force field[44].

Table 2.3: Bond Stretching Potentials[(a)]

	$V_{bond} = (k_r/2)(r - r_0)^2$	
Bonds	r_0 / nm	k_r / kJ mol^{-1} nm^{-2}
Polystyrene		
Csp^3 – Csp^3	0.153	[(b)]259780
Csp^3 – Hsp^3	0.109	[(b)]200000
Csp^2 – Csp^2	0.139	[(b)]393022
Csp^2 – Hsp^2	0.108	[(b)]200000
Csp^3 – Csp^2	0.151	[(b)]265646
Anionic linker molecule		
Csp^3 – Csp^3	0.153	[(b)]259780
Csp^3 – Hsp^3	0.109	[(b)]200000
Csp^3 – Csp^2	0.151	[(b)]265646
C1sp^2 – Hsp^2	0.108	313355
C2sp^2 – Hsp^2	0.108	313355
C1sp^2 – C2sp^2	0.134	547460
Csp^3 – Si	0.184	100000
Si – O	0.163	[(c)]323355
Silica nanoparticle		
Si – O	0.163	[(c)]323984
O – H	0.095	[(c)]533549

(a) For explanations of the symbols, see Table 2.2. Differences in the magnitude of force constants arise from the use of different empirical force fields. References:

(b) Refs. 47-49

(c) Ref. 50

Table 2.4: Bond Angle Potentials[a]

	$V(\theta) = (k_\theta/2)(\theta - \theta_0)^2$	
Bond angles	θ_0 / degrees	k_θ / kJ mol^{-1} rad^{-2}
Polystyrene		
Hsp^3 – Csp^3 – Hsp^3	109.45	306.40
Csp^3 – Csp^3 – Hsp^3	109.45	366.90
Csp^2 – Csp^3 – Csp^3	109.45	366.90
Csp^3 – Csp^3 – Csp^2	109.45	482.30
Csp^3 – Csp^2 – Csp^2	120.00	376.60
Csp^2 – Csp^2 – Csp^2	120.00	376.60
Csp^2 – Csp^2 – Hsp^2	120.00	418.80
Anionic linker molecule		
Csp^3 – C1sp^2 – Hsp^2	120.00	366.90
Csp^3 – Csp^3 – Csp^3	109.45	482.30
Csp^3 – C1sp^2 – C2sp^2	109.45	482.30
Csp^3 – Csp^3 – Hsp^3	109.45	366.90
Csp^3 – Si – Csp^3	109.45	482.00
O – Si – Csp^3	109.45	482.00
Hsp^2 – C2sp^2 – Hsp^2	120.00	[b]272.80
Si – O – H	144.00	[c]209.60
Silica nanoparticle		
Si – O – Si	144.00	[c]209.60
Si – O – H	119.52	[d]228.84
O – Si – O	109.47	[d]469.72

(a) For explanations of the symbols, see Table 2.2.

(b) Ref. 51

(c) Ref. 52

(d) Ref. 50

Table 2.5: Dihedral Angle Potentials[(a)]

	$V(\varphi) = (k_\varphi/2)[1 - \cos 3(\varphi - \varphi_0)]$, cis $\varphi = 0°$	
Dihedral angles	φ_0 / deg	k_φ / kJ mol^{-1}
Polystyrene		
$Csp^3 - Csp^3 - Csp^3 - Csp^3$	180.0	12.0
$Csp^3 - Csp^3 - Csp^3 - Hsp^3$	180.0	12.0 (terminal methyl group)
Anionic linker molecule		
$C2sp^2 - C1sp^2 - Csp^3 - Hsp^3$	180.0	12.0
$Csp^3 - Csp^3 - Csp^3 - Csp^3$	180.0	12.0
$Csp^3 - Si - O - Si$	180.0	12.0
	$V(\varphi) = (k_\varphi/2)(\varphi - \varphi_0)^2$	
Harmonic dihedral angles	φ_0 / deg	k_φ / kJ mol^{-1}
Polystyrene		
$Csp^2 - Csp^2 - Csp^2 - Csp^2$	0.0	167.4
$Csp^2 - Csp^2 - Csp^2 - Hsp^2$	0.0	167.4
$Csp^2 - Csp^2 - Csp^2 - Csp^3$	0.0	167.4
Anionic linker molecule		
$Hsp^2 - C1sp^2 - C2sp^2 - Hsp^2$	0.0	167.4

(a) For explanations of the symbols, see Table 2.2.

The molecular dynamics simulation code, YASP[37], was used at constant temperature T and pressure P, employing Berendsen's thermostat weak coupling[53] to a temperature bath of 590 K and a pressure bath of 101.3 kPa. The coupling times were 0.2 ps (T) and 0.5 ps (P), while a time step of 1 fs was employed. A cutoff radius of 1.0 nm was employed for the nonbonded interactions and a reaction-field correction for the Coulombic[37] interactions. An average effective dielectric constant of the continuum ε_{RF} of 3.7 (experimental dielectric constant: 2.4 – 2.7 for amorphous PS and 4.4 – 4.6 for amorphous silica at room temperature)[41] was assumed. An atomic Verlet neighbor list with a cutoff radius of 1.1 nm was used and updated every 15 time steps. Simulation configurations were sampled every 2000 time steps (2 ps).

A similar procedure to that used by Qian *et al.*[43] was utilized to create the initial configuration of the polystyrene chains. Fully stretched (all *trans*-) polystyrene chains were initially made by replicating two different types of monomers having different absolute configurations (stereochemistry). A uniform random number controlled the resulting stereochemistry of each monomer, R and S configuration having equal probabilities. All chains therefore had different stereochemistry. These chains were placed on a lattice inside a cubic periodic simulation cell at a density below 20 kg/m^3. Polymer chains in the centre of the box were removed to create a cavity into which the silica nanoparticle was inserted.

The silica core was constructed from a lattice of crystalline silica[54]. To construct a nanoparticle of radius *r* and a center located at point *x*, all silicon atoms lying outside this sphere were initially deleted. Secondly, all oxygen atoms that were not connected to the retained silicon atoms were also removed. This procedure guaranteed that silicon atoms that remained on the surface were saturated by oxygen atoms. All silicon atoms that had bonds with three surface oxygen atoms were deleted to reproduce the crystal structure of α-quartz in the core and in accordance with previous work of Brown *et al.*[25]. In their work dealing with silica surfaces and silica nanoparticles, they observed that a silicon atom can be connected to either one or two silanols (oxygen – hydrogen group) but never to three of them. Thirdly, all remaining surface oxygen atoms were saturated with hydrogen to satisfy their chemical bonding. Charges were chosen to ensure a sum of zero over all nanoparticle atoms. If a silicon atom had been deleted, then the three surface oxygen atoms to which it had been attached were also deleted, while the fourth oxygen was saturated with hydrogen. Fourthly, to prepare the nanoparticle for the grafting procedure, random points on the surface of a geometrical sphere with radius *r* and center *x* were selected using the algorithm of Marsaglia[55]. Finally, since the nanoparticle sphere is not perfect, special care was taken to determine where to connect the grafted chains. For this purpose, hydrogen atoms that had coordinate points located nearest to the random points were deleted and replaced by perfectly stretched a-PS chains. But, note that the grafting to the surface occurs via the anionic linker molecule. After having relaxed the isolated grafted silica nanoparticle, it was finally inserted into the earlier created cavity in the midst of the bulk polymer box.

As already mentioned, the density of the initial system configuration was less than 20 kg/m^3 since the polystyrene chains were well-separated on a lattice to allow for their full relaxation at 490 K for 1 ns. The end-to-end distance auto-correlation function decayed to zero during this time. When the system was compressed under isothermal – isobaric conditions, it took at least 3 ns to reach an equilibrated density at 490 K. Owing to the slow relaxation of polystyrene chains at 490 K, annealing simulations were carried out. The system temperature was increased from 490 K to 990 K and simulated at the high temperature for 1 ns. Following this step, it was decreased to 590 K at a rate of 100 K/ ns. Equilibration of the systems was performed for a minimum time of 47.6 ns at 590 K (for the final densities, see Table 2.1) to take advantage of the shorter relaxation time at this temperature compared to 490 K. Production runs were conducted at 590 K for a period of 6 ns while sampling the system configurations every 2000 time steps (2 ps).

2.3. Results and Discussion

2.3.1. Polymer Density around the Nanoparticle

The radial *monomer number* density of the polystyrene phase is shown in Fig. 2.1. It has been obtained by sorting the centers of mass of the repeat units into spherical bins of thickness 0.05 nm around the silica nanoparticle. Having calculated the center of mass of the silica core in every sampling time unit, the position of the nanoparticle surface was defined to be at the selected radius of the nanoparticle (1.5, 2.0, or 2.5 nm). Silica and linker atoms were not included in the density analysis. (Note that equivalent graphs of the polymer atomic *mass* densities show essentially the same behavior; but here the features are less well defined. For this reason, the mass density profiles are included in the Appendix 1 (A1) as Fig. A1.1). In all studied systems, the polymer chains form layers[23-26,56-59] around the nanoparticle, evidenced by an oscillating density profile, Fig. 2.1 (a), (c), and (e). At least 2 maxima are visible at 0.5 nm and ~ 1.0 nm from the surface. The first peak exceeds the bulk monomer and mass densities by at least a factor of 1.4; overall monomer number density profiles even show a factor of 1.9 in Fig. 2.1 (e). This behavior is similar to the density profile of a fluid that wets a surface reasonably well[60]. The density amplitudes around a bare (ungrafted) nanoparticle increase with the diameter of the nanoparticle: the height of the first peak, for example, is 8.3, 8.7, and 9.9 monomers/nm^3 for particles of 3, 4 and 5 nm, respectively. This is easily understood from geometric arguments: a flatter surface (larger particle diameter) allows the monomers less lateral leeway and has a stronger ordering effect. This will be a recurring theme in the discussions below.

The density amplitudes decrease with increasing grafting density. For all particle diameters, the polymer chains in the ungrafted systems have the largest density oscillations, followed by those surrounding a grafted particle with grafting densities of 0.5 and then 1.0 chains/nm^2. The reason here is presumably that the presence of chemically grafted chains on the surface prevents, to differing extents, free chains from adsorbing flat onto the surface and thereby forming discrete layers. Grafted chains themselves, however, contribute to discernible monomer density maxima around the nanoparticles as illustrated in Fig. 2.1 (b), (d) and (f). The tendency for grafted chains to stretch away from the surface increases with increasing grafting density and particle diameter, since the grafted chains become more constrained by their neighbours and are forced to extend more. The grafted chains also inhibit the approach of the free chains to the nanoparticle. This is shown in Fig. 2.1 (b), (d), and (f) as well as in the mass density profiles (Fig. A1.1 (b), (d), and (f)). The strength of the repulsion increases again with increasing particle diameter and grafting density. A larger particle diameter leads to a lower surface curvature and less space between the protruding grafted chains. This observation is consistent with the

prevailing notion that more curvature tends to increase the interpenetration between the free and the grafted chains[36]. Since grafted chains dominate the interfacial region, the free chains form but a reminiscence of the first peak observed near bare nanoparticles and only at the lower grafting density of 0.5 chains/nm^2. At the higher grafting density of 1.0 chains/nm^2, the concentration of monomers of free chains near the surface is too low to show any ordered structure.

There is convergence in the overall density profiles towards the bulk density value at a distance of ~2.0 nm away from the nanoparticle surface for all systems (Fig. 2.1 (a), (c) and (e)). This distance happens to be close to twice the radius of gyration for the studied polymers (free chains). In view of the short chain lengths, it is not clear whether there is a systematic reason or whether this is mere coincidence. However, it is interesting that this observation seems to be reproduced in experimental[61] work that employs longer chains and larger nanoparticles.

Fig. 2.1 (b), (d) and (f) shows that the decomposed monomer density profiles take longer to converge than the overall density. There is a small fraction of grafted monomers still found at distances of about 2.5 nm from the surface. This effect is enhanced with increasing diameter and grafting density. Simultaneously, monomers of free polymer chains can be found within 0.5 nm away from the surface in all studied systems, i.e. well inside the grafted brushes. This observation is evidence that the free polymer chains are able to penetrate and mix with the grafted polymer chains. Furthermore, the shape of the grafted polymer chains density profiles shown in Fig. 2.1 (b), (d), and (f) is similar to that of previous work reported by Borukhov and Leibler[19] of wet brushes, in which grafted chains mix well with free chains. Compared to the idealized step function[62,63] or parabolic[64] approximation for the polymer brush density, the present MD results are more realistic and similar to experimental observations. The stretched-out conformations of grafted chains in this MD simulation study for a grafting density of 1.0 chains/nm^2 is similar to chains appearing in the 'concentrated' regime that has been described in the experimental work of Dukes *et al.*[65]. On the other hand, the collapsing of chains onto the surface under lower grafting density conditions (0.5 chains/nm^2) resembles conformations in what they call the 'semi-dilute' regime.

Decreasing surface curvature and increasing grafting density both have the effect of extending the reach of the grafted chains. Consequently, the ability of free chains to approach the surface is reduced. A good measure to describe the extension of the interphase of different systems is the crossover distance, r_{co}, i.e., the point beyond which the density contribution of the free chains is larger than that of the grafted chains (Table 2.6). It clearly shows that the effect of surface curvature and grafting density: r_{co} shifts away from the nanoparticle surface by at least 0.7 nm when doubling the grafting density. On the other hand, it shifts by at least 0.1 – 0.3 nm when reducing the nanoparticle surface

curvature. Again, a recurring observation is that high nanoparticle surface curvature is associated with increased interpenetration between grafted and free chains. This effect is vital in creating well dispersed grafted nanoparticles in a polymeric matrix. A caveat: while the crossover distance is one measure of the interphase width, the interphase terminates only when there are no more grafted monomers. This happens at a distance of about 1.9-3.6 r_{co} (Fig. 2.1. (b), (d), and (f)).

Table 2.6: Density crossover distance, r_{co} (nm). Below the indicated distances from the nanoparticle surface, the monomer density of the grafted chains exceeds that of the free chains. Above r_{co}, the monomer density contribution of the free chains is larger. The magnitude of the error (±0.025) is equal to half the bin width used in the density calculation.

Nanoparticle diameter ∅ (nm)	Grafted density (0.5 chains/nm^2)	Grafted density (1.0 chains/nm^2)
	r_{co} [nm]	r_{co} [nm]
3	0.825±0.025	1.575±0.025
4	1.125±0.025	1.775±0.025
5	1.225±0.025	1.975±0.025

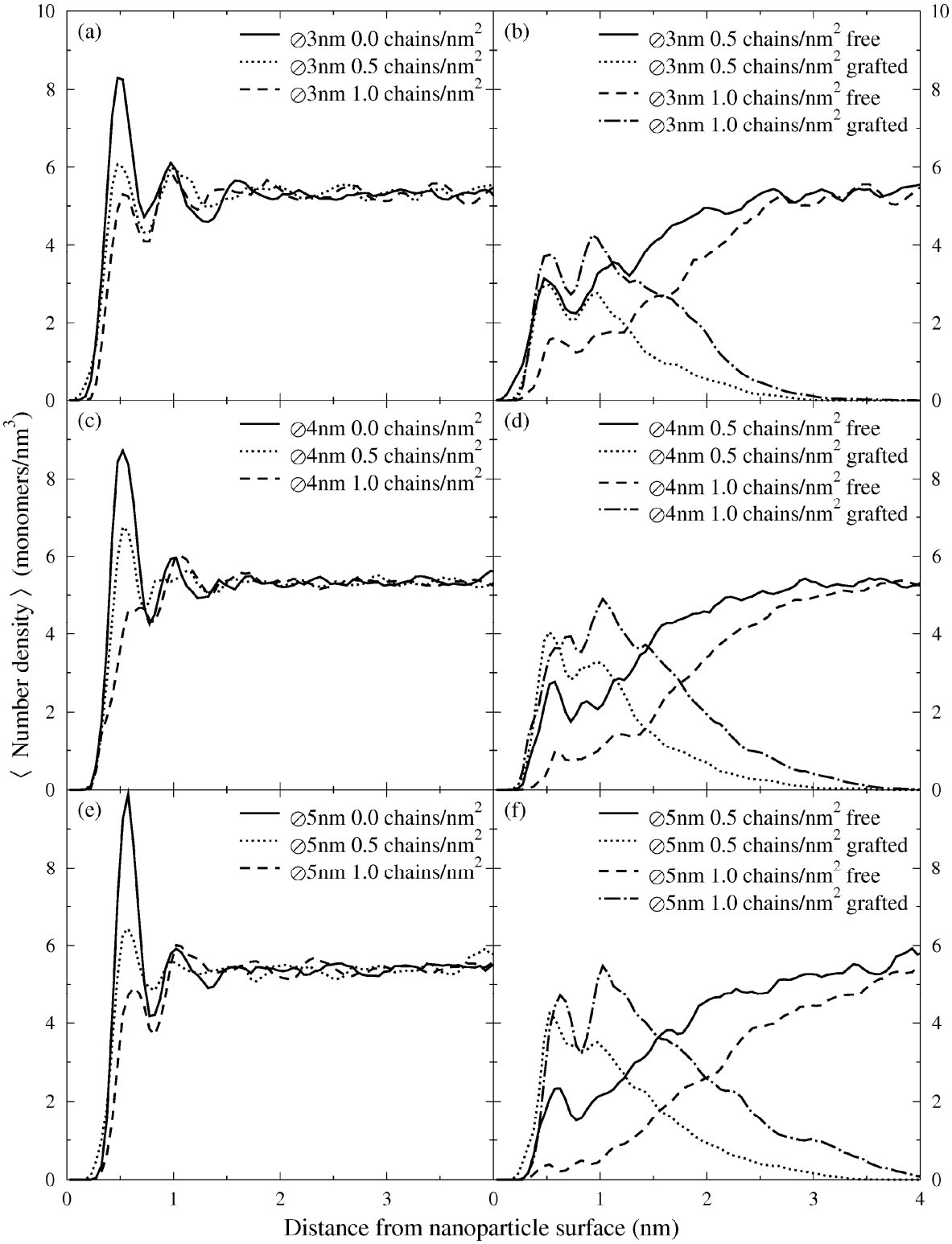

Figure 2.1. Polystyrene monomer number density as a function of the radial distance from the silica nanoparticle. Panels (a), (c), and (e) summarize the overall monomer number density profiles (excluding the linker molecule) for the bare (solid line), medium (dotted line) and high grafted particle (dashed line) systems as a function of the nanoparticle diameter. Panels (b), (d), and (f) show the separated monomer number density profiles of grafted and free chains. The simulations have been performed at T = 590 K and P = 101.3 kPa.

2.3.2. Chain Extension and Orientation

It is interesting to find out if and how the global chain conformation is affected by the distance of the chain (centre-of-mass) from the nanoparticle surface. Fig. 2.2 shows the variation of the squared radius of gyration $\langle R_g^2 \rangle$ of free chains around a bare nanoparticle of different diameters. The profiles are rather independent of the nanoparticle curvature. Polymer chains which are very close to the surface (< 0.5 nm) tend to stretch as also observed by Starr *et al.*[57] Their $\langle R_g^2 \rangle$ is by a factor of about 1.1 – 1.4 larger than the bulk value of ~1.0 nm^2 (labeled by the horizontal line). The reference value of 0.986±0.060 nm^2 was calculated from a simulation of only bulk a-PS. This region is followed by a shallow minimum (~0.5 – ~1.0 nm) in all curves. In consideration of the error bars, it is difficult to say if it is a real feature or an artifact of bad statistics. Beyond 1.0 – 1.3 nm, the radius of gyration approaches bulk behavior. Hence, the interphase thickness as measured by peculiarities of the chain extension is of this order of magnitude. The presence of the surface also influences the orientation of the chains. Fig. 2.3 shows the distance dependence of the angle between the longest axis of the squared radius of gyration tensor and the surface normal of the bare nanoparticle. The observation that the free polymer chains generally prefer to align tangentially to the ungrafted surface is in agreement with conclusions from other researchers[23,66]. In their coarse grained model using Monte Carlo simulations, Vogiatzis *et al.*[23] studied the orientational angles of local chain segments. They also concluded that chain segments in the vicinity of the nanoparticle surface were structured and oriented tangentially to the interface.

The orientational angle θ is schematically shown for the case of a grafted nanoparticle in Fig. 4 and the same definition is applied to the free chains as well. These simulations confirm that the stretching of chains very close to the surface (< 0.5 nm) implies a chain orientation that is tangential to the surface. This is predictable, as chains have to be compressed flat against the surface if they are to approach it closely. This orientational preference decreases steadily to approach the expected bulk average[67-69] of 57.3° at 1.0–1.2 nm. The orientational order, thus, persists to a similar distance from the surface as the chain extension when measured by the mean-squared radius of gyration (see above).

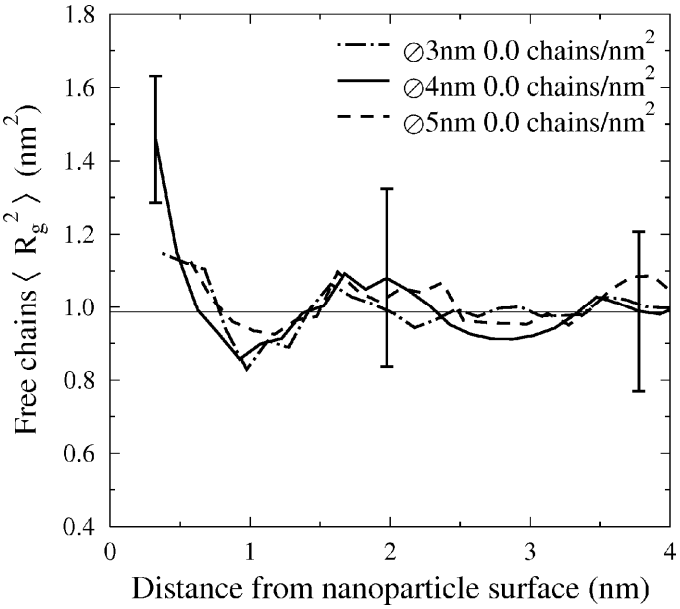

Figure 2.2. Squared radius of gyration of free polymer chains in the vicinity of a bare nanoparticle. The distance measures the separation of the center of mass of the respective chain from the nanoparticle surface. The horizontal line indicates the radius of gyration of free chains (~1.0 nm^2) in the bulk determined for a polymer system without nanoparticles. For clarity of the diagram, representative error bars are shown (here and in the figures to follow).

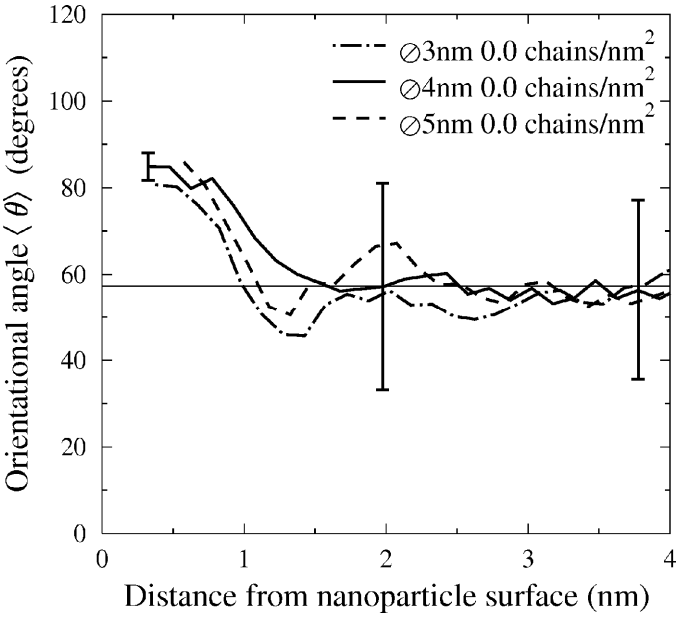

Figure 2.3. Chain orientation as a function of the chain (center-of-mass) distance from the nanoparticle surface for ungrafted systems. The considered nanoparticle diameters were 3, 4, and 5 nm. The orientation angle is calculated between the longest axis of the squared radius of gyration tensor (eigenvector corresponding to its largest eigenvalue, disregarding the sign) and the surface normal. The horizontal line at 57.3 degrees marks the average orientational angle for a random distribution.

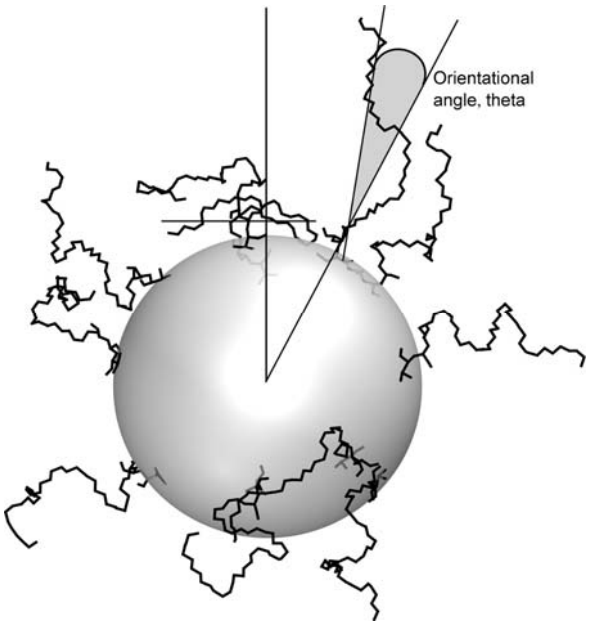

Figure 2.4. Schematic representation of the orientational angle θ between the longest axis of the squared radius of gyration tensor and the surface normal.

The behavior of free chains does not change qualitatively, when the system is switched from a bare to a grafted nanoparticle. Figs. 5 and 6 present the squared radius of gyration and orientational angles for systems with a nanoparticle of 4 nm diameter and different grafting densities as an example (the full set of curves is found in Figs. A1.2 – A1.9 in the Appendix 1). Taking into consideration the error bars and looking at all distributions (Figs. A1.2 – A1.5 of the Appendix 1), one finds that the free chains have a bulk-like $\langle R_g^2 \rangle$, regardless of their separation from the nanoparticle surface. They do not stretch significantly. However, combining Fig. 2.5 (a) and Fig. 2.6 (a) showing data for ρ_{gr} = 0.5 chains/nm^2, we observe that the free chains still orient tangentially to the surface in spite of the absence of stretching. This implies that tangential orientation to the surface normal vector is not restricted to fully stretched-out chains, but that it can also be brought about, for example, by flat chains having pancake shapes. In contrast, free chains nearest to the nanoparticle surface in the high grafting density systems mostly have random orientational angles (Fig. A1.7 – A1.9 (c)). These observations are consistent with a picture of the nanoparticle plus its corona of grafted chains acting as an orienter for the free chains. Grafted chains in the lower ρ_{gr} range intermingle more with the matrix chains (so the overall density converges quickly, cf. Sect 3.1). The free chains close to the surface also orient tangentially. This influence of grafted chains diminishes beyond a separation of 1.0 nm from the surface where the random orientation of free chains begins. At larger ρ_{gr}, free chains have a reduced ability to penetrate and the majority of them lie in the fringes of the grafted chains extension area where they are randomly oriented. However, in some cases, the free chains that have penetrated the

highly dense grafted chains regime are also tangentially oriented and in this case the grafted chains behave as orienters (Fig A1.7 and A1.9 (c)).

The *grafted* chains, on the other hand, show an expected behavior in their extension (Fig. 6). If their centers of mass are close to the surface, they are tangentially oriented. For quite a narrow intermediate region, a random orientation (θ = 57.3°) is observed. At larger separations from the nanoparticle surface, the orientational angle of grafted chains is less than 57.3° which implies that they are stretched and asymptotically align with the surface normal. Despite the tangential orientation, grafted chains close to the surface are not always stretched but rather show a bulk-like $\langle R_g^2 \rangle$ for a small ρ_{gr}. However, for grafted chains that have their center of mass close to the surface, their known tendency to stretch is only observed for the larger nanoparticles with reduced curvature (Fig. A1.4 and A1.5 (d)). On the other hand, mass centers of grafted chains that are located furthest away from the nanoparticle surface correspond to grafted chains that are both stretched and oriented perpendicular to the surface. These chains have a large squared radius of gyration and a small orientation angle with the surface normal. This is exemplified in Figs. 5 and 6 and confirmed for the other systems in the Appendix 1 (Figs. A1.2 – A1.9).

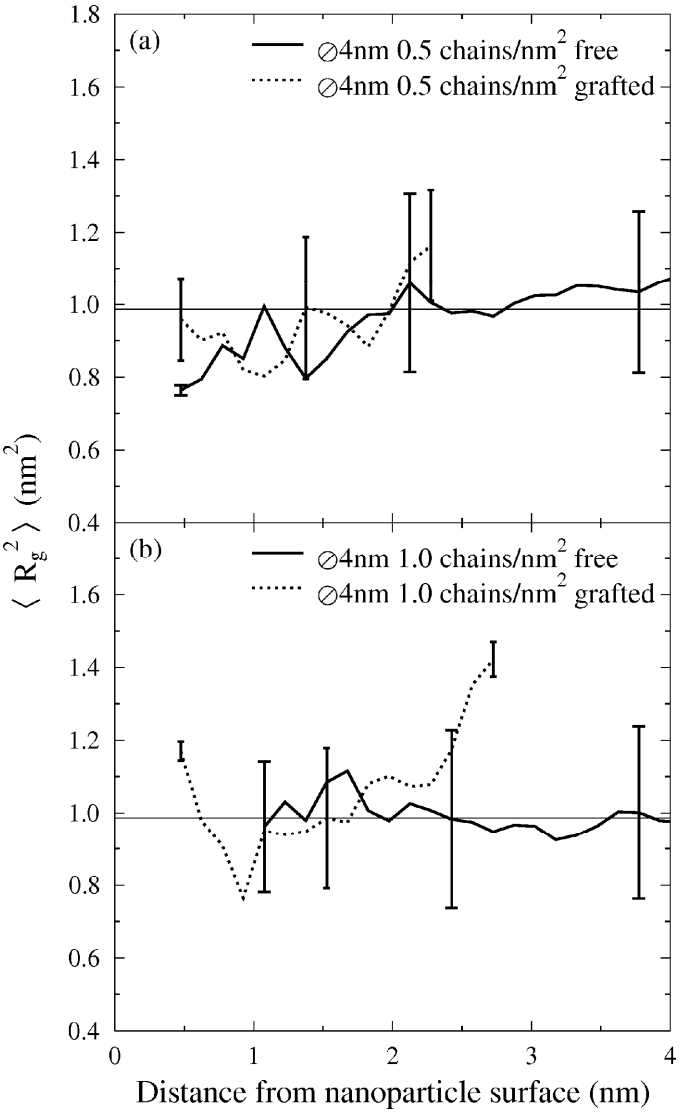

Figure 2.5. Squared radius of gyration of grafted and free chains around a grafted nanoparticle of diameter 4 nm as a function of the distance of their centers of mass from the nanoparticle surface and the grafting density. The horizontal line indicates the squared radius of gyration of free chains (~1.0 nm^2) in the bulk.

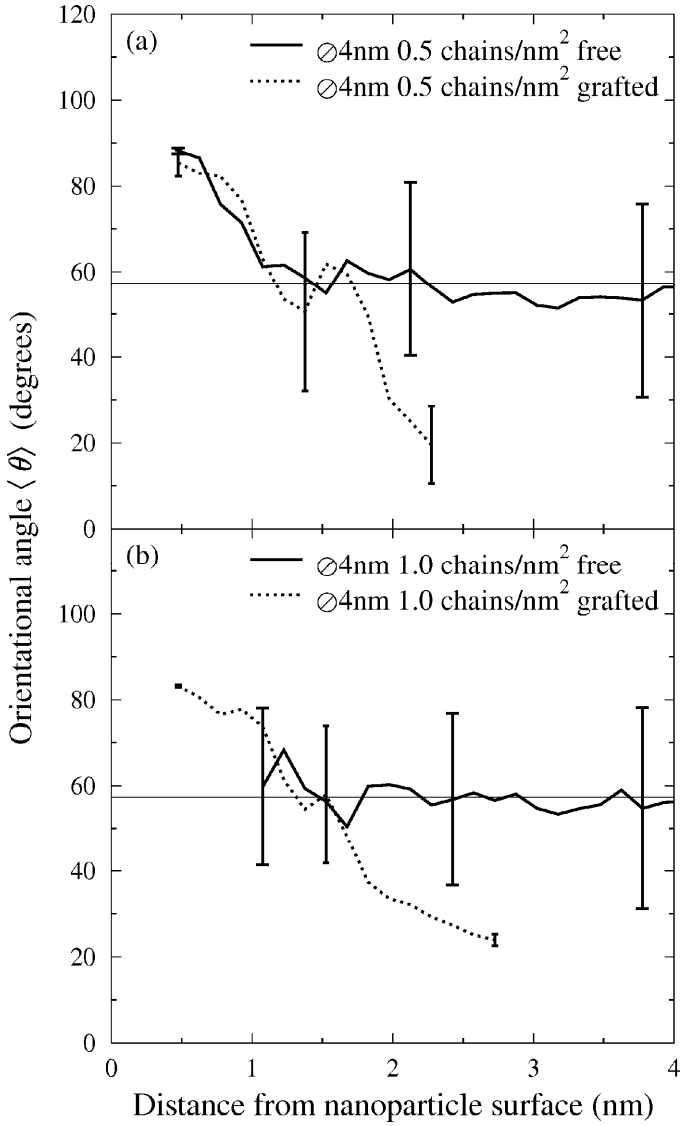

Figure 2.6. Chain orientational angles as a function of the chain (center-of-mass) separation from the surface for systems containing a nanoparticle of 4 nm-diameter and grafted densities 0.5 and 1.0 chains/nm^2. The orientational angle is calculated between the longest axis of the squared radius of gyration tensor (eigenvalue corresponding to its largest eigenvalue, disregarding the sign) and the surface normal. The horizontal line at 57.3 degrees marks the average orientational angle for a random distribution.

A similar orientational behavior can be observed on a more local scale. We have also calculated the orientational angles of chain segments of 1 and 3 monomers. Segment orientations were defined as the unit vector between the backbone carbons carrying the phenyl groups of two adjacent repeat units *i* and *i*+1, as well as between repeat unit *i* and *i*+3, respectively. The orientational angles are defined, as before, as the angle between this intermonomer vector, disregarding its sign, and the surface normal. The distance of a segment from the surface is calculated from the position of the midpoint of the respective intermonomer vector. Similar orientational behavior of both grafted and free chains is observed for both segment lengths. This is shown in Fig. 7 for the nanoparticle with a diameter of 4

nm while the complete data can be found in the Appendix 1 (Fig. A1.10 – A1.17). At very short distances from the surface (0.8 to 1.0 nm), there is – on average – a small preference for a tangential orientation of the segments. Beyond this distance, the segment orientation is random. Note however, that the error bars are large (30 degrees). We can conclude that the orienting effect of the surface on short stretches of the polymer is small and limited to the immediate neighbourhood of the surface. Thus, no longer-reaching interphase manifests itself in *this* property.

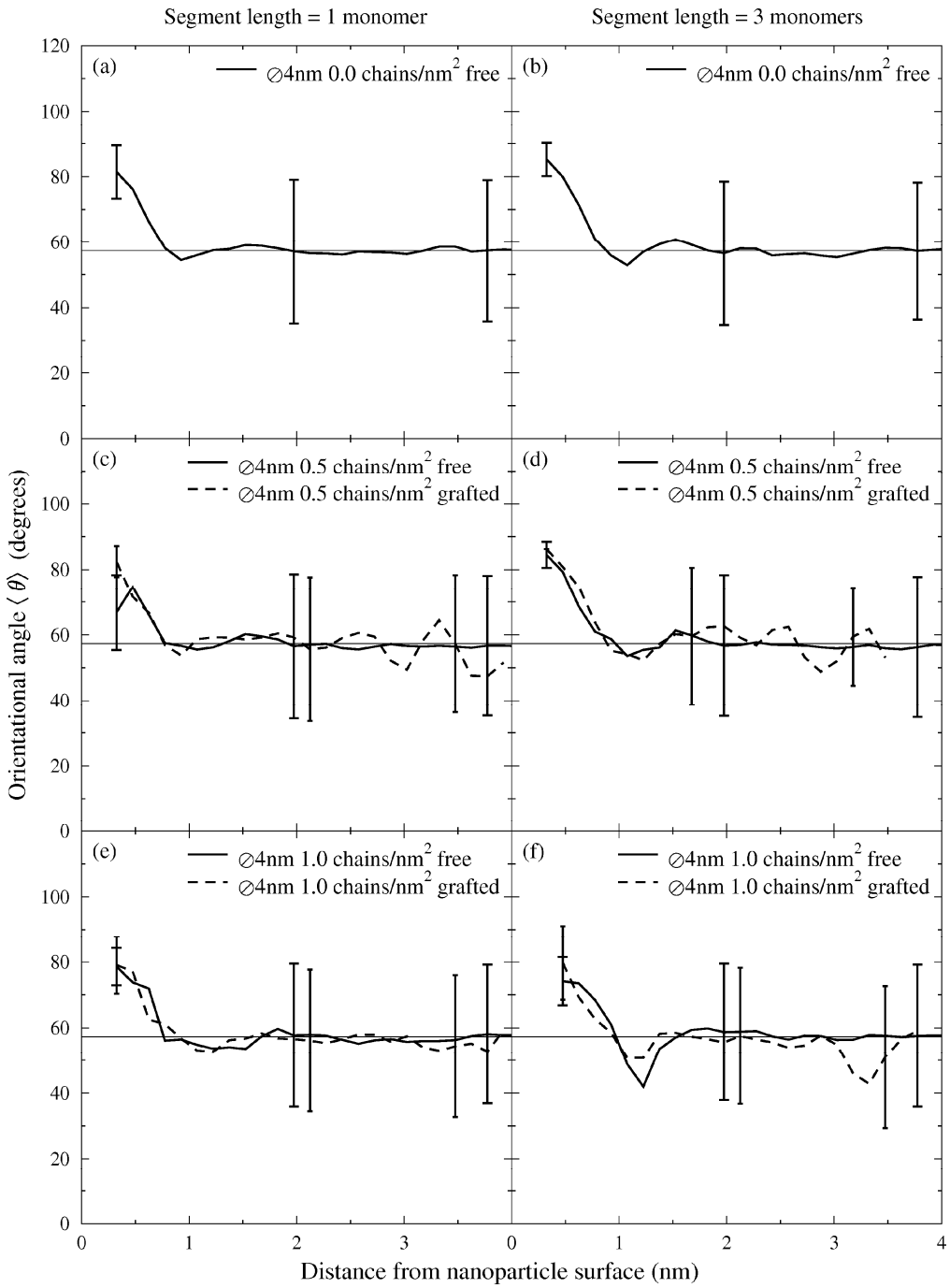

Figure 2.7. Orientation of chain segments of length 1 (left panels (a), (c), and (e)) and length 3 (right panels (b), (d), and (f)) for a bare nanoparticle (top row of panels (a) and (b)), for a nanoparticle of a grafted density of 0.5 chains/nm^2 (center row of panels (c) and (d)) and 1.0 chains/nm^2 (bottom row of panels (e) and (f).

2.4. Summary and Conclusions

The structure of atactic polystyrene in the immediate neighbourhood of a spherical silica nanoparticle with a diameter of 3, 4, and 5 nm has been investigated by MD simulations at the atomistic level. Particular attention has been paid to the influence of the size of the nanoparticle or, equivalently, the curvature of its surface, as well as its grafting state. Ungrafted (bare) nanoparticles as well as a particles grafted with polystyrene chains at grafting densities of 0.5 and 1.0 chains per nm^2 surface area were studied. Grafting densities in this range are frequently employed in experimental work[61] to facilitate the dispersion of nanoparticles in the polymer.

The nanoparticle has a structuring influence on the polymer in its vicinity. This is easily visible in all quantities studied. Studied nanoparticles of all diameters and surface decorations induce: (i) layering of monomers, visible in oscillations of the radial monomer number density, (ii) chain extension, visible in an increase of the squared radius of gyration of the chains, and (iii) chain orientation, visible in the orientation of the longest axis of the gyration tensor being tangential to the surface. The quantitative extent of structural modifications of the polymer and their distance range however, depends on the curvature and grafting state of the nanoparticle. A flatter surface (larger nanoparticle diameter) induces more structure than a more curved one. The reason is geometric: the volume above a circular surface area of a given size is a truncated cone. A flatter surface has a narrower opening angle of the cone. Therefore, if the surface is flat, a polymer molecule adsorbed or grafted to the surface has less space and it interferes more with neighbouring molecules.

A similar argument holds for the different grafting densities. Grafted chains at low grafting density have enough space to make use of their conformational degrees of freedom. This means that they have conformations that are similar to those of bulk polymers and that they leave enough space on the surface for free chains (matrix chains) to approach the surface, too. At a higher grafting density, grafted chains interfere with their neighbours. This has the effect of reducing the available effective volume for each individual grafted chain. They need to stretch away from the surface, and they exclude the free chains. The effects of curvature and grafting density are additive. Still, it must be noted that different structural properties of the polymer are affected to a different degree. All conformational and orientational properties approach their normal, bulk-like behavior within 0.5 – 1.0 nm from the surface and are nearly independent of the nanoparticle size and decoration. The density oscillations reach about twice as far and are more influenced by the nature of the nanoparticle. The farthest reaching structural element is the concentration of grafted chains. Its influence depends

strongly on the nanoparticle size and decoration. Some grafted monomers can be found at 2.5 nm for the most favourable case, in which there is significant interpenetration of grafted and free chains.

At the grafting densities studied here, there are still some free polymers, which intermingle with the grafted chains so that the nanoparticle and polymer are compatibilised. However, there is also evidence for some of the grafted chains to collapse onto the nanoparticle, rather than to entangle with free chains. This is shown in the simulation snapshot in Fig. 4 and by chain orientational angles that are almost perpendicular to the surface normal vector in Fig. 6. A possible consequence is that the mechanical coupling between silica nanoparticles and the surrounding polystyrene is less strong than expected. This is indeed found in experimental investigations[70].

Acknowledgment: Financial support from the European Union through the project "NanoModel" under grant number 211778 is gratefully acknowledged. We would like to acknowledge the SPP1369 for providing the computer resources. Helpful technical discussions in developing the analysis programs with Frédéric Leroy and Gustavo Rondina are especially appreciated. We are also thankful for insightful discussions with Kurt Binder, and last but not least, collaborators within the NanoModel project.

2.5. References

(1) Kraus, G. *Reinforcement of elastomers*; NY: Interscience Publishers: New York, 1965.
(2) Kraus, G. *Angew. Makromol. Chem.* **1977**, *60*, 215-248.
(3) Koenig, J. L. *Accounts Chem. Res.* **1999**, *32*, 1-8.
(4) Zhang, Y.; Ge, S.; Tang, B.; Koga, T.; Rafailovich, M. H.; Sokolov, J. C.; Peiffer, D. G.; Li, Z.; Dias, A. J.; McElrath, K. O.; Lin, M. Y.; Satija, S. K.; Urquhart, S. G.; Ade, H.; Nguyen, D. *Macromolecules* **2001**, *34*, 7056-7065.
(5) Bansal, A.; Yang, H.; Benicewicz, B.; Kumar, S. K.; Schadler, L. S. *J. Polym. Sci. Pol. Phys.* **2006**, *44*, 2944-2950.
(6) Bansal, A.; Yang, H.; Li, C.; Cho, K.; Benicewicz, B.; Kumar, S. K.; Schadler, L. S. *Nature Mater.* **2005**, *4*, 693-698.
(7) Akcora, P.; Liu, H.; Kumar, S. K.; Moll, J.; Li, Y.; Benicewicz, B. C.; Schadler, L. S.; Acehan, D.; Panagiotopoulos, A. Z.; Pryamitsyn, V.; Ganesan, V.; Ilavsky, J.; Thiyagarajan, P.; Colby, R. H.; Douglas, J. F. *Nature Mater.* **2009**, *8*, 354-359.
(8) Uyama, Y.; Kato, K.; Ikada, Y. *Adv. Polym. Sci.* **1998**, *137*, 1-39.
(9) Goddard, E.; Vincent, B.; eds. *ACS Sym. Ser.* **1984**, *240*.
(10) Mackay, M. E.; Tuteja, A.; Duxbury, P. M.; Hawker, C. J.; Van Horn, B.; Guan, Z.; Chen, G.; Krishnan, R. S. *Science* **2006**, *311*, 1740-1743.
(11) Raviv, U.; Giasson, S.; Kampf, N.; Gohy, J.-F.; Jérôme, R.; Klein, J. *Nature* **2003**, *425*, 163-165.
(12) Klein, J. *Science* **2009**, *323*, 47-48.
(13) Mackay, M. E.; Dao, T. T.; Tuteja, A.; Ho, D. L.; Van Horn, B.; Kim, H.-C.; Hawker, C. J. *Nature Mater.* **2003**, *2*, 762-766.
(14) Valentin, J. L.; Mora-Barrantes, I.; Carretero-González, J.; López-Manchado, M. A.; Long, D. R.; Saalwächter, K. *Macromolecules* **2010**, *43*, 334-346.
(15) Tsagaropoulos, G.; Eisenburg, A. *Macromolecules* **1995**, *28*, 396-398.
(16) Chevigny, C.; Gigmes, D.; Bertin, D.; Jestin, J.; Boué, F. *Soft Matter* **2009**, *5*, 3741-3753.
(17) Chevigny, C.; Jestin, J.; Gigmes, D.; Schweins, R.; Di-Cola, E.; Dalmas, F.; Bertin, D.; Boué, F. *Macromolecules* **2010**, *43*, 4833-4837.
(18) Kumar, S. K.; Krishnamoorti, R. *Annu. Rev. Chem. Biomol. Eng.* **2010**, *1*, 37-58.
(19) Borukhov, I.; Leibler, L. *Macromolecules* **2002**, *35*, 5171-5182.
(20) Frischknecht, A. L.; McGarrity, E. S.; Mackay, M. E. *J. Chem. Phys.* **2010**, *132*, 204901-204907.
(21) Hooper, J. B.; Schweizer, K. S. *Macromolecules* **2005**, *38*, 8858-8869.
(22) Hooper, J. B.; Schweizer, K. S. *Macromolecules* **2006**, *39*, 5133-5142.
(23) Vogiatzis, G.; Voyiatzis, E.; Theodorou, D. N. *Eur. Polym. J.* **2010**, *doi: DOI: 10.1016/j.eurpolymj.2010.09.017*.
(24) Barbier, D.; Brown, D.; Grillet, A.-C.; Neyertz, S. *Macromolecules* **2004**, *37*, 4695-4710.
(25) Brown, D.; Mélé, P.; Marceau, S.; Albérola, N. D. *Macromolecules* **2003**, *36*, 1395-1406.
(26) Borodin, O.; Smith, G. D.; Bandyopadhyaya, R.; Byutner, O. *Macromolecules* **2003**, *36*, 7873-7883.
(27) Eslami, H.; Müller-Plathe, F. *J. Phys. Chem. B* **2009**, *113*, 5568-5581.
(28) Alaghemandi, M.; Böhm, M. C.; Illya, G.; Müller-Plathe, F. p in preparation.
(29) Grest, G. S. *J. Chem. Phys.* **1996**, *105*, 5532-5542.
(30) Lo Verso, F.; Egorov, S. A.; Milchev, A.; Binder, K. *arXiv:1005.0235v1 [cond-mat.soft]* **2010**.
(31) Kalb, J.; Dukes, D.; Kumar, S. K.; Hoy, R. S.; Grest, G. S. *arXiv:1008.1022v1 [cond-mat.soft]* **2010**.
(32) Klos, J.; Pakula, T. *J. Chem. Phys.* **2003**, *118*, 1507-1514.
(33) Klos, J.; Pakula, T. *J. Chem. Phys.* **2003**, *118*, 7682-7690.
(34) Klos, J.; Pakula, T. *Macromolecules* **2004**, *37*, 8145-8151.
(35) Cordeiro, R. M.; Zschunke, F.; Müller-Plathe, F. *Macromolecules* **2010**, *43*, 1583-1591.

(36) Trombly, D. M.; Ganesan, V. *J. Chem. Phys.* **2010**, *133*, 154904-154911.
(37) Müller-Plathe, F. *Comput. Phys. Commun.* **1993**, *78*, 77-94.
(38) Vaia, R. A.; Maguire, J. F. *Chem. Mater.* **2007**, *19*, 2736-2751.
(39) Hübner, E.; Allgaier, J.; Meyer, M.; Stellbrink, J.; Pyckhout-Hintzen, W.; Richter, D. *Macromolecules* **2010**, *43*, 856-867.
(40) Höcker, H.; Blake, G. J.; Flory, P. J. *Trans. Faraday Soc.* **1971**, *67*, 2251-2257.
(41) Lide, D. R. *CRC Handbook of Chemistry and Physics*, 74th ed.; CRC Press: Boca Raton, Florida, 1993.
(42) Müller-Plathe, F. *Macromolecules* **1996**, *29*, 4782-4791.
(43) Qian, H.-J.; Carbone, P.; Chen, X.; Karimi-Varzaneh, H. A.; Liew, C. C.; Müller-Plathe, F. *Macromolecules* **2008**, *41*, 9919-9929.
(44) Jorgensen, W. L.; Maxwell, D. S.; Tirado-Rives, J. *J. Am. Chem. Soc.* **1996**, *118*, 11225-11236.
(45) Lopes, P. E. M.; Murashov, V.; Tazi, M.; Demchuk, E.; MacKerell, J., Alexander D. *J. Phys. Chem. B* **2006**, *110*, 2782-2792.
(46) Allen, M. P.; Tildesley, D. J. *Computer Smulations of Liquids*; Clarendon, Oxford, 1987.
(47) Algaer, E.; Alaghemandi, M.; Böhm, M. C.; Müller-Plathe, F. *J. Phys. Chem. A* **2009**, *113*, 11487-11494.
(48) Lussetti, E.; Terao, T.; Müller-Plathe, F. *J. Phys. Chem. B* **2007**, *111*, 11516-11523.
(49) Valavala, P. K.; Odegard, G. M. *Rev. Adv. Mater. Sci.* **2005**, *9*, 34-44.
(50) Ermoshin, V.; Smirnov, K. S.; Bougeard, D. *J. Mol. Struct.* **1997**, *410-411*, 371-374.
(51) Blom, C. E.; Altona, C.; Oskam, A. *Mol. Phys.* **1977**, *34*, 177-192.
(52) Newton, M. D. *Phys. Chem. Miner.* **1980**, *6*, 305-312.
(53) Berendsen, H. J. C.; Postma, J. P. M.; van Gunsteren, W. F.; DiNola, A.; Haak, J. R. *J. Chem. Phys.* **1984**, *81*, 3684-3690.
(54) Wells, A. F. *Structural Inorganic Chemistry*; Oxford Science Publications, 1984.
(55) Marsaglia, G. *Ann. Math. Stat.* **1972**, *43*, 645-646.
(56) Allegra, G.; Raos, G.; Vacatello, M. *Prog. Polym. Sci.* **2008**, *33*, 683-731.
(57) Starr, F. W.; Schrøder, T. B.; Glotzer, S. C. *Macromolecules* **2002**, *35*, 4481-4492.
(58) Vacatello, M. *Macromolecules* **2001**, *34*, 1946-1952.
(59) Vacatello, M. *Macromol. Theor. Simul.* **2002**, *11*, 757-765.
(60) Bucior, K.; Yelash, L.; Binder, K. *Phys. Rev. E* **2009**, *79*, 031604-031616.
(61) Kim, C. J.; Spehr, T.; Stühn, B., 2010; p personal communication.
(62) Alexander, S. *J. Phys. (France)* **1977**, *38*, 977-981.
(63) de Gennes, P. G. *Macromolecules* **1980**, *13*, 1069-1075.
(64) Milner, S. T.; Witten, T. A.; Cates, M. E. *Macromolecules* **1988**, *21*, 2610-2619.
(65) Dukes, D.; Li, Y.; Lewis, S.; Benicewicz, B. C.; Schadler, L. S.; Kumar, S. K. *Macromolecules* **2010**, *43*, 1564-1570.
(66) Brown, D.; Marcadon, V.; Mélé, P.; Albérola, N. D. *Macromolecules* **2008**, *41*, 1499-1511.
(67) Morikawa, E.; Saile, V.; Okudaira, K. K.; Azuma, Y.; Meguro, K.; Harada, Y.; Seki, K.; Hasegawa, S.; Ueno, N. *J. Chem. Phys.* **2000**, *112*, 10476-10481.
(68) Bergström, J. S.; Boyce, M. C. *Macromolecules* **2001**, *34*, 614-626.
(69) Palmer, J. S.; Boyce, M. C. *Acta Biomater.* **2008**, *4*, 597-612.
(70) Harton, S. E.; Kumar, S. K.; Yang, H.; Koga, T.; Hicks, K.; Lee, H.; Mijovic, J.; Liu, M.; Vallery, R. S.; Gidley, D. W. *Macromolecules* **2010**, *43*, 3415-3421.

3. Interface and Interphase Dynamics of Polystyrene Chains near Grafted and Ungrafted Silica Nanoparticles

ABSTRACT: The chain and segmental dynamics of free and grafted 20-monomer atactic polystyrene chains surrounding a silica nanoparticle have been investigated employing atomistic molecular dynamics simulations. The effect of the nanoparticle curvature and grafting density on the mean-square displacement of free polystyrene chains and also on the mean relaxation time of various intramolecular vectors was investigated as a function of separation from the surface. Confinement, reduced surface curvature, and densification resulted in a reduction of the mean-square displacement and an increase in the mean relaxation time of the C_α-H bond vector and chain end-to-end vector in the vicinity of the surface. Therefore, the presence of a surface has a significant influence on the dynamics of the surrounding polymer chains especially the ones in the interfacial region. Depending on the property investigated, the thickness of the interphase, i.e. the distance beyond which the polymer has bulk behavior, varies between 1 and 3 nm, corresponding to 1-3 radii of gyration of the bulk polymer.

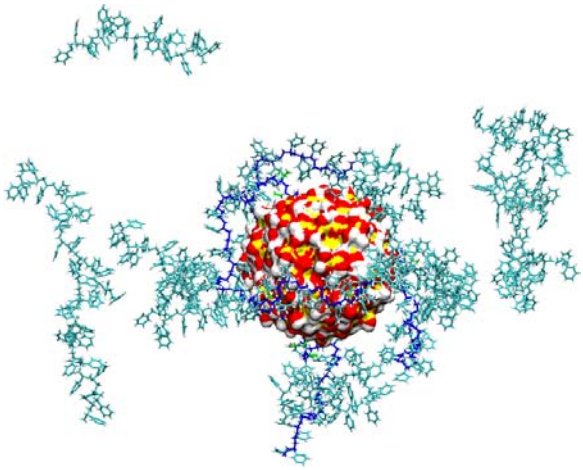

3.1. Introduction

The possibility of achieving significant enhancements in material properties (mechanical, electrical, optical, thermal, etc.) by adding minute amounts of nanoparticles as filler particles (rods, platelets, spheres, icosahedra, sheets) has spurred research in polymer nanocomposites[1-24]. At the nanometer scale, the size of the filler particles is often of the same order of magnitude as that of the polymer coil resulting in a drastic increase in the nanoparticle-polymer interfacial surface area. Also at this small scale, the filler particle surface curvature and filler-polymer interactions play significant roles in influencing the structural arrangement, mobility, and overall relaxation of the polymer chains[17,25,26].

Similar to our previous work[20] on static and structural properties of nanocomposites formed by spherical nanoparticles and atactic polystyrene (a-PS), we have employed atomistic molecular dynamics (MD) simulations to extend our research to dynamic quantities. For these MD simulations, we have chosen both a-PS grafted and ungrafted silica nanoparticles embedded into an a-PS matrix. Furthermore, we have performed simulations of the pure polymer bulk. In our earlier work[20], we showed that the nanoparticle influences the polymer structural properties. We have commented on density enhancement (layering) in the vicinity of the surface, parallel orientation of chains and their segments along the nanoparticle surface, and polymer swelling as shown by an increased radius of gyration. We now present an analysis of the nanoparticle effect on the polymer dynamics as a function of the distance from the particle surface. We have analyzed the effect on the polymer chains' translation in different shells surrounding the nanoparticle as well as the reorientation dynamics of several intramolecular vectors pertaining to different chain segments. This was compared to the molecular dynamics simulations and experiments of Harmandaris and co-workers[27] who studied the temperature and pressure dependence of the bulk dynamics of a-PS. We have also determined the temperature and pressure effects on the polymer chain dynamics in different regions surrounding the spherical nanoparticles.

Since the properties of polymer nanocomposites are a direct result of the polymer behavior at the polymer-solid interface, the study of the polymer dynamics at interfaces or surfaces has been and continues to be in the focus of intensive research by both experimental[12,28-34] and computational[10,24,34-43] methods. Understanding of the interface effect on the polymer may contribute to the design of high-tech applications that involve, for example, coating, lubrication, wetting, and adhesion.[44] The nature of the surface (smooth or rough)[45], the kind of surface-polymer interactions (repulsive or attractive, physisorption or chemisorption)[13,24-26], the interaction between grafted (polymer brush) and melt chains[33], as well as the size of the interfacial surface area and curvature[46] have a significant influence on the polymer dynamics. Simultaneously, the modified dynamics leads to changes of polymer diffusion, viscosity, and glass transition temperature. Many studies have been carried out to determine whether the polymer dynamics is enhanced in systems containing thin polymer films[14,28-30] as well as nanoparticles[2,14,25,32,47,48]. Bansal et al.[6] and Sen et al.[8] have presented arguments that treat polymer films and nanocomposites as equivalent systems as far as interfaces are concerned.

We will now briefly review some of the experimental findings on the dynamics of polymers at interfaces and highlight some points of debate to which we make a computational contribution in this work. Firstly, Mortezaei and co-workers[25,46,49] have reported that the mobility of polystyrene chains close to hydrophilic ('untreated') silica particles is slowed. Under these conditions, the interfacial polymer layer has been immobilized by adhesion. On the contrary, 'treated' hydrophobic silica

particles (i.e. grafted with vinyltriethoxysilane as a surface modifier) had a weaker adhesion resulting in a decrease of the volume fraction of the immobilized interfacial polymer. They also have reported that any increase of the interfacial surface area enhanced the fraction of slowed-down free polymer chains. Similarly, Whittington et al.[48] also observed slower polymer dynamics in a nanocomposite that consisted of silica nanoparticles in polystyrene relative to bulk polystyrene. They attributed the observed enhanced thermal stability in polymer nanocomposites to the reduced mobility of surface polymer chains. Similarly, Robertson and Rackaitis[50] have reported that carbon black filler particles slow the dynamics of polybutadiene chains close to the surface.

On the contrary, Oh and Green[33] who studied chain dynamics in an athermal polymer/nanoparticle mixture of polystyrene grafted gold nanoparticles in a polystyrene melt observed that melt polystyrene chains experience a local reduction in the friction coefficient, ζ, when in contact with the short (10-monomer grafted chains) 'dry' brush layer of the nanoparticle, denoted as $AuPS_{10}$. This resulted in faster overall relaxation rates, that is, enhanced dynamics (recall that the longest polymer relaxation time, τ, is proportional to ζ). On the other hand, the increased elastic energy penalty of deforming longer grafted chains (481 monomers) resulted in reduced interpenetration of the brush layer by the host melt chains (50 monomers)[51]. Simultaneously, the grafted chain mobility was also slowed down significantly in the $AuPS_{481}$ nanocomposite as this reduction decreases exponentially with grafted chain length. Their findings suggest that the dynamics of polystyrene are enhanced in the presence of short grafted chains and reduced when longer grafted chains are used. We have sought to understand the changes in the dynamics of polystyrene chains when in contact with a polystyrene grafted and bare silica surface.

The work of Kropka et al.[31] on the peculiarities of dynamical properties in poly(methyl methacrylate)-(PMMA)-C_{60} nanocomposites showed how small concentrations of C_{60} increase the longest relaxation time of the polymer. The increase in the relaxation time of the polymer resulted from transient immobilization of polymer segments at the particle surface leading to the chains feeling an enhanced effective friction. They reported that the PMMA-C_{60} interfacial interactions created a fraction of slowly relaxing polymer domains. In their later work, Kropka et al.[32] also showed by incoherent neutron scattering of C_{60}−polymer mixtures that local polymer chain backbone motions in the glassy state were suppressed relative to those of the pure polymer. Despite the seemingly direct link between attractive interfacial interactions and their effect on the polymer dynamics, Akcora et al.[12] have argued that a universal behavior for the local motion of polymers in the vicinity of solid surfaces does not exist. Rather, they attributed the observations to the chemical specificity of a given scenario.

This therefore might be one reason why some researchers[34] reported for example that the local segmental dynamics of poly(vinyl acetate) adjacent to silica particles are similar to the bulk behavior.

Yet another contribution to this debate presented by Priestly et al.[30] suggested that hydrogen bonds formed between PMMA and a silica substrate suppress any cooperative segmental mobility as well as the smaller motions that are associated with structural relaxations. They also reported a near-elimination of the physical aging process within 25 nm of the substrate and a slowed-down aging over distances of at least 100 nm from the substrate. Similarly, experimental work on a poly(2-vinyl pyridine) – silica model nanocomposite by Rittigstein et al.[28] revealed that confinement on the polymer chains can extend to *hundreds of nanometers and even to the microscale* in the presence of strong attractive interactions. On the other hand, the work of Yang et al.[29] on a system without strong hydrogen bonds revealed that a mobile surface layer of less than 2.3 nm reduced the effective viscosity of unentangled, short-chain 24-mer polystyrene films on silicon.

Although the majority of experimental work that we have reviewed suggests that attractive interfacial-polymer interactions lead to a suppression of the polymer segmental mobility, Bogoslovov and co-workers[34] observed no such evidence for poly(vinyl acetate) (PVAc) in the presence of spherical silica particles of ~100 nm diameter. They explained that their data of enhanced filler-polymer interaction results from a silica surface treatment with tetrasulfidosilane. The reviewed results indicate that there is great need for an experimental and theoretical understanding of the "non-universality" of polymer interface dynamics. McKenna[52] has also summarized some of these discrepancies or inconsistent results explaining whether polymer dynamics increase or decrease at surfaces and the impact on the polymer glass-transition temperature for example.

We will now present some of the computer modeling and theoretical approaches which have been employed to understand the dynamics of polymers at interfaces. Using stochastic molecular dynamics simulations and the Kremer-Grest[53] bead-spring coarse-grained polymer model, Goswami and Sumpter[41] observed a slower anomalous diffusion of polymer chains in polymer nanocomposites. They attributed this decrease in the dynamics to attractive interactions between monomers and nanoparticles. The chains surrounding spherical nanoparticles exhibited Rouse-like motion, an intermediate subdiffusive regime that was followed by the usual Fickian diffusion. In other work, Egorov[54] studied the diffusion of Lennard-Jones spheres representing the nanoparticles in polymer melts of n spherical segments using mode-coupling theory. The diffusion coefficient of the nanoparticles, which directly affects that of surrounding polymer chains, decreased with increasing nanoparticle-polymer interaction strength. Also, coarse-grained molecular dynamics simulations of Torres et al.[42] of ultrathin films revealed that the strength of the substrate-polymer interactions determined the relaxation and diffusion rates of polymer chains. Strongly attractive substrates created "slow" regions while "free or solid"

surfaces enhanced the molecular mobility. Furthermore, Binder et al.[26] also showed by coarse-grained models of polymer chains interacting with hard walls that the polymer density was reduced near repulsive walls while a layer of enhanced density was created close to an attractive wall. As a result of the structure of the density profile induced by the attractive or repulsive nature of the surface, the local polymer mobility was larger near the repulsive walls where there is a reduced mass density. Their findings were in agreement with the experimental work of Van Alsten et al.[55]

Atomistic MD simulations of poly(ethylene oxide) (PEO) sandwiched between two TiO_2 surfaces by Borodin et al.[37] revealed that the density of PEO close to the surface played only a minor role in the interfacial PEO relaxation. Instead, Coulombic interactions between the polymer and the surface significantly increased the structural and conformational relaxation times of the interfacial PEO. Vogel[35] has also made similar observations in another atomistic MD study of PEO between two parallel surfaces of TiO_2.

Yelash et al.[10] also observed slowed dynamics in an atomistic 1,4-polybutadiene melt at a graphite surface. In their work, they attributed the slow dynamics not only to packing effects and intramolecular rotation (conformational) barriers present in the polymer bulk but also to the slow monomer desorption kinetics at the surface which leads to slow layer exchange dynamics. Similarly, Müller-Plathe and co-workers[36,56,57] reported a reduction in the conformational and structural relaxations at the graphite-polyamide-6,6 (oligomers) interface using atomistic and coarse-grained MD simulations. Another example of a first adsorption layer exhibiting slowed dynamics at a graphite surface was reported in the atomistic MD simulations of Hamandaris et al.[43] of polyethylene. Atomistic MD simulations on a silica surface have also been performed by Brown et al.[3], Barbier et al.[4], and Smith et al.[38]. In the work of Brown and co-workers[3], linear chains with CH_2 united-atoms have been used to represent the polymer chains while Barbier and co-workers[4] have used poly(ethylene oxide) oligomers surrounding a spherical α-quartz silica surface. Lastly, Smith et al.[38] employed poly(dimethylsiloxane) chains in the vicinity of a flat β-cristobalite silica surface. Their results revealed slowed-down polymer dynamics at the interface.

Our current work intends to identify factors which influence the polymer dynamics at interfaces or on surfaces. The parameters varied in our simulations are the nanoparticle diameter (which simultaneously determines the surface curvature and interfacial surface area) and the grafting density (ρ_{gr}, chains/nm^2). Our contribution will augment experimental findings in which it is more difficult to locally resolve dynamical quantities. Furthermore, explicit atomistic models have the advantage of being more material-specific in the investigation of the intermolecular energetics. This has the

advantage that the polymer relaxation processes in the vicinity of surfaces can be quantified in greater detail in comparison to using coarse-grained models[58].

3.2. Model and Simulation Details

All-atom molecular dynamics (MD) simulations were carried out on nanocomposite systems consisting of atactic polystyrene (a-PS, -[C_8H_8]-$_n$) in contact with either an ungrafted or an a-PS-grafted spherical silica (SiO_2) nanoparticle as in or previous work[20]. Simulations were generally performed at a temperature, T, of 590 K and pressure, P, of 101.3 kPa. The exception was during the investigations of the influence of T and P on the reorientation of intramolecular vectors where T varied from 490 to 690 K while P was increased from 101.3 to 40520 kPa. Nanoparticles with diameters of 3, 4, and 5 nm have been chosen to vary the surface curvature while grafting densities of 0.0 (bare, ungrafted), 0.5, and 1.0 chains/nm^2 were contrasted. Both free and grafted a-PS polymer chains in our model system have n = 20 monomers, since at present only low molecular weight polymers can be investigated atomistically in reasonable time and length scales. The grafted chains are attached to the silica surface via a linker unit, (-[$H_2C(H(C_2H_3)C]_3(CH_3)_2Si$-), also employed in experiments[59]. In all studied systems, the minimum number of polymer chains is 202, that is, the sum of both free and grafted chains. For example, a particle of 3 nm diameter has 14 or 28 grafted chains for grafting densities of 0.5 and 1.0 chains/nm^2, and is surrounded by 188 or 174 free chains, respectively. Those which have diameters of 4 and 5 nm have 25 and 40 grafted chains for a grafting density of 0.5 chains/nm^2 while being surrounded by 202 and 162 free chains, respectively. For the higher grafting case of 1.0 chains/nm^2, the 4 nm diameter has 50 grafted and 177 free chains while the 5 nm diameter has 80 grafted and 122 free chains. In all cases, the ungrafted particles are surrounded by 202 free a-PS chains. The cubic simulation box sizes vary between 9.23 and 9.71 nm. The bulk a-PS melt mass density was 910.9 ± 1.5 kg/m^3 at 590 K and 101.3 kPa (experimental[60] density at the same temperature and pressure = 904.0 ± 0.1 kg/m^3) while that of the silica nanoparticle was 2770.6 ± 7.6 kg/m^3 (density of natural quartz[61] = 2635 – 2660 kg/m^3).

The force field parameters (containing the Lennard-Jones and Coulomb terms) for the polymer and anionic linker molecule are based on the OPLS-AA force field[62] for hydrocarbons and have been designed to describe mixtures of a-PS with benzene[63] and ethylbenzene[64]. On the other hand, the silica Lennard-Jones and Coulomb interaction parameters were obtained from a model that describes bulk crystalline silica[65]. For a complete description of the studied systems and force field parameters, we refer to our previous work[20] where the same parameters have been employed.

Simulation runs were carried out in the isothermal-isobaric (*NPT*) ensemble using the molecular dynamics simulation code YASP[66]. During the MD simulations, the Berendsen[67] thermostat and barostat were used to maintain the system at prescribed temperatures T and pressures P. Coupling times of 0.2 ps (T) and 0.5 ps (P) were chosen. The integration has been performed employing the Verlet-leapfrog integration algorithm with a time step of 1 fs. Nonbonded interactions and the Verlet neighbor list (updated every 15 time steps) had cutoff radii of 1.0 and 1.1 nm, respectively. The reaction-field correction for the Coulombic[66] interactions was employed, assuming the average effective dielectric constant of the continuum ε_{RF} to be 3.7 (experimental dielectric constant: 2.4 – 2.7 for amorphous PS and 4.4 – 4.6 for amorphous silica at room temperature)[61].

To allow sampling of different configurations, the temperature was elevated from the set-up temperature of 490 K to 990 K. Later, it was decreased at 100 K/ns for 5 ns and final equilibration runs were performed at 590 K. To investigate the effect of temperature on the reorientational dynamics of intramolecular vectors, a further decrease in temperature steps of 10 K was carried out, simulating for 0.5 ns in the *NVT* ensemble and then for 1.25 ns in the *NPT* ensemble at each temperature. Following this, production simulations were performed for a further 4 ns at both 540 K and 490 K. Equilibrated systems at 590 K were further simulated at 640 K and 690 K also for 4 ns having made a single temperature step increase from the lower (590 K) to the higher temperatures. The influence of pressure was studied by increasing the pressure from 101.3 to 20260 and 40520 kPa at 590 K and simulating the systems for 4 ns. During production, configurations were sampled every 2000 time steps (2 ps). The mean-square displacement analysis performed at a temperature of 590 K and pressure of 101.3 kPa was done from a 50 ns production run. At the same temperature and pressure, the reorientation of chain segment vectors has been done by averaging 3 different trajectory files of length 16 ns.

3.3. Results and Discussion

3.3.1. Mean-Square Displacement of Polymer Chains

As a measure of the mobility of free chains, their center of mass (COM) mean-square displacement (MSD) was calculated. Shells of equal thickness (either 0.5 or 1.0 nm) surrounding the spherical nanoparticle were constructed to define different spatial regions as a way to investigate how far reaching the silica surface influences the polymer chain dynamics. Note that 1 nm is approximately the unperturbed radius of gyration (R_g) of the considered polymer chain[20]. Representative MSD plots for this motion, $\langle(R_{COM}(t) - R_{COM}(0))^2\rangle$, with $\langle\ldots\rangle$ denoting the ensemble average in the particular shell or for all polymer chains in the reference bulk a-PS melt (T = 590 K, P = 101.3 kPa) and $R_{COM}(t)$ is the

position of the chain COM at a given time *t*, are shown in Fig. 3.1. The MSD of every polymer chain was counted for the shell in which its COM spent the most residence time during the 50 ns production runs. While the chains COMs resided for at least 50% of the time in a shell of 1 nm thickness, their residence time increased in shells closer to the surface due to confinement. Despite the increasing migration between shells at larger surface separation, chain COMs still spent on average about 75% of the simulation time in a given shell.

For one illustrative example, we use a finer shell width (0.5 nm), namely for the chain MSDs in a system containing the 4 nm diameter particles of different grafting densities (Fig. 3.1). Chain residence times in these narrower shells are shorter; thus their minimum residence time reduces to 40%. Still, the MSDs in the four inner shells are distinctly different. Error bars from a comparison of 3 shorter trajectories of 15 ns each with different average shell populations were negligible as the MSD in each shell remained distinctly different. There is no MSD data for shell 1 and/or 2 for the grafted particles because free chains cannot penetrate the grafted polymer layers at close distance, as we have reported in our previous work[20] on structural properties of the same system. For the free a-PS chains, the following general trend can be extracted from Fig. 3.1: with decreasing separation from the nanoparticle surface, the MSD is reduced, i.e. the chains exhibit attenuated dynamics. In contrast to the polymer chain behavior near the nanoparticle surface, the free chains residing in the outer shells approach bulk-like MSDs. However, even for the bulk 20 monomer a-PS melt, we only observe Rouse diffusion dynamics characterized by an MSD slope of 0.5 compared to the Einstein diffusive limit of 1. This is due to the long time scale of Einstein diffusion, which is not accessible in this type of simulation. (Note: Both slopes have been added to Fig. 3.1.) Consequently, we have not calculated the diffusion coefficient. However, we have found that our bulk MSD data is similar to that of an 18 monomer bulk a-PS melt[27]. While the free polymer chains in shells nearer to the surface have reduced MSDs due to confinement and increased density[20], those in shells further away from the surface experience a reduced effect. At a distance of 2.5-3.0 nm, the chains approach bulk-like movement. In addition, it is observed for all grafting densities that the chains closest to the nanoparticle exhibit a qualitatively different diffusion behavior; their MSD follows a power law with an exponent visibly below 0.5.

We compare the chain mobilities using shells of 1 nm width to investigate the effect of the surface curvature and grafting density (Table 3.1 and Fig. A2.1-3 in the Appendix 2). As the systems are subdiffusive and diffusion coefficients thus not meaningful, we use the centre-of-mass MSD after 40 ns as a comparative measure of the chain mobility. Near the particle surface (< 1nm) it is a factor 2-3 lower than in the outer shell (2-3 nm) for the bare nanoparticles A similar decrease is also observed when comparing MSDs as a function of distance from the surface when the surface is grafted. At the

same time, the MSD of free chains in general decreases more in the vicinity of the particle when the particle is larger. This is a consequence of a surface curvature which decreases with particle size. This geometrical change promotes chain and segmental tangential orientation to the surface, denser packing within the interphase region, in addition to simply providing more geometrical hindrance to diffusion[20]. Therefore, the confinement experienced by the free chains not only increases when they are closer to the surface but also when the surface curvature is reduced as the particle surface then approximates more and more the limit of a flat surface. From recent calculations, it follows that the surface-polymer attractions[13,25,26,37] also play an increasing role with an increase in the interfacial surface area. In the employed force-field, the silica nanoparticles as well as the phenyl ring atoms have partial charges. In single nanoparticle simulations, the interfacial surface area doubles and almost triples when moving from a particle with a diameter of 3 nm to one of 4 and 5 nm, respectively. Therefore, all these factors have a combined effect of reducing the free chains MSDs in shells that are both closer to the surface and even more so in those surrounding particles of decreasing surface curvature.

Furthermore, the average MSDs of free chains COMs in the first shells around grafted particles are less that in the same shell surrounding bare particles (Table 3.1). The reason for the further reduced MSDs within the distance of 0 – 1 nm from the surface is the intermixing of free chains with grafted chains, which in turn have an excluded volume for free chains and a lower mobility, as they are fixed to the silica surface. The grafted chains affect the dynamics of the free chains in other ways (see below). However, the numbers in Table 3.1 reflect the possible competition between the nanoparticle surface and the grafted chains on the mobility of the free chains. Clearly, the surface reduces the mobility of free chains. At the same time, while grafted chains 'screen' the free chains from interacting directly with the surface, the motion of the same grafted chains to expelling the free chains from approaching the surface increases the MSD of free chains. This is indicated by normalized MSD values in Table 3.1 of 0.35 and 0.44 nm^2 in the first shell (0-1 nm) surrounding 3 nm diameter particles of grafting densities 0.5 and 1.0 chains/nm^2, respectively. Therefore, the exclusion of free chains by the grafted chains dominates in the higher grafting case while both the excluded volume of the grafted chains and the surface cooperatively reduce the free chains MSD in the lower grafting case.

The MSD after 40 ns has also been calculated for the grafted chains (not shown), in full knowledge that they cannot diffuse. It is generally found that their mobility is greatest when their centre of mass is predominantly found in the shell separated 1-2nm from the nanoparticle surface. This is not too surprising, since the closer chains are more squashed against the nanoparticle and in general experience a higher polymer density[20] which restricts their motion. In the other limit, a chain, whose

center of mass resides predominantly at large distances from the nanoparticle surface (2-3 nm shell), maintains a stretched conformation and is less mobile for that reason.

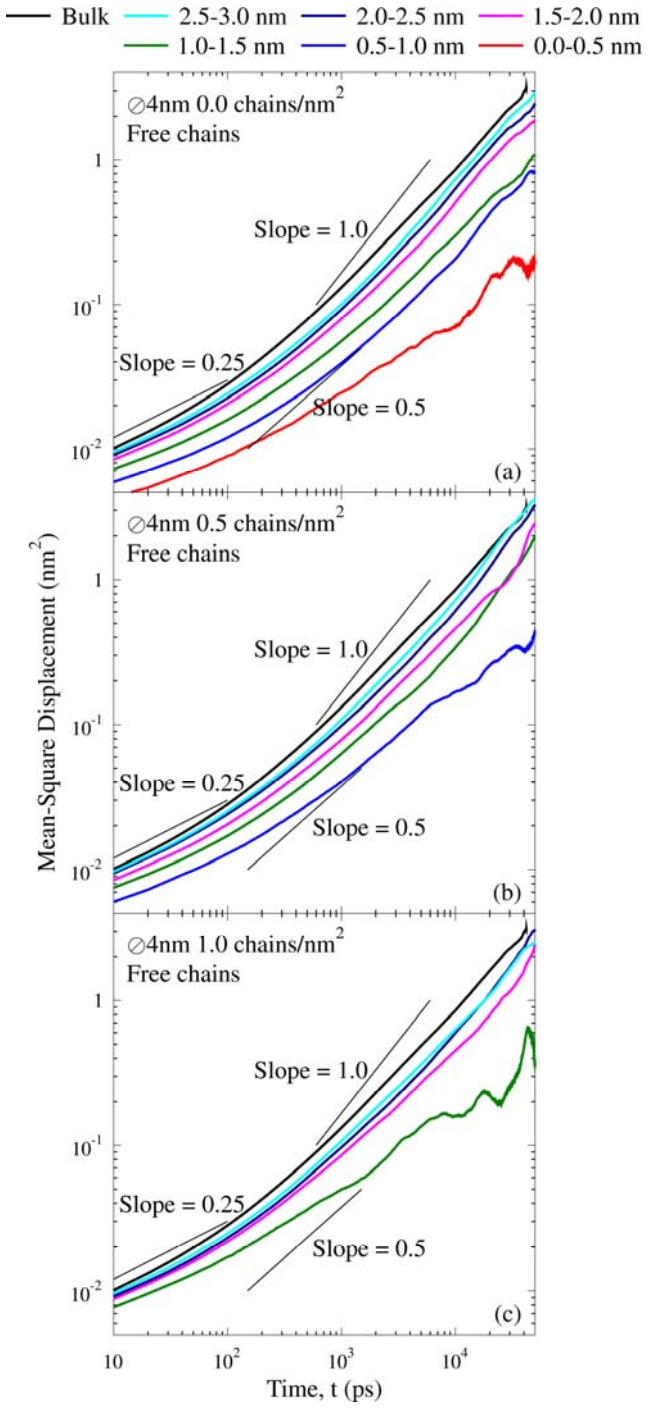

Figure 3.1. Center of mass mean-square displacement (MSD) of free 20 monomer polystyrene chains which reside the most in one of the 6 shells surrounding spherical particles of diameter = 4 nm and different grafting density. The simulations have been performed at T = 590 K and P = 101.3 kPa. Each of the shells has a width of 0.5 nm. Shell 1 (0.0-0.5 nm) is missing in panel (b) while both shells 1 (0.0-0.5 nm) and 2 (0.5-1.0 nm) are not present in panel (c) because the ability of free polymer chains to penetrate the grafted chains regime reduces with increasing grafting density. The physical meaning of the added slopes (thin black lines) of 0.25, 0.5, and 1.0 has been explained in the text.

Table 3.1: Normalized mean-square displacements (MSDs), MSD_{Shell} / MSD_{Bulk}, after 40 ns

Free bulk chains MSD = MSD_{Bulk} = 2.97 nm^2			
Shell: distance from the nanoparticle surface	**Nanoparticle diameter ∅ = 3 nm**	**Nanoparticle diameter ∅ = 4 nm**	**Nanoparticle diameter ∅ = 5 nm**
	Free chains, Grafting density = 0.0 chains/nm^2		
0 – 1 nm	0.49	0.22	0.18
1 – 2 nm	0.88	0.41	0.36
2 – 3 nm	1.03	0.77	0.55
	Free chains, Grafting density = 0.5 chains/nm^2		
0 – 1 nm	0.35	0.11	0.13
1 – 2 nm	0.88	0.52	0.29
2 – 3 nm	0.86	0.89	0.62
	Free chains, Grafting density = 1.0 chains/nm^2		
0 – 1 nm	0.44	–	–
1 – 2 nm	0.64	0.48	0.25
2 – 3 nm	0.89	0.74	0.66

The data in the table above is for the normalized chain center of mass mean-square displacements (MSD_{Shell} / MSD_{Bulk}) of 20-monomer atactic polystyrene chains at a temperature of 590 K and atmospheric pressure. MSD_{Shell} symbolizes the value derived for the considered shell while MSD_{Bulk} represents the bulk value. For high grafting densities of 1.0 chains/nm^2 for the 4 and 5 nm diameter particles, there are no free chains in the first shell (0-1 nm).

3.3.2. Reorientation of Intramolecular Vectors

The analysis of both the local segmental and chain dynamics is useful to understand the nanoparticle induced changes on the properties of the surrounding polymer chains. To study both the free and grafted chain and local segmental reorientation dynamics in the modeled nanocomposites, we have investigated the relaxation times of various intramolecular vectors which include those shown in the schematic representation in Fig. 3.2.

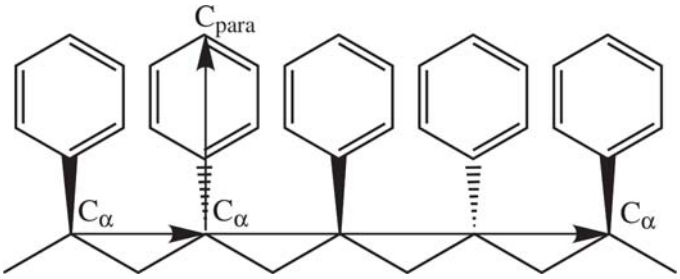

Figure 3.2. This schematic diagram is of a 5 monomer polystyrene chain to show the one monomer (C_α-C_α) long, three monomers (C_α ... C_α) long, and C_α-C_{para} segment vectors considered in the study of the chain segmental dynamics by calculating the reorientation $P_1(t)$ and $P_2(t)$ time-autocorrelation functions of theses vectors. The hydrogen atoms have been omitted in this figure.

In addition to the one monomer (C_α-C_α), three monomers (C_α … C_α), and C_α-C_{para} vectors, the reorientation of the C_α-H and the end-to-end vector was also studied. For the latter, both C atoms are the terminal C_α of free chains, while one of the two terminal C atoms of a-PS bonds to the linker molecule in the case of grafted chains. Since the induced structural orientation of the one monomer and three monomers segments is similar[20], we have only focused on reorientation results of the three monomers segment in this work. Also, having observed that the reorientation of the C_α-C_{para} and C_α-H vectors is of a similar magnitude, focus has been put on the C_α-H bond vector.

The advantage of calculating relaxation correlation times is that - in principle - they can be compared to those obtained experimentally. The vector of interest in dielectric spectroscopy (DS) studies is C_α-C_{para} while the quantity of interest is the first Legendre polynomial[68]: $P_1(t) = \langle \cos(\theta(t)) \rangle$. On the other hand, the spin relaxation time in nuclear magnetic resonance (NMR) spectroscopy studies can be directly related to the reorientation of the C-H bond vector in which case the quantity of interest is the second Legendre polynomial[68]: $P_2(t) = 1.5\langle \cos^2(\theta(t)) \rangle - 0.5$. In both cases, $\theta(t)$ is the angle by which the vector has rotated in a time t and $\langle \ldots \rangle$ denotes the ensemble average. The relaxation times τ_1 and τ_2 are obtained as time integrals of the corresponding correlation function; see below. A similar investigation of polymer chain segment vector relaxation times has been carried out by Harmandaris and co-workers[27] to investigate the effect of temperature and pressure on a pure melt of 18 monomer a-PS chains. They reported that the ratio of the mean relaxation time at all temperatures obtained from the $P_1(t)$ and $P_2(t)$ curves, that is, τ_1/τ_2 varied between 2.2 and 2.7, similar to our results in which this ratio is 2.7 for the C_α-H segment reorientation. For more details, see below. In addition, earlier work of Ediger et al.[69] correlated NMR experiments with the results of the segmental dynamics of a pure melt of 20 monomer a-PS that had been obtained from MD simulations. They also observed a similar non-exponential decay of the $P_2(t)$ curves as in our melt a-PS system and this validates our model system. Our contribution explains the influence of the surface curvature and grafting density on the dynamics

of both free and grafted chains. In a series of simulations, we determine how they deviate from the bulk polymer dynamics.

We have again employed the shell construction in calculating the $P_1(t)$ and $P_2(t)$ time-autocorrelation functions for the various intramolecular vectors. For the present problem, the vectors contribute to the statistics of that shell where their midpoint has the greatest residence time. An exception is the end-to-end vector which contributes to the statistics of that shell where the chain COM resides the most. The logarithmic plots of the $P_2(t)$ time-autocorrelation functions in a period of 16 ns for the C_α-H and 3 monomer segment vector around a bare nanoparticle are shown in Fig. 3.3 (a-c) and (d-f), respectively, as examples of local vectors of free chains. A finer 0.5 nm resolution of the shell thickness has been chosen to have a better local resolution. The other local vectors, C_α-C_α and especially C_α-C_{para} behave similar to the C_α-H vector, and so have not been shown. In all autocorrelations, there is a fast initial decrease in the first 10 ps which corresponds to the so-called primitive relaxation (bond and angle vibrations and librations) followed by the segmental (α-) relaxation at longer times. The results observed by Harmandaris and co-workers[27] in neat PS agree with this behavior. Similar to the relaxation of the end-to-end vector at the chain level are the trends for the C_α-H and the 3 monomer segment vector autocorrelation functions; compare Fig. 3.3 (a-c) with (d-f): (i) The segments close to the nanoparticle (< 1 nm) relax significantly slower than bulk chain segments, whereas the outer shells quickly approach bulk dynamics. The reasons for the 'surface-near' changes are the same as given above for the mean-square displacements: adhesion and steric hindrance. (ii) The relaxation of segments close to the nanoparticle becomes slower with increasing particle diameter (i.e. decreasing curvature) while the slow region extends further into the more distant shells. Compare, for example, the autocorrelation functions in the 2.5-3.0 nm shell in Figs. 3.3a to 3.3c and 3.3d to 3.3f. For the 3 nm nanoparticle (Fig. 3.3 (d)), it is virtually identical to the bulk autocorrelation function, whereas the decay is clearly slower for the 5 nm system. This is an effect of decreasing surface curvature, as for example also the increase in polymer density from small to larger particles. Again, we refer to Fig. 3.1 of our recent MD study[20]. These two trends are qualitatively the same for the reorientation autocorrelation of all vectors investigated. However, from Fig. 3.3 it is also evident that the strongest slowing down is always found in the layer nearest to the nanoparticle (< 1 nm). This coincides with the distance at which static orientational anomalies disappear. Short polymer segments feel an orienting effect of the surface up to 1 nm. Beyond that distance, they are randomly oriented[20].

As a measure of long-scale relaxation, we also present the autocorrelation functions of the end-to-end vectors of free chains around the bare particle in Fig. 3.4 (a-c) for a period of 50 ns. The same qualitative trends as already shown in Fig. 3.3 are observable. Note, however, that the overall decay of

the autocorrelation functions is slower with increasing vector length. To give an idea of this behavior, we have calculated the relaxation times via the P_2(t) correlation functions according to the procedure outlined below in the bulk at 590 K. The values of these times are 6.4 ns for the end-to-end vector, 2.4 ns for a segment of three monomers, and 0.6 ns for the C_α-H bond vector.

As an example to quantify the vector relaxation as a function of the separation from the surface, the mean reorientational relaxation times, $\langle \tau \rangle$, of the C_α-H bond vector were obtained from the time integral of the $P_2(t)$ curve. For practical reasons, they were least-squares fitted by a Kohlrausch-Williams-Watts (KWW) stretched exponential function whose time integral is analytical.

$$\langle \tau \rangle = \int_0^\infty P_1(t)\,dt \approx \int_0^\infty \exp\left(-\left(t/\tau_\kappa\right)^\beta\right) dt = \frac{\tau_\kappa}{\beta}\Gamma\left(\frac{1}{\beta}\right) \qquad (3.1)$$

In equation 3.1, the parameter $\langle \tau \rangle$ is the mean relaxation time obtained from the area under the curve $P_2(t)$, t is time, β is the stretching exponent, and $\Gamma(1/\beta)$ is the complete gamma function. In the case of an exponential decay with $\beta = 1$, the parameter τ_κ would be equal to the mean relaxation time $\langle \tau \rangle$. The KWW function provides a very reasonable fit, as can be seen in the examples shown in the next section (cf. Fig. 3.6). We note here that some of the autocorrelation functions, most notably for the end-to-end vectors and segment vectors in the immediate vicinity of the surface, did not converge to zero in the accessible simulation time of 50 ns (cf. Fig. 3.4). We have nonetheless followed the above procedure and used the KWW function fitted to the initial decay of the autocorrelation to extrapolate it to long times. We are aware that the resulting reorientation times are, at best, order-of-magnitude estimates and should be taken with care.

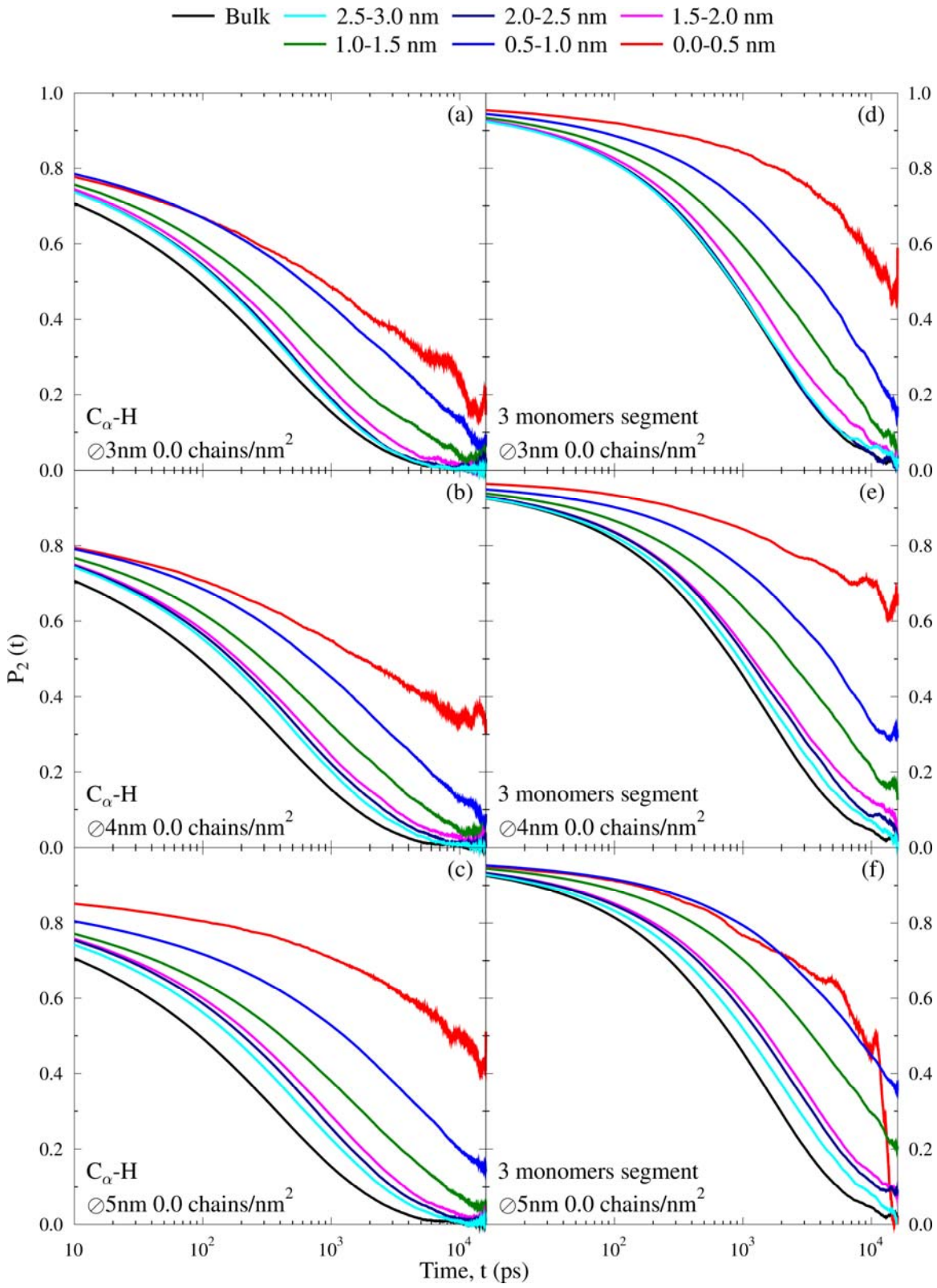

Figure 3.3. $P_2(t)$ **time-autocorrelation function for the** C_α**-H bond vector (left panels) and the 3 monomers segment vector (right panels) of free polymer chains surrounding bare nanoparticles during a 16 ns simulation period. Sampling for the respective shells has been explained in the text. The simulations have been performed at** T **= 590 K and** P **= 101.3 kPa.**

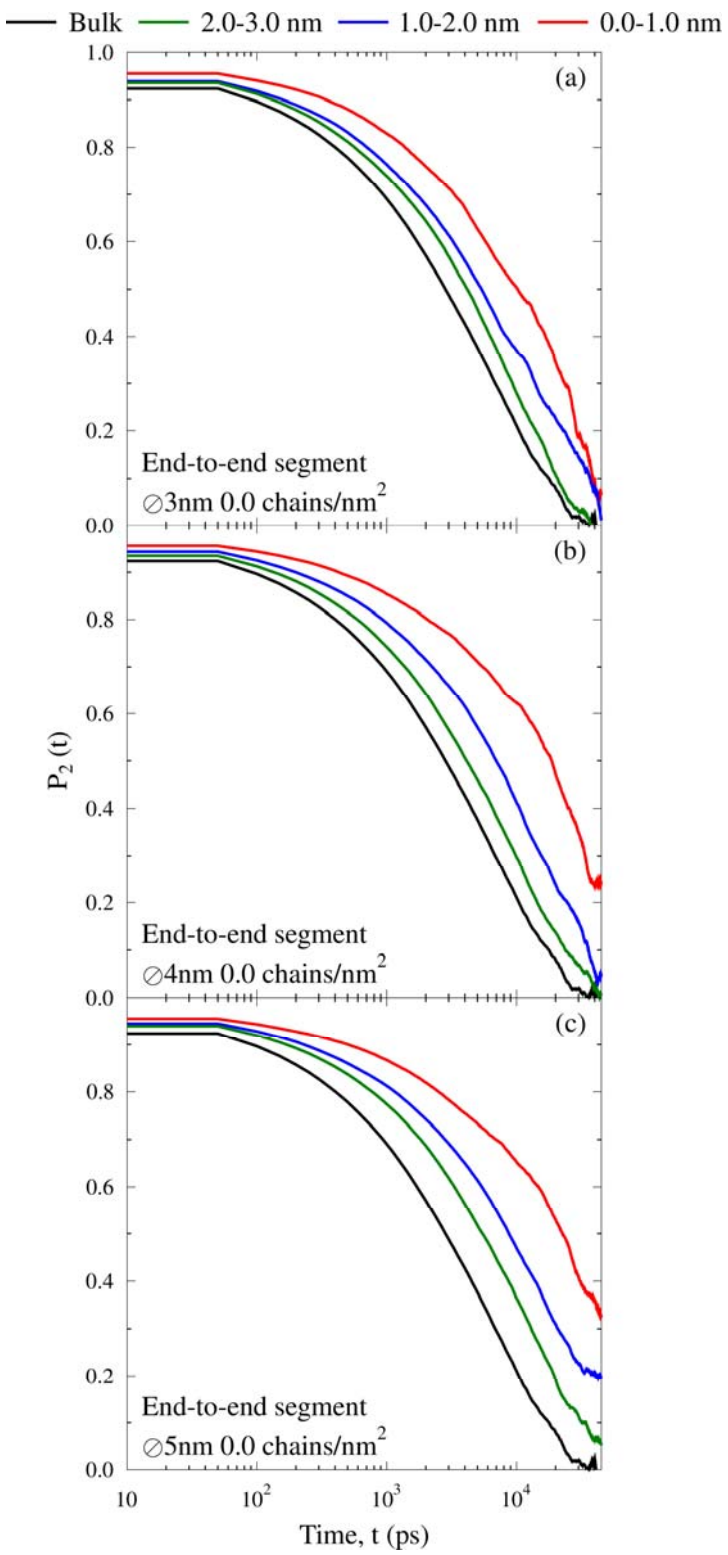

Figure 3.4. $P_2(t)$ time-autocorrelation function for the end-to-end vector of free chains surrounding bare silica spherical particles of different diameters at T = 590 K and P = 101.3 kPa during a 50 ns simulation period. Sampling of the respective shells took into account only those chains whose center of mass resided predominantly in that particular shell.

Having computed the normalized mean relaxation times in each of the shells relative to a bulk a-PS melt at the same T = 590 K and P = 101.3 kPa, $\langle\tau\rangle_{Shell}$ / $\langle\tau\rangle_{Bulk}$, a comparison which shows the effect of the surface curvature and grafting density is given in Fig. 3.5 for the C_α-H vector. Shells that are 0.25 nm wide were chosen to have a finer resolution as a function of the separation from the surface. In the very first shell (0-0.25 nm) rather large relaxation times (2-3 orders higher than bulk) are found, which are however not included in the figure due to their large scatter. We find that the dynamics of local segments of both free and grafted chains are affected to a different extent in the various shells. There is usually a strong slowing-down in the closest layers (< 1 nm), with the reorientational relaxation time increasing by factors between 4 and 30 over the bulk value taking into account the large error bars. Segment vectors located beyond 2 nm from the surface are only moderately affected; their relaxation times increase by factors between 1.1 and 2.0. The effect on the segments located > 2.5 nm away is marginal, with relaxation times only a few percent larger or smaller than in the bulk. The trend of stronger slowing-down with increasing particle diameter as already found for other dynamical quantities again appears for the segment reorientations. For the grafted chains, it can be noted that their segments reorient generally with similar speeds as the free-chain segments in the same shell. However, there is a difference between these local reorientations of free and grafted chains for small particle diameters (3 and 4 nm) and large distances (> 2 nm). Whereas the free-chain dynamics approaches bulk behavior (Fig. 3.5 a, c, e), the outer monomers of the grafted chains actually relax faster than bulk chains (Fig. 3.5 b, d). This is noteworthy, as this is the only point where we observe an increase of the polymer dynamics apparently caused by the nanoparticle. The precise reason for this faster relaxation remains unclear, but it is obvious that this effect decreases with particle diameter, disappearing altogether for the largest particle (Fig. 3.5 f).

With the reorientation of the C_α-H vector reflecting very localized dynamics, it is no surprise that the grafting density has only a small effect on them, if any at all. The unusually fast reorientation for a diameter of 4 nm and a grafting density of 1.0 chains/nm^2 (Fig. 3.5c) is probably due to very limited statistics, as few free chains can penetrate the grafted brush. This topic has been discussed several times above.

In the chosen double-logarithmic presentation of Fig. 3.5 it becomes clear that the dependence of the local reorientation times on the distance from the surface appears to follow power laws. The reorientation of the C_α-H vector of *grafted* chains (Fig. 3.5 b, d, f) seem to follow single power law r^{-m}, with m increasing from 1.15 (∅ = 3 nm) via 1.87 (∅ = 4 nm) to 2.21 (∅ = 5 nm). This reflects once more the fact that a flatter surface has a longer-ranged effect on the polymer dynamics, and is thus in line with the findings above. Note however, that this correlation has been checked only under

conditions where a “flatter surface” simultaneously implies a “larger surface area”. The distance dependence of the C_α-H reorientation of the *free* chains also follows a power law. In contrast to the grafted chains, however, there appear two domains with different exponents (Fig. 3.5 a, c, e). Close to the surface (< 1.625 nm) the exponent *m* depends on the particle diameter, increasing from 1.50 to 2.11 and then to 2.61 between highest and lowest surface curvature. At larger distances (> 1.625 nm) we find a second, smaller exponent which also has a dependence on the particle diameter. It increases from 0.19 (∅ = 3 nm) via 0.55 (∅ = 4 nm) to 0.86 (∅ = 5 nm). It therefore appears that the dynamics of free chain segments close to the surface has a strong distance dependence, which itself is affected by the surface curvature. At larger separation from the surface, the distance dependence is smaller and less influenced by the surface curvature in the now familiar way: a lower curvature leads to a more far-reaching influence on the dynamics. The distance which separates both regimes is approximately 1.625 nm, close to a value corresponding that is 1.5 times the radius of gyration of the unperturbed chain (~1 nm), and also to approximately 3 times the monomer diameter. As to why grafted and free chains behave qualitatively differently, we can only speculate. A possible reason is that grafted chains have monomers that are close to the surface. Thus a monomer of a grafted chain far from the surface is necessarily connected to chain parts at closer distances and may feel their influence on its own reorientation dynamics. In contrast, the monomer of a free chain at the same far distance will most likely not belong to a chain which has also segments close to the surface. Therefore, its behavior will carry less influence from near-surface dynamics.

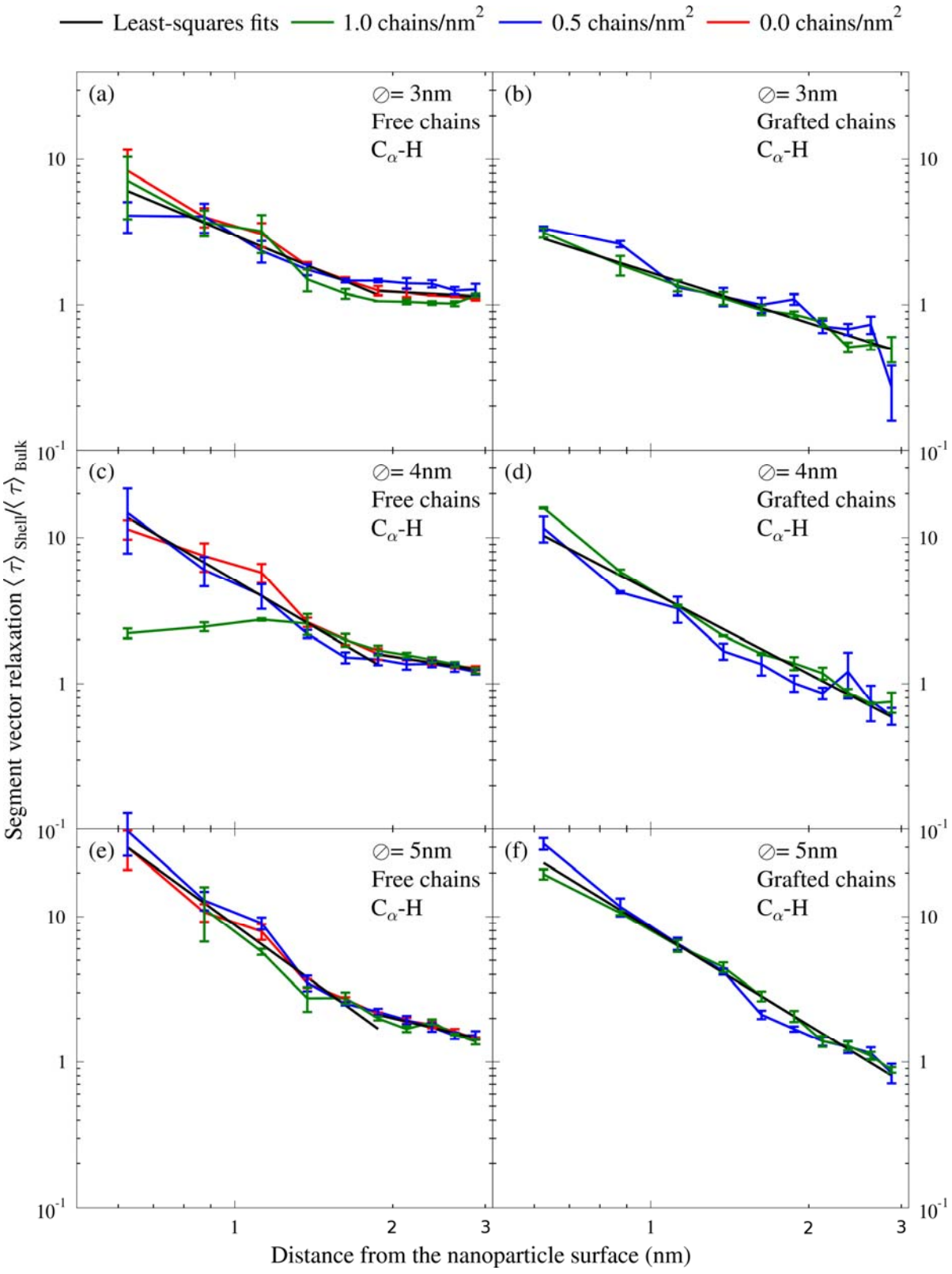

Figure 3.5: $P_2(t)$ based normalized mean relaxation times relative to the bulk value (τ_{bulk} = 0.6 ns) for the C_α-H bond vector of both free and grafted chains as a function of the distance from the nanoparticle surface which varied in curvature. Sampling for the respective shells of thickness 0.25 nm took into account only those bond vectors whose mid-point resided the most in that particular shell. The simulations have been performed at T = 590 K and P = 101.3 kPa. The error bars are the error of the average value computed in determining the standard deviation. The straight black lines are least-squares fits to all curves simultaneously in the corresponding range (except (c), where the 1.0 chains/nm^2 curve has been omitted from the fit).

While the normalized relaxation times of the local vectors are qualitatively similar when comparing the C_α-H vector to C_α-C_{para} for example, the end-to-end vectors have much longer relaxation times (see Table 3.2). Also their slowing-down near the nanoparticle with respect to bulk behavior is stronger. In all shells, even the outermost, the end-to-end relaxation is more affected than the local segment relaxation. A particular strong hindrance of reorientation is observed in the first shell (< 1 nm). Here, the mean distance of the chain from the surface is less than its unperturbed R_g and an increase of 2-3 orders of magnitude is estimated for the grafting density of 0.5 chains/nm^2. The reason is intermingling of free chains with grafted chains, which due to their attachment to the surface can only sway, but not fully reorient. It is reasonable to expect that this slows the free chains, too. For the grafting density of 1 chain/nm^2, one would expect even slower reorientation. However, at this density and the lower curvatures (4 and 5 nm diameter), the grafted brushes effectively expel free chains from this region: The distance at which there is more free polymer than grafted polymer has been found to be 1.8 and 2 nm for particles of 4 and 5 nm diameter, respectively[20]. This result shows that it is not only the chain dynamics as determined by shell MSDs but also the chain segmental dynamics that are slowed-down with decreasing surface curvature.

Table 3.2: $P_1(t)$ normalized end-to-end vector relaxation time $\langle\tau\rangle_{SHELL}$ / $\langle\tau\rangle_{BULK}$

Free bulk chains = $\langle\tau\rangle$ = 20.2 nanoseconds (ns)			
Shell: distance from nanoparticle surface	**Nanoparticle diameter ∅ = 3 nm**	**Nanoparticle diameter ∅ = 4 nm**	**Nanoparticle diameter ∅ = 5 nm**
	Free chains, Grafting density = 0.0 chains/nm^2		
0 – 1 nm	2.7	3.9	12.7
1 – 2 nm	2.0	3.0	5.7
2 – 3 nm	1.2	1.1	2.2
	Free chains, Grafting density = 0.5 chains/nm^2		
0 – 1 nm	3.5	~6000	~600
1 – 2 nm	2.1	1.74	20
2 – 3 nm	1.2	1.67	1.9
	Free chains, Grafting density = 1.0 chains/nm^2		
0 – 1 nm	2.3	–	–
1 – 2 nm	3.4	2.9	5.1
2 – 3 nm	1.4	1.2	1.8

$P_1(t)$ normalized end-to-end vector relaxation time relative to a bulk a-PS melt at T = 590 K and P = 101.3 kPa. The mean relaxation time, $\langle\tau\rangle$, was obtained from the integral of a Kohlrausch-Williams-Watts (KWW) stretched exponential function after performing a least-squares fit to the observed reorientational autocorrelation function in a period of 50 ns. The parameter $\langle\tau\rangle$ in the first shell (0-1 nm) for grafting density = 0.5 chains/nm^2 are orders of magnitude larger due to very slow reorientation times. For high grafting densities, there are no free chains in the first shell (0-1 nm); see also the numbers considered in Table 3.1.

3.3.3. Temperature and Pressure Influence on the Reorientation of the C_α-H Bond Vector

In practical applications, polymers are exposed to a variety of temperature and sometimes pressure conditions which determine how well they can be processed and thus the resulting material characteristics, e.g. mechanical and electrical properties. Whenever property changes are observed, they indicate modifications of the polymer structure and dynamics at the nano-scale. As such, it is important to understand how dynamic polymer properties are altered by temperature and pressure changes. Therefore, we have investigated the temperature and pressure effect on the reorientation of the C_α-H bond vector which is can be measured by NMR spectroscopy. Fig. 3.6 summarizes the

influence of either temperature (panels a-d) or pressure (panels e-h) on the $P_2(t)$ time-autocorrelation function of the C_α-H vector. As a representative example, we have chosen the relaxation of the segment vectors of the free chains in three shells of thickness = 1.0 nm surrounding a 4 nm bare particle. In studying the influence of temperature, the pressure was kept constant at 101.3 kPa while the temperature was varied between 490 and 690 K in steps of 50 K. To observe the influence of the pressure, the temperature was kept constant at 590 K while pressure values of 101.3, 20260, and 40520 kPa were chosen.

The density of the simulated bulk a-PS changes from 855.2±3.6 kg/m^3 at 690 K to 883.3±3.2 kg/m^3, 910.9±1.5 kg/m^3, 941.1±2.7 kg/m^3, 967.9±2.1 kg/m^3 at 640 K, 590 K, 540 K, and 490 K, respectively. This density reduction with decreasing temperature slows down the segmental dynamics by a factor of 4 in the bulk a-PS melt when reducing the temperature from 590 to 490 K. A similar decrease has been observed in each of the shells surrounding the nanoparticle, with the slowest $P_2(t)$ curve decay always occurring at the lowest temperature (see Fig. 3.6 (a-c)). The reorientation times at different temperatures were obtained as outlined in Section 3.2 for a three shell resolution. Their distribution indicates a Williams-Landel-Ferry temperature dependence at lower temperatures. The high temperature region between 590 and 690 K was subjected to an Arrhenius fit (not shown) in order to estimate very roughly the activation energy for C_α-H reorientation at different distances from the nanoparticle surface. The activation energy evaluated in the present study converges with increasing distance (0-1 nm: 89 kJ/mol; 1-2 nm: 76 kJ/mol; 2-3 nm: 70 kJ/mol) toward the value for the bulk (66 kJ/mol). Still, it is about 1.4 times higher in the first layer around the nanoparticle than in the bulk.

On the other hand, even though a reduction in the segmental dynamics is also observed when increasing the pressure from 101.3 to 40520 kPa at 590 K, the magnitude is much smaller due to less efficient densification effects within the employed pressure range. The density of the bulk a-PS at 590 K only increases from 910.9±1.5 kg/m^3 at a pressure of 101.3 kPa to 930.1±2.7 kg/m^3, and 945.9±2.4 kg/m^3 at 20260 kPa, and 40520 kPa, respectively. However, distinction can still be clearly made when comparing the dynamics in each of the shells under different pressure conditions. In summary, the general observed trend is that of slower segmental dynamics with decreasing temperature, increasing pressure, and decreasing separation from the silica surface.

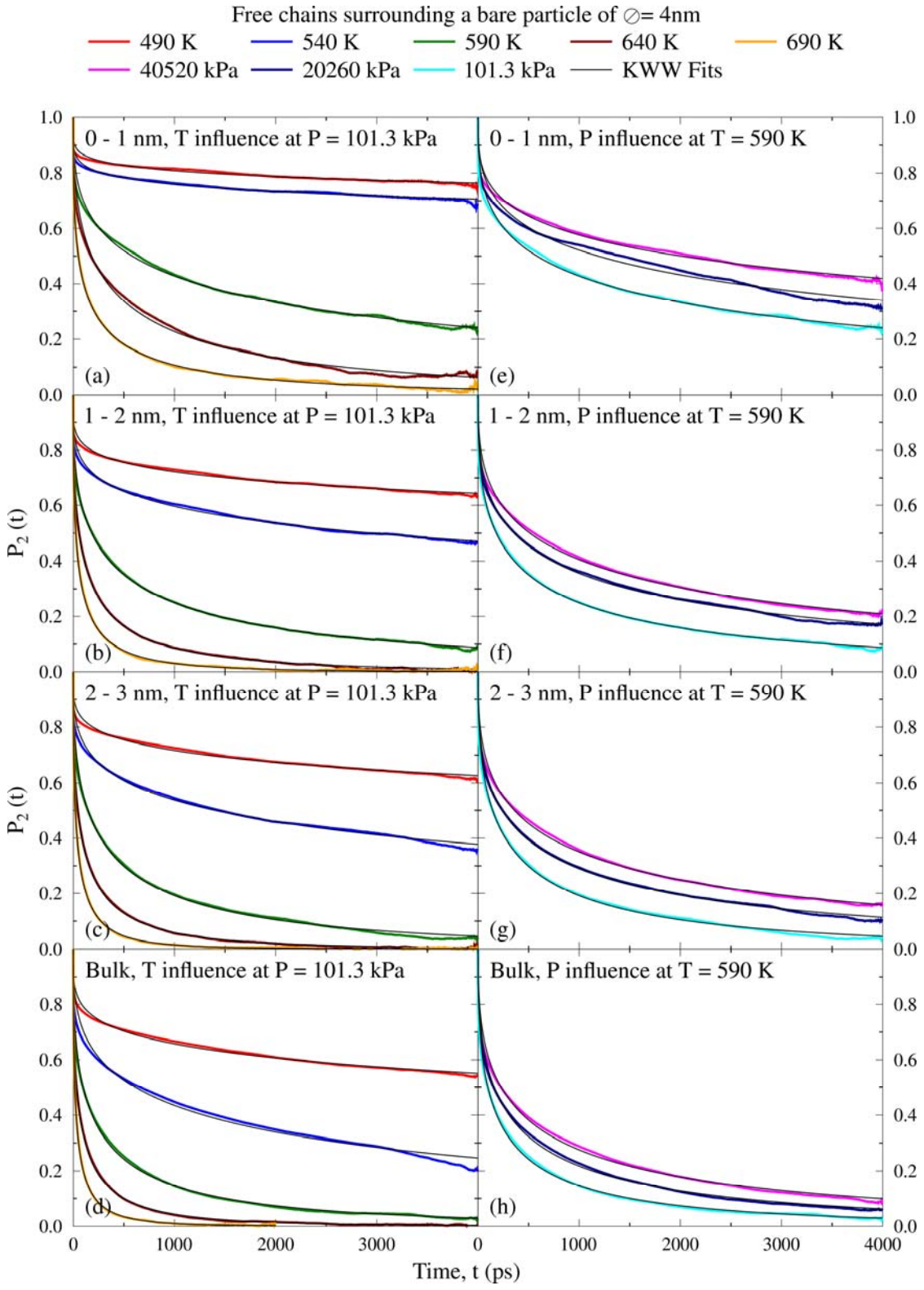

Figure 3.6. $P_2(t)$ time-autocorrelation function for the C_α-H bond vector of free chains surrounding a 4 nm diameter bare particle as a function of temperature (left panels) and pressure (right panels). The KWW fits are shown in black while sampling for the respective shells took into account only those bond vectors whose mid-point resided the most in that particular shell. The simulations have been performed at T = 590 K (right hand panels) and P = 101.3 kPa (left hand panels).

3.4. Summary and Conclusions

The chain and segmental dynamics of atactic polystyrene melts (molecular weight ~ 2000 g/mol, i.e. 20 monomers) in the interfacial and interphase region surrounding a spherical silica nanoparticle of diameters 3.0, 4.0, and 5.0 nm have been investigated by MD simulations at the atomistic level. We have determined the average mean-square displacement of the center of mass of the polymer chains in different spatial regions (shells) surrounding the spherical nanoparticle. Similarly, the reorientation of intramolecular vectors (C_α-H bond vector, three monomers segment, and the end-to-end vector) as indicated either by $P_1(t)$ or $P_2(t)$ relaxation curves has been investigated. With these data, the intramolecular segment mean relaxation times have been computed as a function of separation from the surface.

The global chain dynamics are described by the centre-of-mass mean-square displacement as well as by the relaxation of the end-to-end vector. Both quantities indicate a strong slowing down of the chain motion near the nanoparticle. Within a distance from the surface corresponding to one R_g (i.e. the radius of gyration of an unperturbed bulk chain) the dynamics is reduced by at least several times, in some cases by several orders of magnitude. In contrast, the chain dynamics is almost normal and bulk-like if the polymer chain is more than 2 R_g away from the surface. The dynamic behavior of matrix polymer chains is affected both by the grafting state of the nanoparticle (moderately) and its diameter or surface curvature (strongly). A lower curvature radius (our nanoparticles have curvature radii corresponding to 1.5, 2.0 and 2.5 R_g) leads to slower polymer dynamics and to an increased thickness of the "slow zone" around the particle. This is due to both increased geometric hindrance and – in the case of grafted particles – increased crowding of the grafted brushes.

The local polymer dynamics has been monitored by the reorientation of various intramolecular vectors; they also show similar behavior. Taking the methine C_α-H bond vector as an example, we can show that also the local mobility is considerably slowed by the presence of the nanoparticle. The grafting state of the surface has little influence on the local reorientation, but the surface curvature which in the chosen setup is also coupled to the surface area, has a pronounced effect. The C_α-H reorientation near the surface is slowed by about a factor of 8 compared with the bulk for a particle of 3 nm diameter. This reduction in dynamics is increased to a factor of 30 for the 5-nm particle. The reorientation dynamics as a function of distance from the surface has been found empirically to be governed by power laws of the type r^{-m}. The exponent m is generally sensitive to the surface curvature and increases with the diameter of the nanoparticle. This indicates that the zone of slowed dynamics expands, as the surface becomes flatter. An interesting feature is found for the free chains, which show

two regimes roughly separated by a distance of ~1.5 R_g from the surface. Below this boundary, the exponent is large (1.5 to 2.6) and curvature dependent, whereas above this limit m is smaller (< 1) though still curvature dependent. Also the activation energy for the segment orientation at close distance from the surface (< 1 R_g) is markedly different from the rest of the system, being ~1.4 times the activation energy in the outer shell (> 2 R_g) or in the bulk.

We therefore find for the dynamical properties that both the chain mobility and the segment mobility are significantly slowed close to the nanoparticle surface. Chain mobility is affected even at a distance of 2-3 R_g from the surface, whereas segment mobility becomes bulk-like beyond 2 R_g. It is interesting to juxtapose the dynamical interphase thickness with the interphase thickness calculated previously by various structural features [20] for the same system. Density oscillations cease after 2 R_g. Monomers of surface-grafted chains are no longer found after 3-4 R_g, depending on surface curvature and grafting density. The chains' sizes and orientations become bulk-like and random after about 1.5 R_g, whereas the segment orientation becomes random already just below 1 R_g. The emerging picture is therefore that most surface-induced modifications of the polymer properties have a range of about 2 R_g. Segment properties may converge earlier, whereas the whole-chain dynamics may extend further. The interphase, defined by whatever property, however, has a thickness of this order of magnitude. Note that these statements are specific to the system at hand. Care should be taken when generalising them to other chain lengths, as the 20-mers studied here are far from the length where the polymer behavior becomes generic. Moreover, the position dependence of the segmental structure and dynamics may well be governed by the monomer diameter, rather than the chain length R_g, as the dominating length scale. In our short polymers, the two scales just happen to be similar in magnitude.

Acknowledgment: Financial support from the European Union through the project "NanoModel" under grant number 211778 is gratefully acknowledged. We would like to acknowledge the DFG Priority Program 1369 for providing the computer resources. Fruitful discussions with Evangelos Voyiatzis, Frédéric Leroy, Simon Butler, Mohammad Rahimi, Azadeh Ghanbari, Enrico Riccardi, and colleagues in the NanoModel project are especially appreciated.

3.5. References

(1) Vacatello, M. *Macromolecules* **2001**, *34*, 1946-1952.
(2) Starr, F. W.; Schrøder, T. B.; Glotzer, S. C. *Macromolecules* **2002**, *35*, 4481-4492.
(3) Brown, D.; Mélé, P.; Marceau, S.; Albérola, N. D. *Macromolecules* **2003**, *36*, 1395-1406.
(4) Barbier, D.; Brown, D.; Grillet, A.-C.; Neyertz, S. *Macromolecules* **2004**, *37*, 4695-4710.
(5) Everaers, R.; Sukumaran, S. K.; Grest, G. S.; Svaneborg, C.; Sivasubramanian, A.; Kremer, K. *Science* **2004**, *303*, 823-826.
(6) Bansal, A.; Yang, H.; Li, C.; Cho, K.; Benicewicz, B.; Kumar, S. K.; Schadler, L. S. *Nature Mater.* **2005**, *4*, 693-698.
(7) Sen, S.; Xie, Y.; Kumar, S. K.; Yang, H.; Bansal, A.; Ho, D. L.; Hall, L.; Hooper, J. B.; Schweizer, K. S. *Phys. Rev. Lett.* **2007**, *98*, 128302-128305.
(8) Sen, S.; Xie, Y.; Bansal, A.; Cho, K.; Schadler, L.; Kumar, S. K. *Eur. Phys. J. Spec. Top.* **2007**, *141*, 161-165.
(9) Akcora, P.; Liu, H.; Kumar, S. K.; Moll, J.; Li, Y.; Benicewicz, B. C.; Schadler, L. S.; Acehan, D.; Panagiotopoulos, A. Z.; Pryamitsyn, V.; Ganesan, V.; Ilavsky, J.; Thiyagarajan, P.; Colby, R. H.; Douglas, J. F. *Nature Mater.* **2009**, *8*, 354-359.
(10) Yelash, L.; Virnau, P.; Binder, K.; Paul, W. *Phys. Rev. E* **2010**, *82*, 50801-50804.
(11) Lo Verso, F.; Egorov, S. A.; Milchev, A.; Binder, K. *J. Chem. Phys.* **2010**, *133*, 184901-184910.
(12) Akcora, P.; Kumar, S. K.; Sakai, V. G.; Li, Y.; Benicewicz, B.; Schadler, L. S. *Macromolecules* **2010**, *43*, 8275-8281.
(13) Jancar, J.; Douglas, J. F.; Starr, F. W.; Kumar, S. K.; Cassagnau, P.; Lesser, A. J.; Sternstein, S. S.; Buehler, M. J. *Polymer* **2010**, *51*, 3321-3343.
(14) Harton, S. E.; Kumar, S. K.; Yang, H.; Koga, T.; Hicks, K.; Lee, H.; Mijovic, J.; Liu, M.; Vallery, R. S.; Gidley, D. W. *Macromolecules* **2010**, *43*, 3415-3421.
(15) Kumar, S. K.; Krishnamoorti, R. *Annu. Rev. Chem. Biomol. Eng.* **2010**, *1*, 37-58.
(16) Dukes, D.; Li, Y.; Lewis, S.; Benicewicz, B. C.; Schadler, L. S.; Kumar, S. K. *Macromolecules* **2010**, *43*, 1564-1570.
(17) Kalb, J.; Dukes, D.; Kumar, S. K.; Hoy, R. S.; Grest, G. S. *Soft Matter* **2010**, *7*, 1418-1425.
(18) Vogiatzis, G.; Voyiatzis, E.; Theodorou, D. N. *Eur. Polym. J.* **2010**, *47*, 699-712.
(19) Chevigny, C.; Jestin, J.; Gigmes, D.; Schweins, R.; Di-Cola, E.; Dalmas, F.; Bertin, D.; Boué, F. *Macromolecules* **2010**, *43*, 4833-4837.
(20) Ndoro, T. V. M.; Voyiatzis, E.; Ghanbari, A.; Theodorou, D. N.; Böhm, M. C.; Müller-Plathe, F. *Macromolecules* **2011**, *44*, 2316-2327.
(21) Milano, G.; Santangelo, G.; Ragone, F.; Cavallo, L.; Di Matteo, A. *J. Phys. Chem. C* **2011**, *115*, 15154-15163.
(22) Chevigny, C.; Dalmas, F.; Di Cola, E.; Gigmes, D.; Bertin, D.; Boue, F.; Jestin, J. *Macromolecules* **2011**, *44*, 122-133.
(23) Ghanbari, A.; Ndoro, T. V. M.; Leroy, F.; Rahimi, M.; Böhm, M. C.; Müller-Plathe, F. *Submitted to Macromolecules* **2011**.
(24) Liu, J.; Wu, Y.; Shen, J.; Gao, Y.; Zhang, L.; Cao, D. *Phys. Chem. Chem. Phys.* **2011**, *13*, 13058-13069.
(25) Mortezaei, M.; Famili, M. H. N.; Kokabi, M. *Compos. Sci. Technol.* **2011**, *71*, 1039-1045.
(26) Binder, K.; Milchev, A.; Baschnagel, J. *Annu. Rev. Mater. Sci.* **1996**, *26*, 107-134.
(27) Harmandaris, V. A.; Floudas, G.; Kremer, K. *Macromolecules* **2011**, *44*, 393-402.
(28) Rittigstein, P.; Priestly, R. D.; Broadbelt, L. J.; Torkelson, J. M. *Nat. Mater.* **2007**, *6*, 278-282.
(29) Yang, Z.; Fujii, Y.; Lee, F. K.; Lam, C.-H.; Tsui, O. K. C. *Science* **2010**, *328*, 1676-1679.
(30) Priestly, R. D.; Ellison, C. J.; Broadbelt, L. J.; Torkelson, J. M. *Science* **2005**, *309*, 456-459.
(31) Kropka, J. M.; Putz, K. W.; Pryamitsyn, V.; Ganesan, V.; Green, P. F. *Macromolecules* **2007**, *40*, 5424-5432.
(32) Kropka, J. M.; Sakai, V. G.; Green, P. F. *Nano Letters* **2008**, *8*, 1061-1065.

(33) Oh, H.; Green, P. F. *Nat. Mater.* **2009**, *8*, 139-143.
(34) Bogoslovov, R. B.; Roland, C. M.; Ellis, A. R.; Randall, A. M.; Robertson, C. G. *Macromolecules* **2008**, *41*, 1289-1296.
(35) Vogel, M. *Macromolecules* **2009**, *42*, 9498-9505.
(36) Eslami, H.; Müller-Plathe, F. *J. Phys. Chem. B* **2009**, *113*, 5568-5581.
(37) Borodin, O.; Smith, G. D.; Bandyopadhyaya, R.; Byutner, O. *Macromolecules* **2003**, *36*, 7873-7883.
(38) Smith, J. S.; Borodin, O.; Smith, G. D.; Kober, E. M. *J. Polym. Sci.: Part B: Polym. Phys.* **2007**, *45*, 1599-1615.
(39) Dionne, P. J.; Ozisik, R.; Picu, C. R. *Macromolecules* **2005**, *38*, 9351-9358.
(40) Dionne, P. J.; Picu, C. R.; Ozisik, R. *Macromolecules* **2006**, *39*, 3089-3092.
(41) Goswami, M.; Sumpter, B. G. *Phys. Rev. E* **2010**, *81*, 41801-41808.
(42) Torres, J. A.; Nealey, P. F.; de Pablo, J. J. *Phys. Rev. Lett.* **2000**, *85*, 3221-3224.
(43) Harmandaris, V. A.; Daoulas, K. C.; Mavrantzas, V. G. *Macromolecules* **2005**, *38*, 5796-5809.
(44) Jones, R. A. L.; Richards, R. W. *Polymers at surfaces and interfaces*; Cambridge University Press: Cambridge, UK, 1999.
(45) Scheidler, P.; Kob, W.; Binder, K. *Europhys. Lett.* **2002**, *59*, 701-707.
(46) Mortezaei, M.; Farzi, G.; Kalaee, M. R.; Zabihpoor, M. *J. Appl. Polym. Sci.* **2011**, *119*, 2039-2047.
(47) Chen, L.; Zheng, K.; Tian, X.; Hu, K.; Wang, R.; Liu, C.; Li, Y.; Cui, P. *Macromolecules* **2010**, *43*, 1076-1082.
(48) Whittington, A. P.; Nguyen, S. T.; Kim, J.-H. *Nanoscape* **2009**, *6*, 26-30.
(49) Mortezaei, M.; Famili, M. H. N.; Kalaee, M. R. *J. Reinf. Plast. Comp.* **2011**, *30*, 593-599.
(50) Robertson, C. G.; Rackaitis, M. *Macromolecules* **2011**, *44*, 1177-1181.
(51) Xu, J.; Qiu, F.; Zhang, H.; Yang, Y. *J. Polym. Sci. B* **2006**, *44*, 2811-2820.
(52) McKenna, G. B. *Eur. Phys. J. E* **2003**, *12*, 191-194.
(53) Kremer, K.; Grest, G. S. *J. Chem. Phys.* **1990**, *92*, 5057.
(54) Egorov, S. A. *J. Chem. Phys.* **2011**, *134*, 84903-84908.
(55) Van Alsten, J. G.; Sauer, B. B.; Walsh, D. J. *Macromolecules* **1992**, *25*, 4046-4048.
(56) Eslami, H.; Müller-Plathe, F. *J. Phys. Chem. B* **2010**, *114*, 387-395.
(57) Eslami, H.; Karimi-Varzaneh, H. A.; Müller-Plathe, F. *Macromolecules* **2011**, *44*, 3117-3128.
(58) Wolfgang, P.; Smith, G. D. *Rep. Prog. Phys.* **2004**, *67*, 1117-1185.
(59) Hübner, E.; Allgaier, J.; Meyer, M.; Stellbrink, J.; Pyckhout-Hintzen, W.; Richter, D. *Macromolecules* **2010**, *43*, 856-867.
(60) Höcker, H.; Blake, G. J.; Flory, P. J. *Trans. Faraday Soc.* **1971**, *67*, 2251-2257.
(61) Lide, D. R. *CRC Handbook of Chemistry and Physics*, 74th ed.; CRC Press: Boca Raton, Florida, 1993.
(62) Jorgensen, W. L.; Maxwell, D. S.; Tirado-Rives, J. *J. Am. Chem. Soc.* **1996**, *118*, 11225-11236.
(63) Müller-Plathe, F. *Macromolecules* **1996**, *29*, 4782-4791.
(64) Qian, H.-J.; Carbone, P.; Chen, X.; Karimi-Varzaneh, H. A.; Liew, C. C.; Müller-Plathe, F. *Macromolecules* **2008**, *41*, 9919-9929.
(65) Lopes, P. E. M.; Murashov, V.; Tazi, M.; Demchuk, E.; MacKerell, J., Alexander D. *J. Phys. Chem. B* **2006**, *110*, 2782-2792.
(66) Müller-Plathe, F. *Comput. Phys. Commun.* **1993**, *78*, 77-94.
(67) Berendsen, H. J. C.; Postma, J. P. M.; van Gunsteren, W. F.; DiNola, A.; Haak, J. R. *J. Chem. Phys.* **1984**, *81*, 3684-3690.
(68) Abramowitz, M.; Stegun, I. A. *Handbook of Mathematical Functions with Formulas, Graphs, and Mathematical Tables*, 9th ed.; Dover Publications: New York, 1972.
(69) He, Y.; Lutz, T. R.; Ediger, M. D.; Ayyagari, C.; Bedrov, D.; Smith, G. D. *Macromolecules* **2004**, *37*, 5032-5039.

4. Conclusions and Outlook

This PhD thesis is a summary of the successful use of the molecular dynamics simulation tool, YASP[1], to investigate the changes in the structural and dynamical properties of atactic polystyrene near a spherical silica surface. The studied surface has either been grafted with atactic polystyrene of the same length as the surrounding bulk polymer melt or was left without any surface modifiers. Additionally, the diameter of the nanoparticles was varied to have different surface curvature and nanoparticle size effects. These parameters together with the nanoparticle grafting density influenced the extent of interpenetration between the grafted and free polymer chains and thereby revealing the width of the interphase region. Wherein, the polymer properties deviate from the bulk characteristics as a consequence of the surface effect. In a contrasting case, the unmodified nanoparticles revealed the behavior of the free polymer chains in direct contact with the surface to form the surface-polymer interface region. The static and dynamic properties of these 'interface' polymers were compared to those of grafted chains in the same location which form a different kind of polymer-surface interface region.

Firstly, this study revealed that the two types of nanoparticles, with and without any grafting, do indeed influence both the structural and dynamical properties of the polymer chains in the interface as well as the interphase region. A much more pronounced effect on the polymer chains in the interface region was observed due to their close proximity to the surface in comparison to polymer chains in the interphase region. The observed densification[2-6] or layering of the combined free and grafted polymer chains surrounding the nanoparticles extended to regions as far away as twice the polymer radius of gyration. This result indicated favorable swelling of the polymer chains around the nanoparticles. Such behavior together with the very good mixing between the grafted (0.5 chains/nm^2) and free chains would be favorable for the propagation of mechanical stress from the bulk polymer and also useful in reducing adhesive failure. At the same time, densification resulted in slower polymer dynamics, particularly in the interface region compared to the interphase region. The latter has been confirmed by reduced polymer chains center-of-mass mean-square displacement and much longer reorientation times of intramolecular chain segments. Consequently, this has important practical implications because the creation of slower polymer domains in the vicinity of the surface can lead to a delay in the polymer aging process. This is beneficial in increasing the material's practical lifespan. Simultaneously, experimental measurements have shown that such slow domains lead to a higher polymer glass transition temperature[7,8] in the interface region. Further simulations with polymer chains that are longer than the 20-mers studied in this work should be able to confirm this experimental observation and also investigate changes in the material mechanical properties. The latter depends on

the width of the interphase region and how well the grafted and free polymer chains interpenetrate to allow for propagation of mechanical stress. Results from the density profiles revealed that an intermediate grafting density of 0.5 chains/nm^2 was favorable for intermixing between grafted and free chains.

Secondly, both surface modified and unmodified nanoparticles induce a tangential orientation of the grafted and free polymer chains as well as their segments. However, this effect occurs only within a distance that is equal to the polymer radius of gyration i.e. ~ 1 nm for 20-mer bulk polystyrene chains. Such surface induced tangential orientations make it more difficult for the polymer chains to diffuse and thus slow down the relaxation of intramolecular segments.

Thirdly, results from both the density profiles of free and grafted chains, mean-square displacements and chain intramolecular segment relaxations are influenced significantly by the nanoparticle surface curvature. The reduced surface curvature, exemplified by the nanoparticle with the greatest diameter of 5 nm, led to enhanced densification. This is because the polymer chains can more easily attain a pancake-like conformation along the flatter increased surface area. At the same time, the influence of the larger particle on the polymer chain's dynamics extended much further away from the surface. These observations underscore the importance of both surface area and curvature in designing nanoparticles. This is so because seemingly minute changes like moving from a particle diameter of 3 to 5 nm can have a significant impact on the properties of polymer chains in its vicinity.

Finally, concerning the observed results from this work, it has been shown that the grafting state of a nanoparticle also plays a key and critical role in determining the interphase width and how well grafted and free chains intermix. This has a direct influence on the dispersion state of the nanoparticles in a polymer melt, a quantity that is important in determining the final material properties. A high grafting density of 1.0 chains/nm^2 resulted in a significant expulsion of free chains from approaching the surface in this case. For an intermediate grafting density of 0.5 chains/nm^2, greater interpenetration between the grafted and free polymer chains was allowed. Furthermore, the distance at which the concentration of both grafted and free polymer chains is equal was also shown to shift further away from the surface with increasing particle size and grafting density. These observations again reveal a strong interplay amongst the various parameters and highlight the importance of understanding their effects in the design of polymer nanocomposites.

With regards to the present and future work, the same model system that has been developed and analyzed in this PhD thesis is the backbone of coarse-graining work which will be presented elsewhere. Coarse-grained simulations have the advantage of investigating much longer polymer chains and several nanoparticles in a single system within accessible simulation times. This is made possible by the simplifications which group several atoms into single 'super atoms thereby reducing

degrees of freedom and allowing for much faster relaxation times of the polymer chains for example. Results from this technique are powerful in that they can explore typical experimental chain lengths together with several nanoparticles to investigate nanoparticle dispersion. Moreover, this work is also being used in the calculation of mechanical and thermodynamic polymer properties to determine the effect of the nanoparticle surface at the atomistic level. At both levels of resolution, it is important to investigate model systems with more than one nanoparticle to observe how the particle-particle interactions influence the current observations. In view of simulating longer polymer chains while also having a good description of the polymer-surface interface region, this model system is also a good candidate for performing hybrid molecular dynamics simulations. In this novel computer simulation approach, the interface region is treated with atomistic detail while the interphase region is at the coarse-grained level. This approach therefore takes advantage of the benefits of both atomistic and coarse-grained simulations. Additionally, calculating the surface interfacial free energy and separating the enthalpic and entropic contributions in these complex systems will undoubtedly lead to a better understanding of the current results. Such knowledge will give both the modeler and experimentalist significant control in tailoring polymer nanocomposites for specific purposes. Therefore, experience and knowledge gathered in this PhD thesis work provides key input parameters in the design of novel materials whose benefits will further propel technological advances in the present ‘nano era’.

4.1. References

(1) Müller-Plathe, F. *Comput. Phys. Commun.* **1993**, *78*, 77-94.
(2) Brown, D.; Mélé, P.; Marceau, S.; Albérola, N. D. *Macromolecules* **2003**, *36*, 1395-1406.
(3) Barbier, D.; Brown, D.; Grillet, A.-C.; Neyertz, S. *Macromolecules* **2004**, *37*, 4695-4710.
(4) Bucior, K.; Yelash, L.; Binder, K. *Phys. Rev. E* **2009**, *79*, 031604-031616.
(5) Vogiatzis, G.; Voyiatzis, E.; Theodorou, D. N. *Eur. Polym. J.* **2010**, *47*, 699-712.
(6) Yelash, L.; Virnau, P.; Binder, K.; Paul, W. *Phys. Rev. E* **2010**, *82*, 50801-50804.
(7) Mortezaei, M.; Famili, M. H. N.; Kokabi, M. *Compos. Sci. Technol.* **2011**, *71*, 1039-1045.
(8) Tsagaropoulos, G.; Eisenburg, A. *Macromolecules* **1995**, *28*, 396-398.

Appendix 1

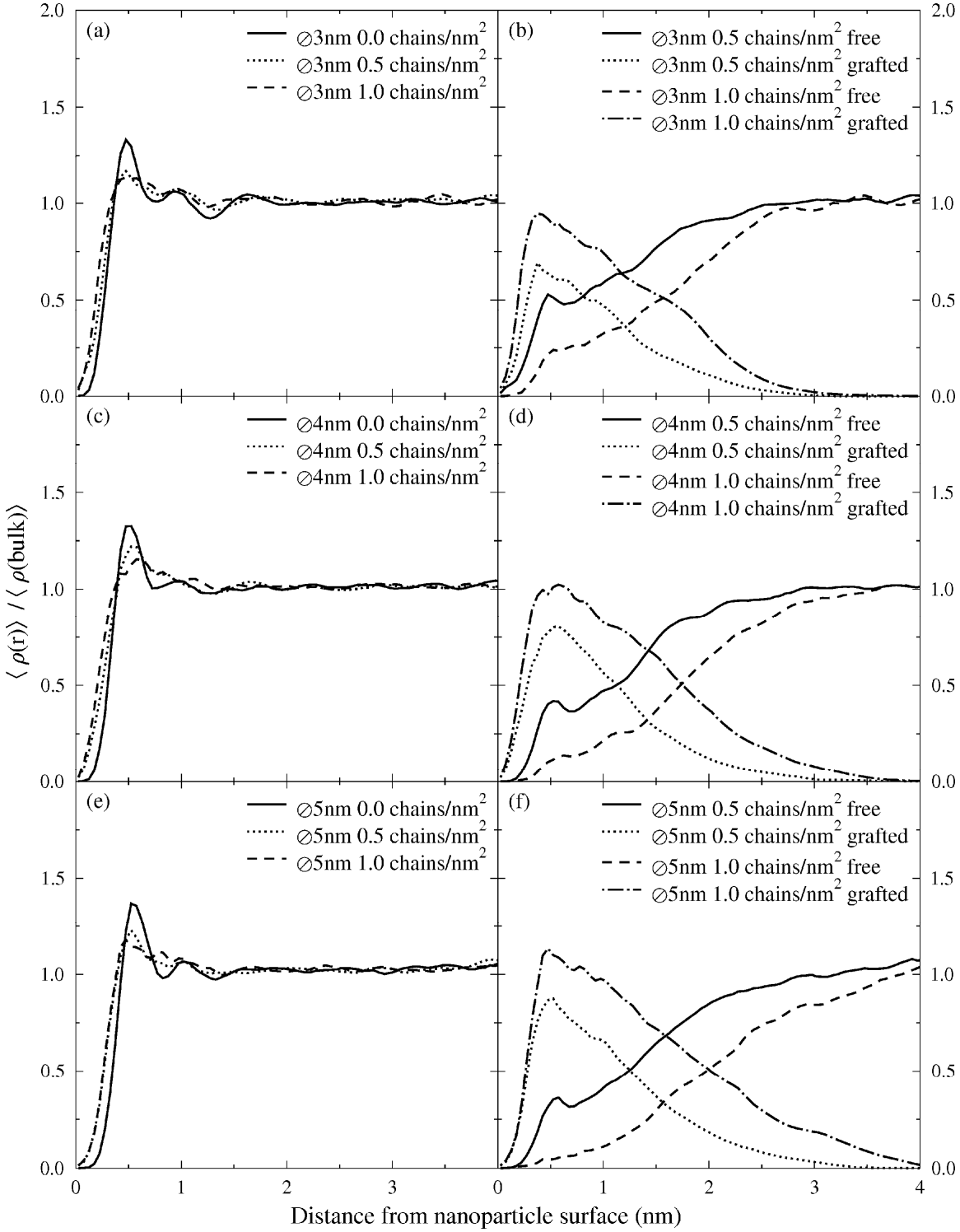

Figure A1.8. Polystyrene mass density profiles as a function of the radial distance from the silica nanoparticle. Panels (a), (c), and (e) summarize the overall polymer mass density profiles (excluding linker atoms) for the bare (solid line), medium (dotted line) and high grafted density (dashed line) systems as a function of nanoparticle diameter. Panels (b), (d), and (f) show the separated mass density profiles of grafted and free chains. These simulations have been performed at T = 590 K and P = 101.3 kPa.

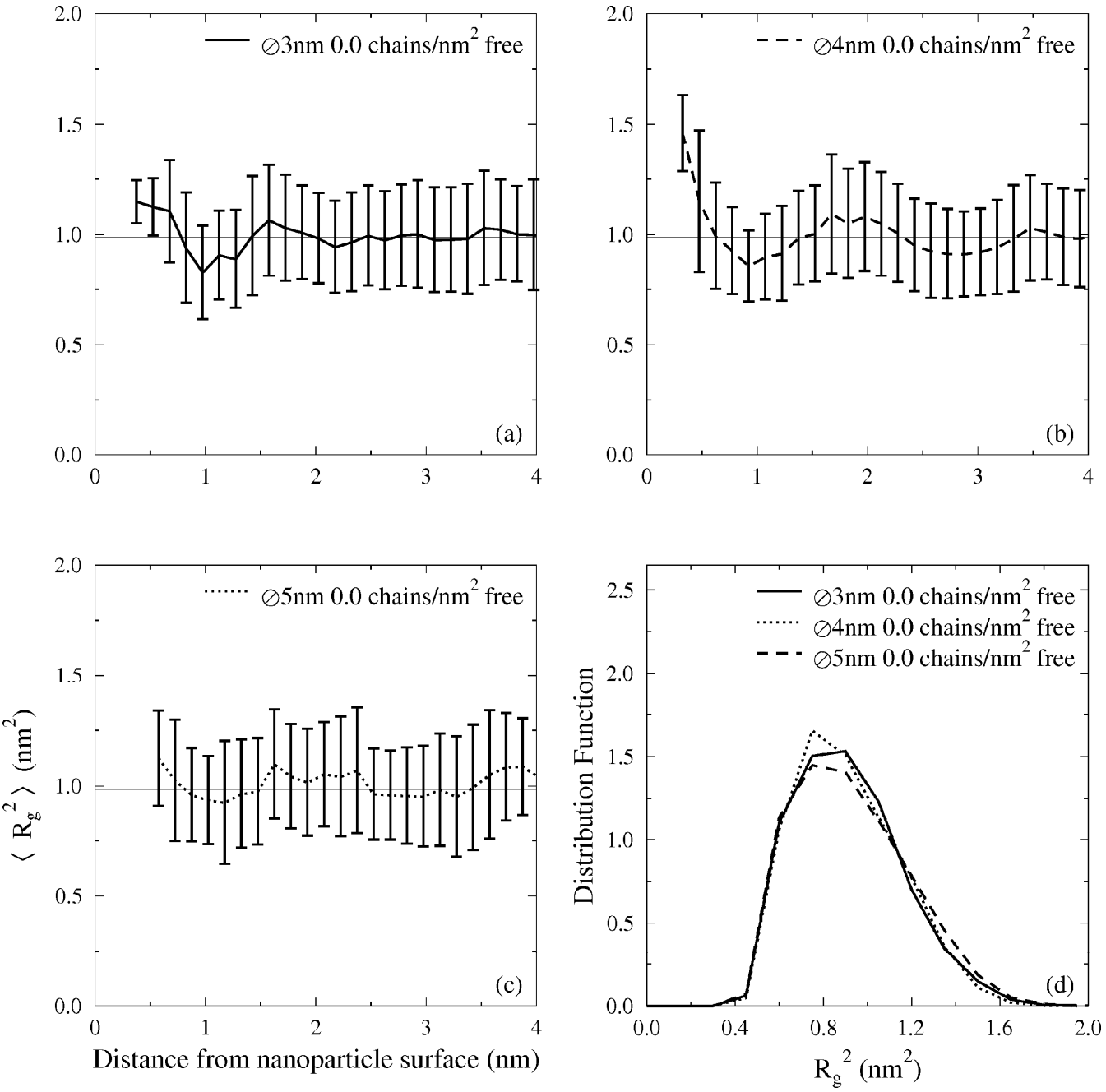

Figure A1.2. Panels (a), (b), and (c) summarize the squared radius-of-gyration of free a-PS polymer chains around bare nanoparticles while graph (d) shows the corresponding histograms (in arbitrary units) at *T* = 590 K and *P* = 101.3 kPa. The horizontal line (also drawn in Figures SI-3, 4, and 5) containing squared radius-of-gyration data) at ~1 nm^2 corresponds to the average squared radius-of-gyration of the bulk. The vertical error bars on the data points are the mean standard deviation values.

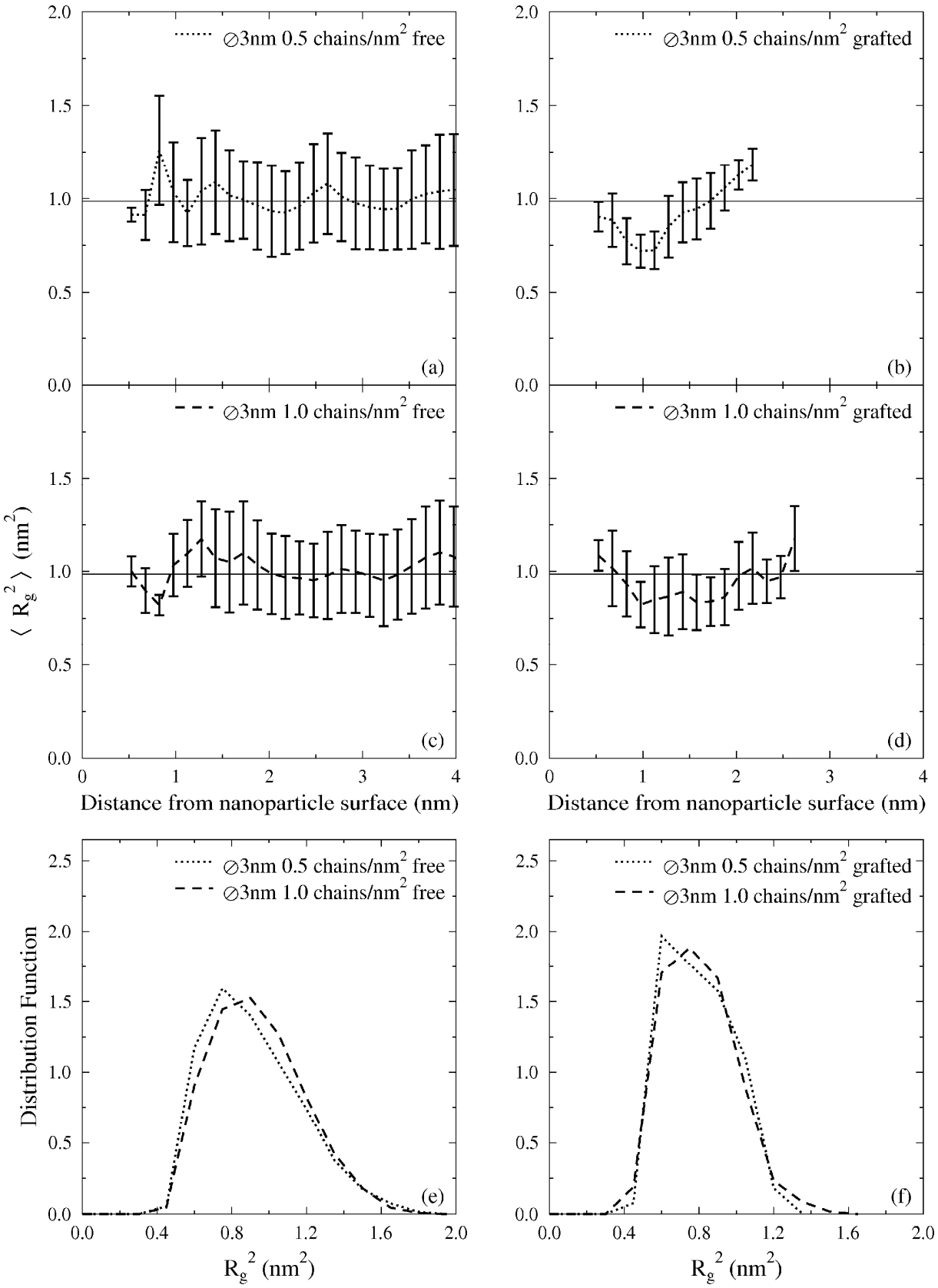

Figure A1.3. Squared radius-of-gyration values for systems containing grafted 3 nm-diameter nanoparticles of medium and high grafted densities. Panels (a) and (c) summarize values pertaining to the free a-PS chains while panels (b) and (d) refer to those of grafted polymer chains. Panels (e) and (f) are the corresponding histograms (in arbitrary units) for free and grafted chains, respectively, at T = 590 K and P = 101.3 kPa.

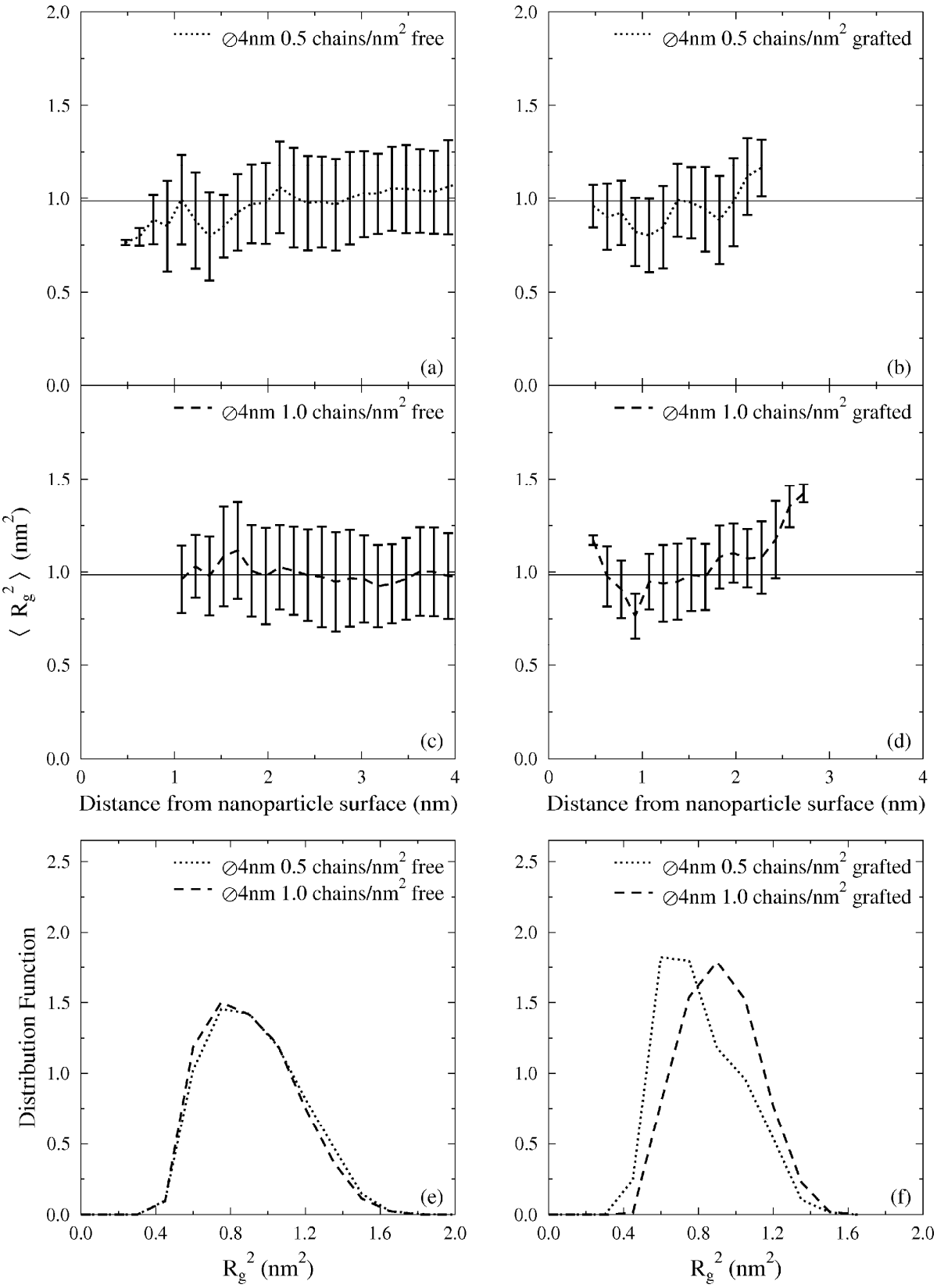

Figure A1.4. Squared radius of gyration values for systems containing grafted 4 nm-diameter nanoparticles of medium and high grafted densities. Panels (a) and (c) summarize values pertaining to the free a-PS chains while panels (b) and (d) refer to those of grafted polymer chains. Panels (e) and (f) are the corresponding histograms for free and grafted chains, respectively, at T = 590 K and P = 101.3 kPa.

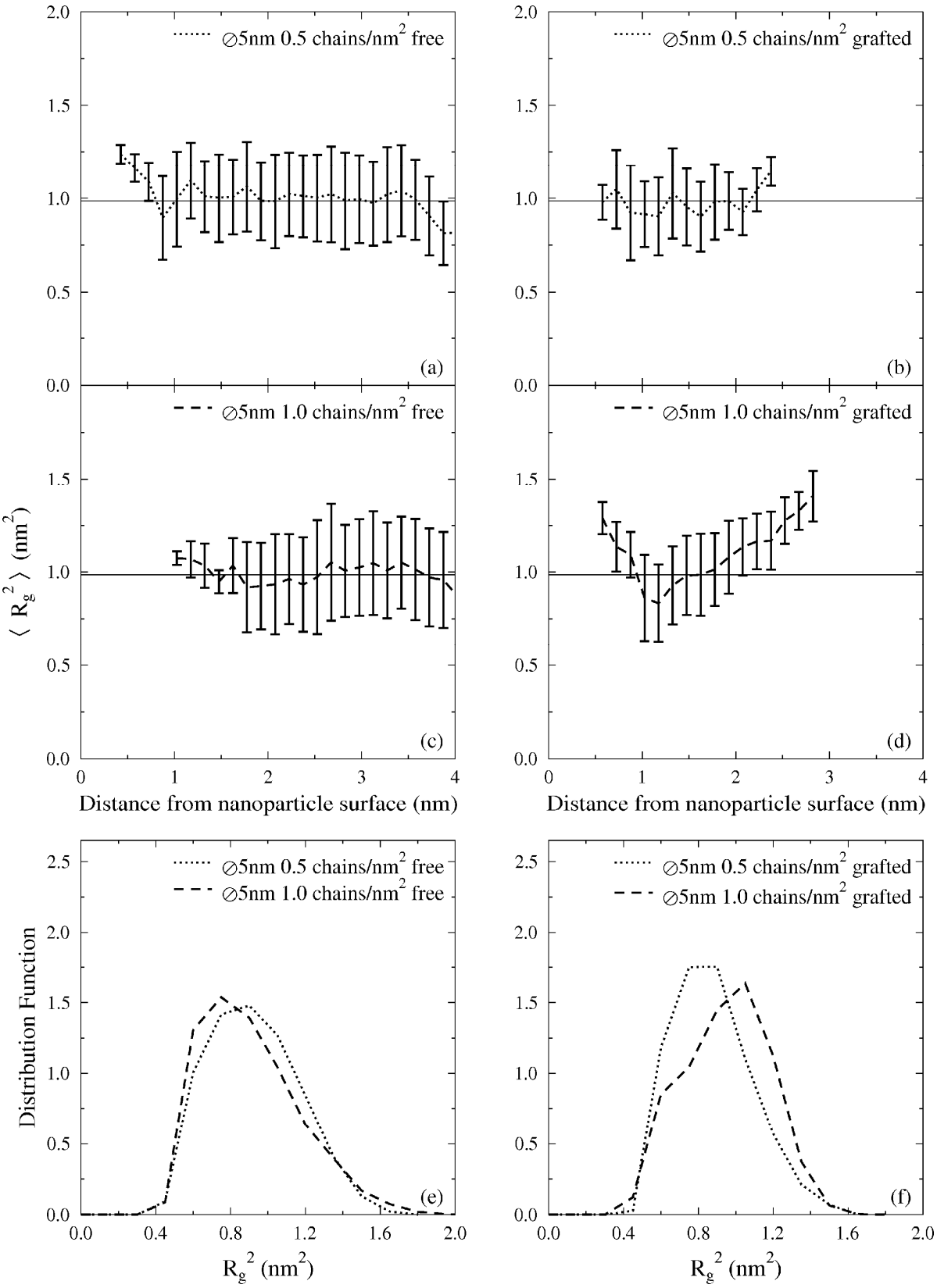

Figure A1.5. Squared radius of gyration values for systems containing grafted 5 nm-diameter nanoparticles of medium and high grafted densities. Panels (a) and (c) summarize values pertaining to the free a-PS chains while panels (b) and (d) refer to those of grafted polymer chains. Panels (e) and (f) are the corresponding histograms for free and grafted chains, respectively, at T = 590 K and P = 101.3 kPa.

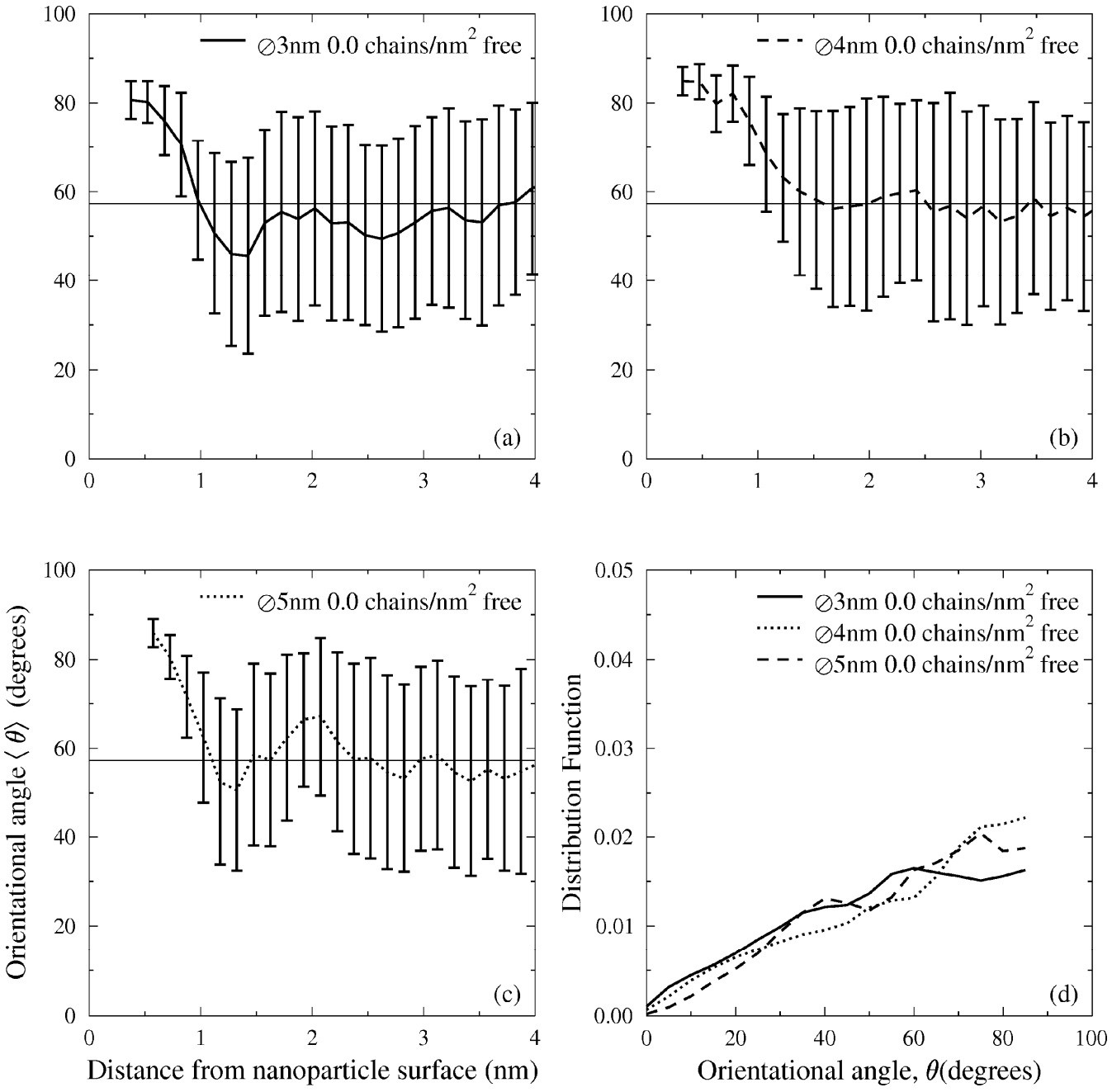

Figure A1.6. Panels (a), (b), and (c) summarize the chain orientational angles (between the vector corresponding to the largest eigenvalue of the radius of gyration tensor and the surface normal) of free a-PS polymer chains around a bare nanoparticle while panel (d) shows the corresponding histograms (in arbitrary units) at T = 590 K and P = 101.3 kPa. The horizontal line at an angle of 57.3 degrees corresponds to the average bulk orientational angle and this is also drawn in Figures A1.7 to 17. The unexpected distribution function profile is a consequence of restricting the definition of all orientational angles to the first quadrant. The vertical error bars on the data points are the standard deviation values.

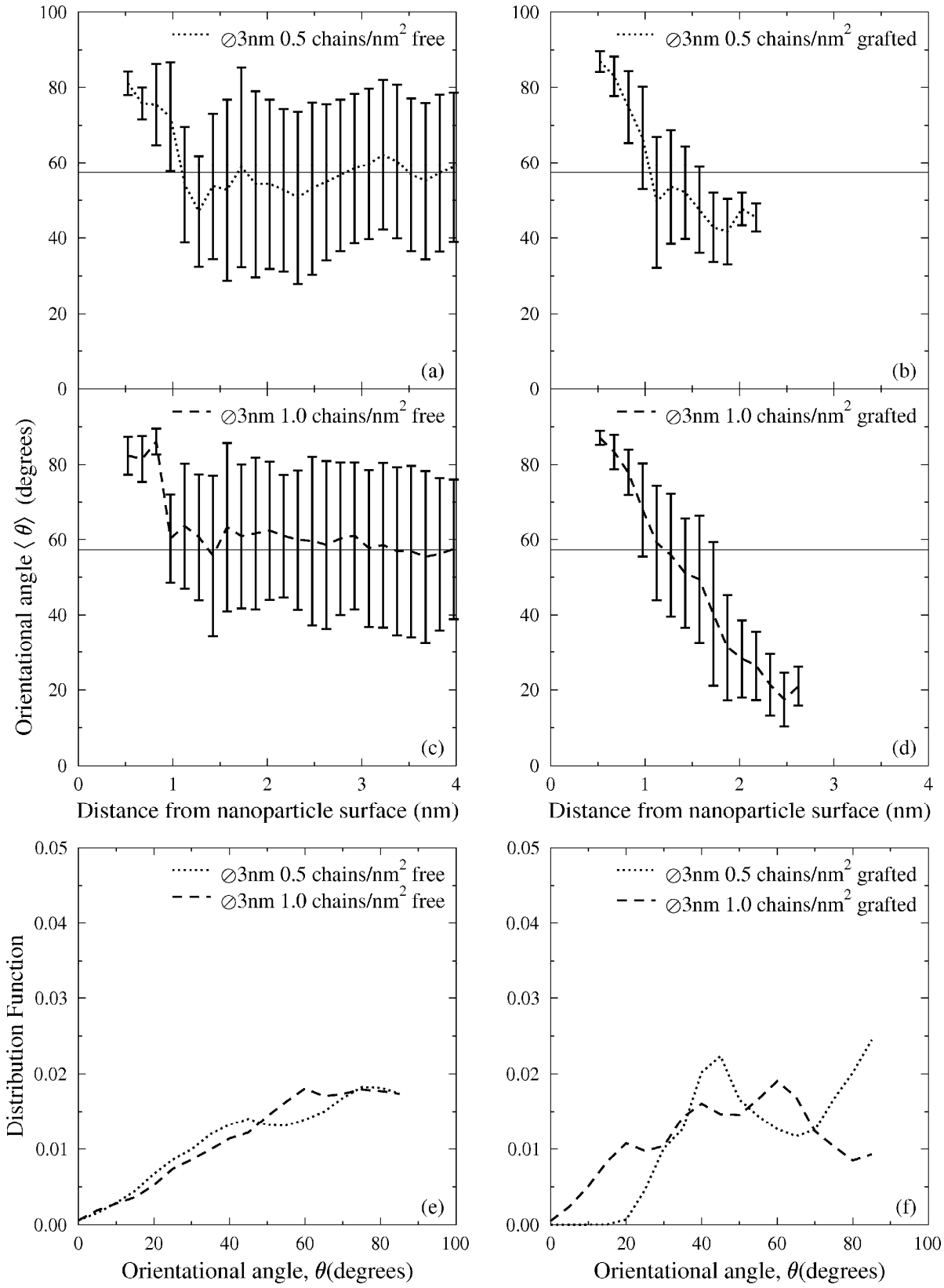

Figure A1.7. Orientational angle between the longest axis of the squared radius-of-gyration tensor and the surface normal for systems containing grafted 3 nm-diameter nanoparticles of medium and high grafted densities. Panels (a) and (c) summarize values pertaining to the free a-PS chains while panels (b) and (d) refer to those of grafted polymer chains. Panels (e) and (f) are the corresponding histograms for free and grafted chains, respectively, at T = 590 K and P = 101.3 kPa.

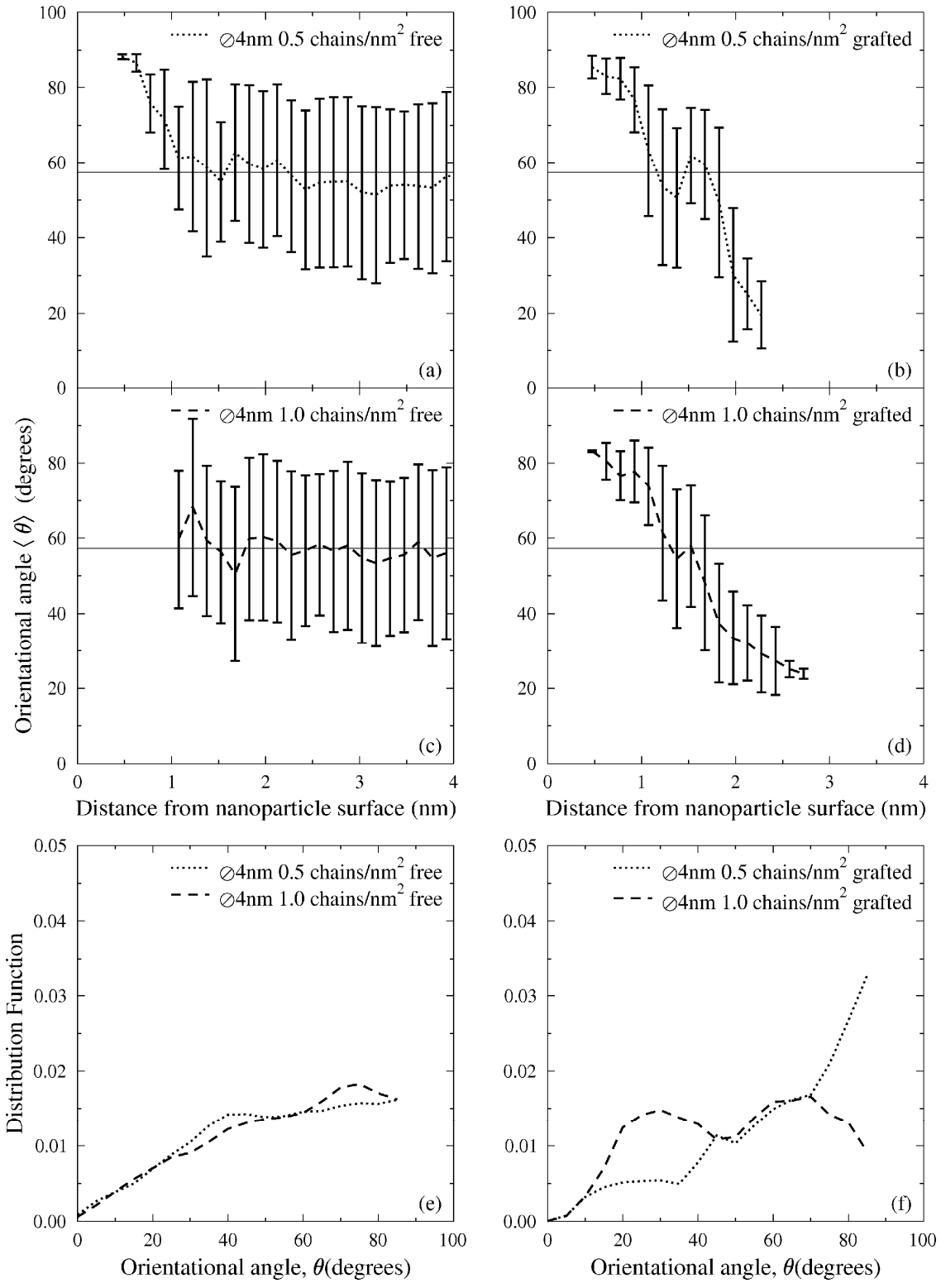

Figure A1.8. Orientational angle between the longest axis of the squared radius of gyration tensor and the surface normal for systems containing grafted 4 nm-diameter nanoparticles of medium and high grafted densities. Panels (a) and (c) summarize values pertaining to the free a-PS chains while panels (b) and (d) refer to those of grafted polymer chains. Panels (e) and (f) are the corresponding histograms for free and grafted chains, respectively, at T = 590 K and P = 101.3 kPa.

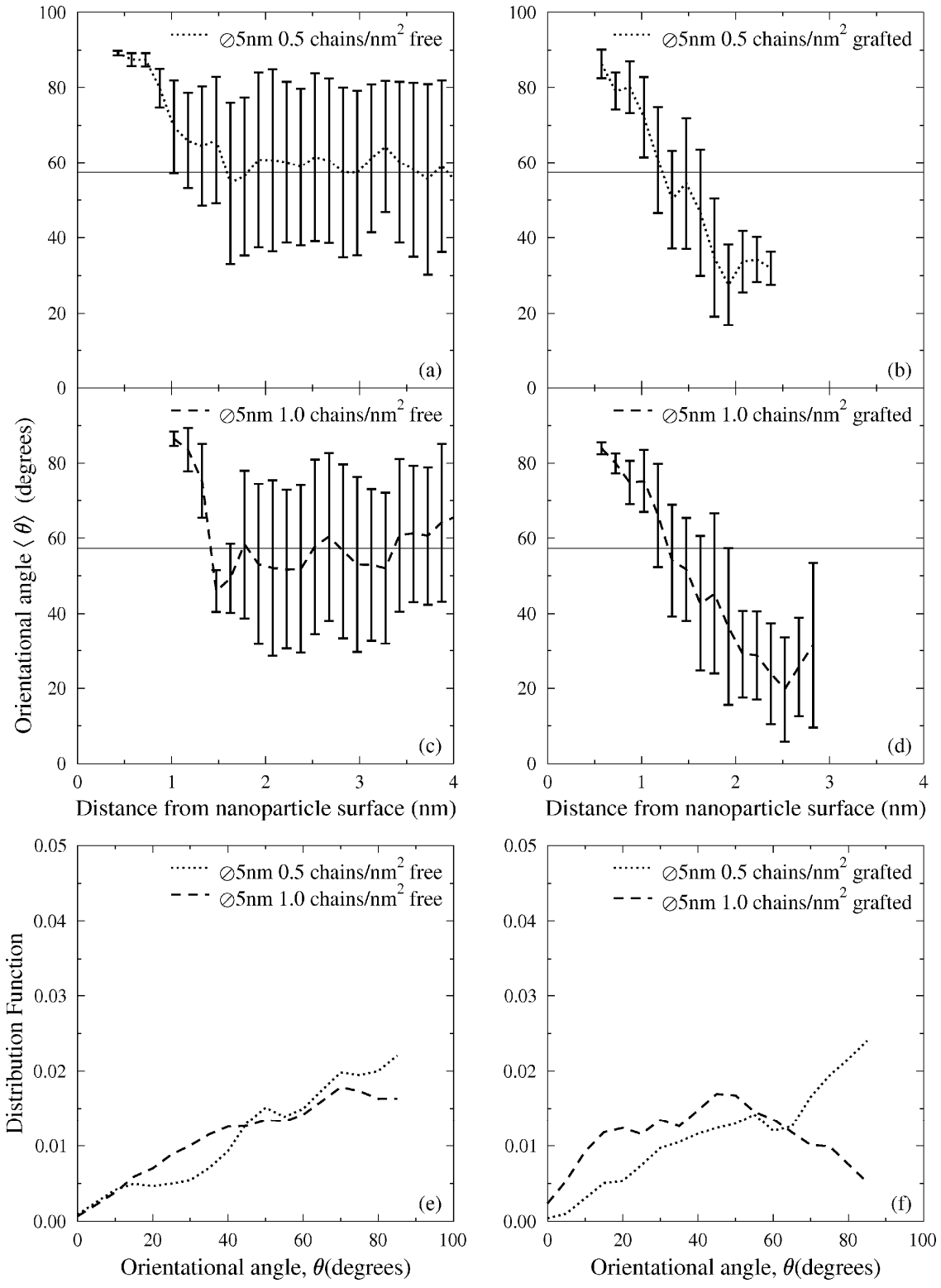

Figure A1.9. Orientational angle between the longest axis of the squared radius of gyration tensor and the surface normal for systems containing grafted 5 nm-diameter nanoparticles of medium and high grafted densities. Panels (a) and (c) summarize values pertaining to the free a-PS chains while panels (b) and (d) refer to those of grafted polymer chains. Panels (e) and (f) are the corresponding histograms for free and grafted chains, respectively, at T = 590 K and P = 101.3 kPa.

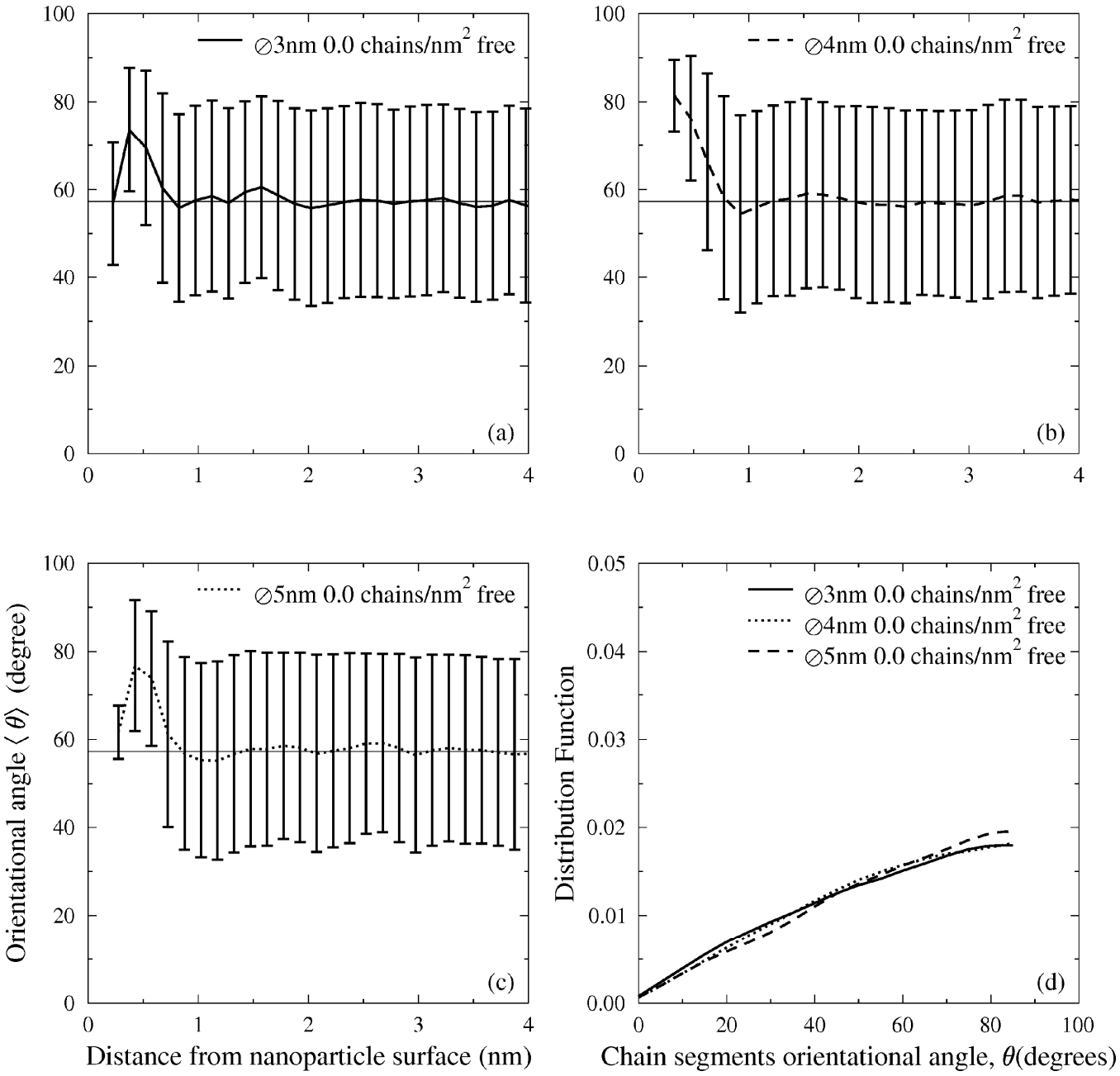

Figure A1.10. Orientational angle between the vectors connecting 1st-neighbor monomers (*i* and *i*+1) of free polymer chains and the surface normal for systems containing bare nanoparticles of diameter 3 nm (a), 4 nm (b), and 5 nm (c) at *T* = 590 K and *P* = 101.3 kPa.

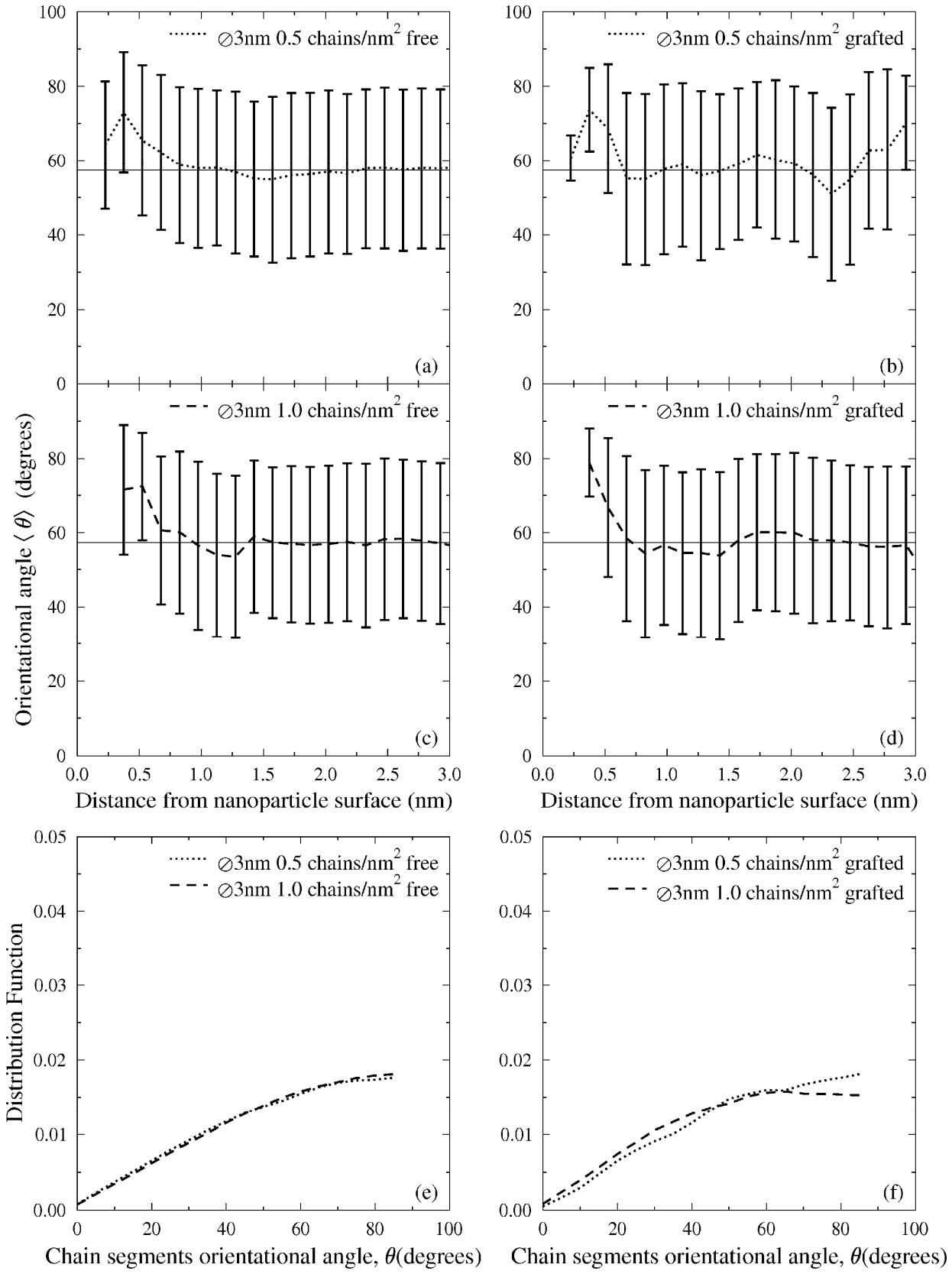

Figure A1.11. Orientational angle between the vectors connecting 1st-neighbor monomers (*i* and *i*+1) of free and grafted polymer chains and the surface normal for systems with nanoparticles of diameter 3 nm and grafted densities 0.5 chains/nm^2 (panels (a) and (c) and 1.0 chains/nm^2 (panels (b) and (d)) at *T* = 590 K and *P* = 101.3 kPa.

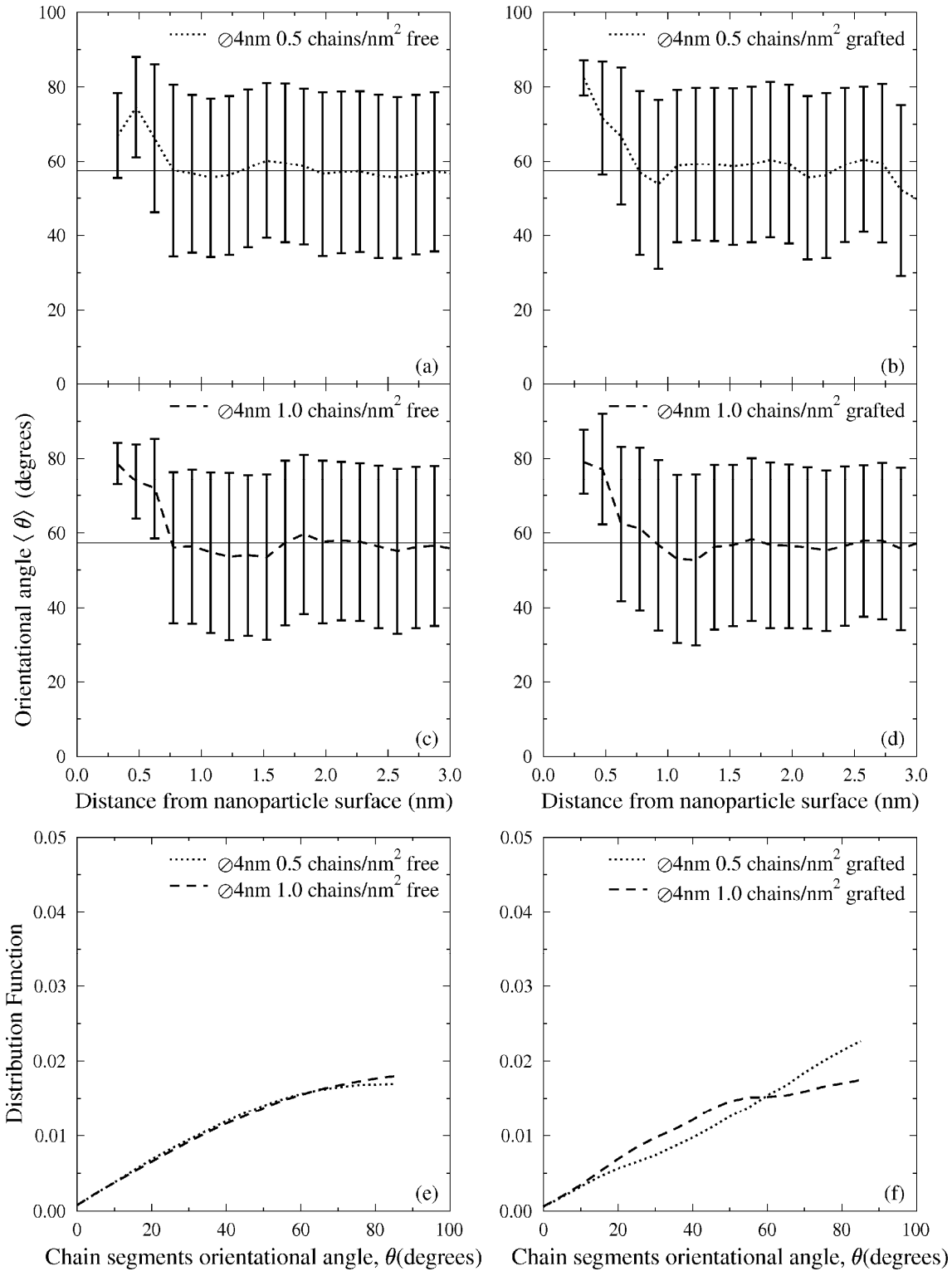

Figure A1.12. Orientational angle between the vectors connecting 3rd-neighbor monomers (*i* and *i*+1) of free and grafted polymer chains and the surface normal for systems with nanoparticles of diameter 4 nm and grafted densities 0.5 chains/nm^2 (panels (a) and (c) and 1.0 chains/nm^2 (panels (b) and (d)) at T = 590 K and P = 101.3 kPa.

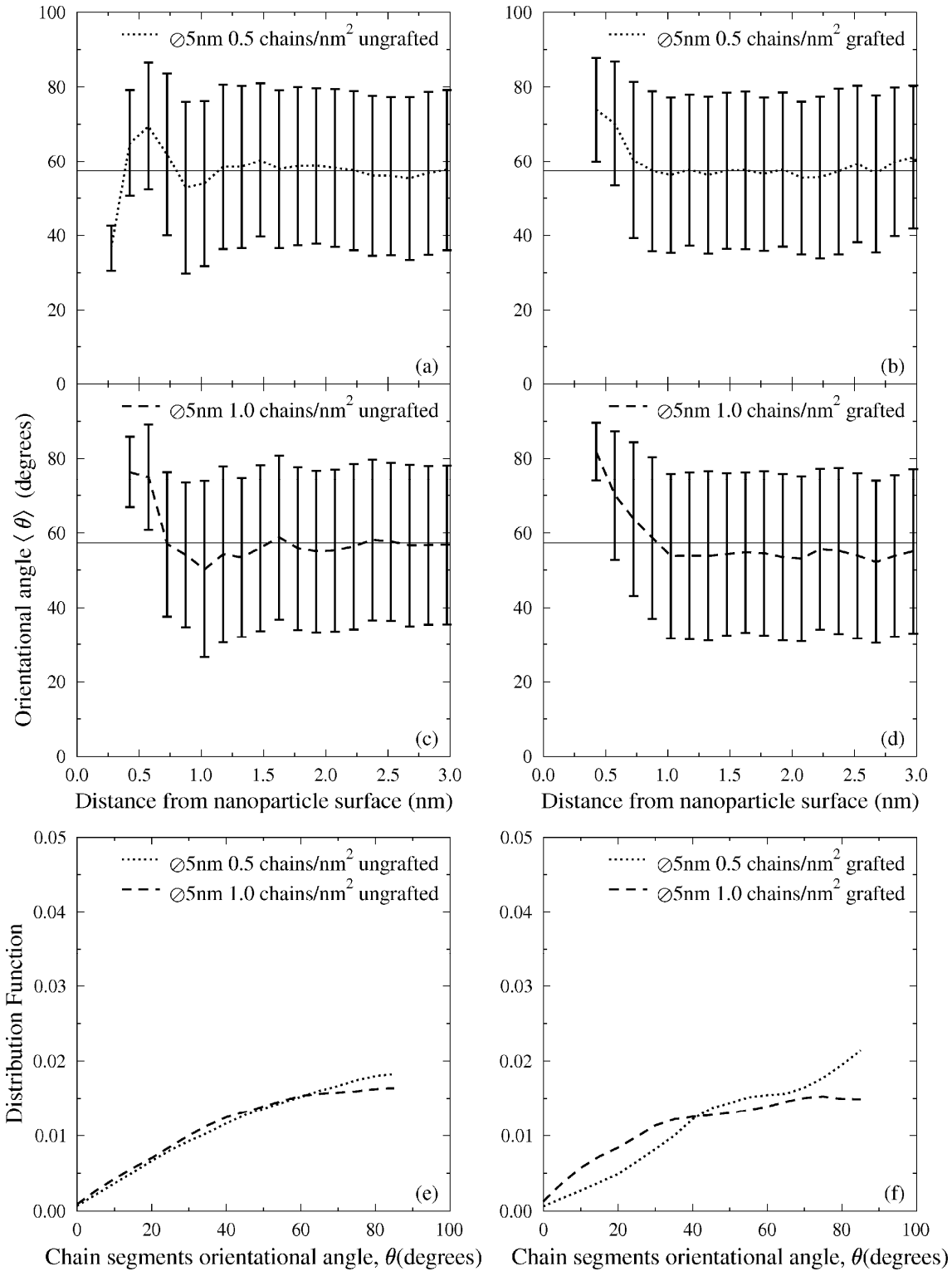

Figure A1.13. Orientational angle between the vectors connecting 3rd-neighbor monomers (*i* and *i*+1) of free and grafted polymer chains and the surface normal for systems with nanoparticles of diameter 3 nm and grafted densities 0.5 chains/nm^2 (panels (a) and (c) and 1.0 chains/nm^2 (panels (b) and (d)) at T = 590 K and P = 101.3 kPa.

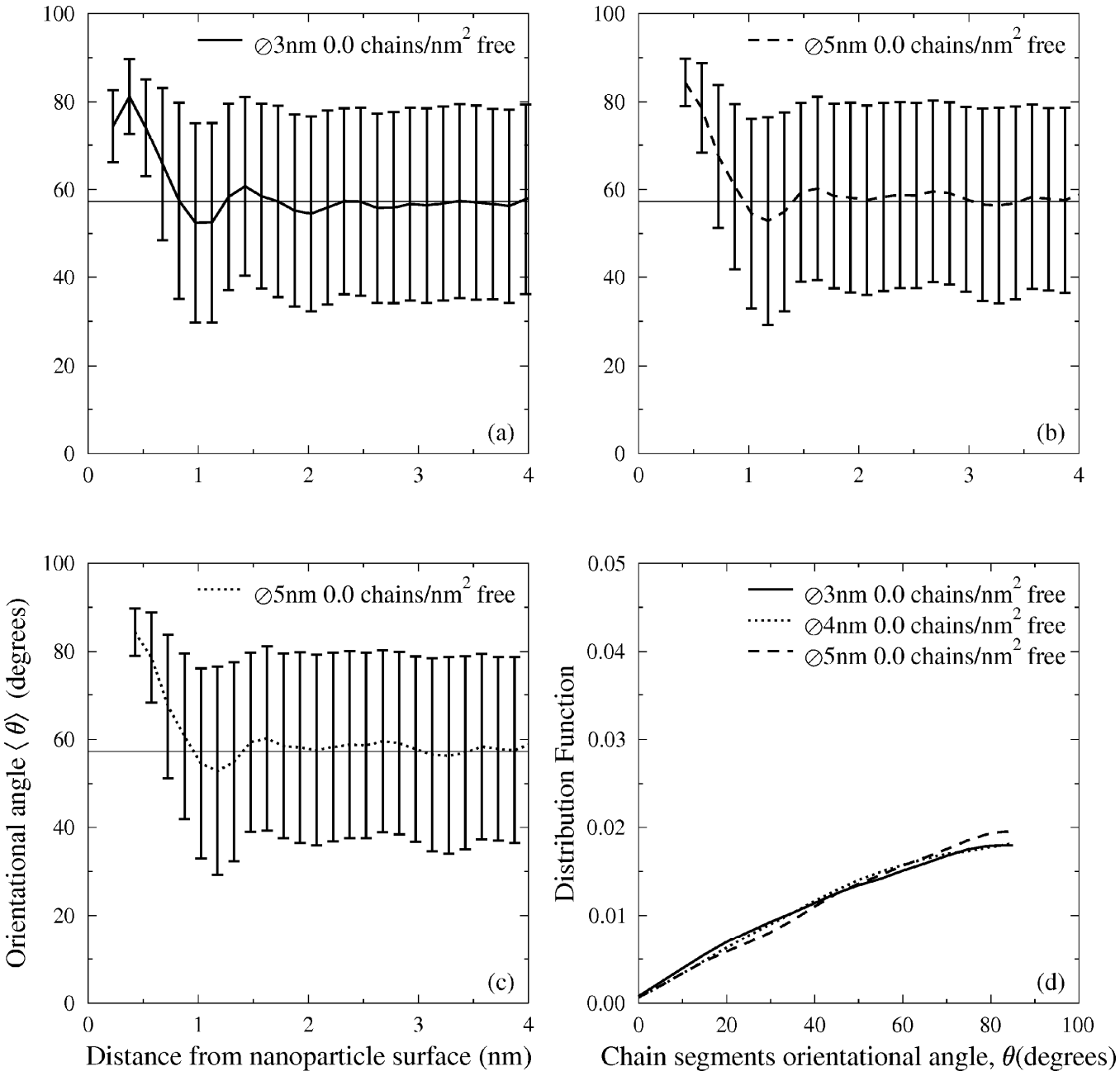

Figure A1.14. Orientational angle between the vectors connecting 3rd-neighbor monomers (*i* and *i*+3) of free polymer chains and the surface normal for systems containing bare nanoparticles of diameter 3 nm (a), 4 nm (b), and 5 nm (c) at *T* = 590 K and *P* = 101.3 kPa.

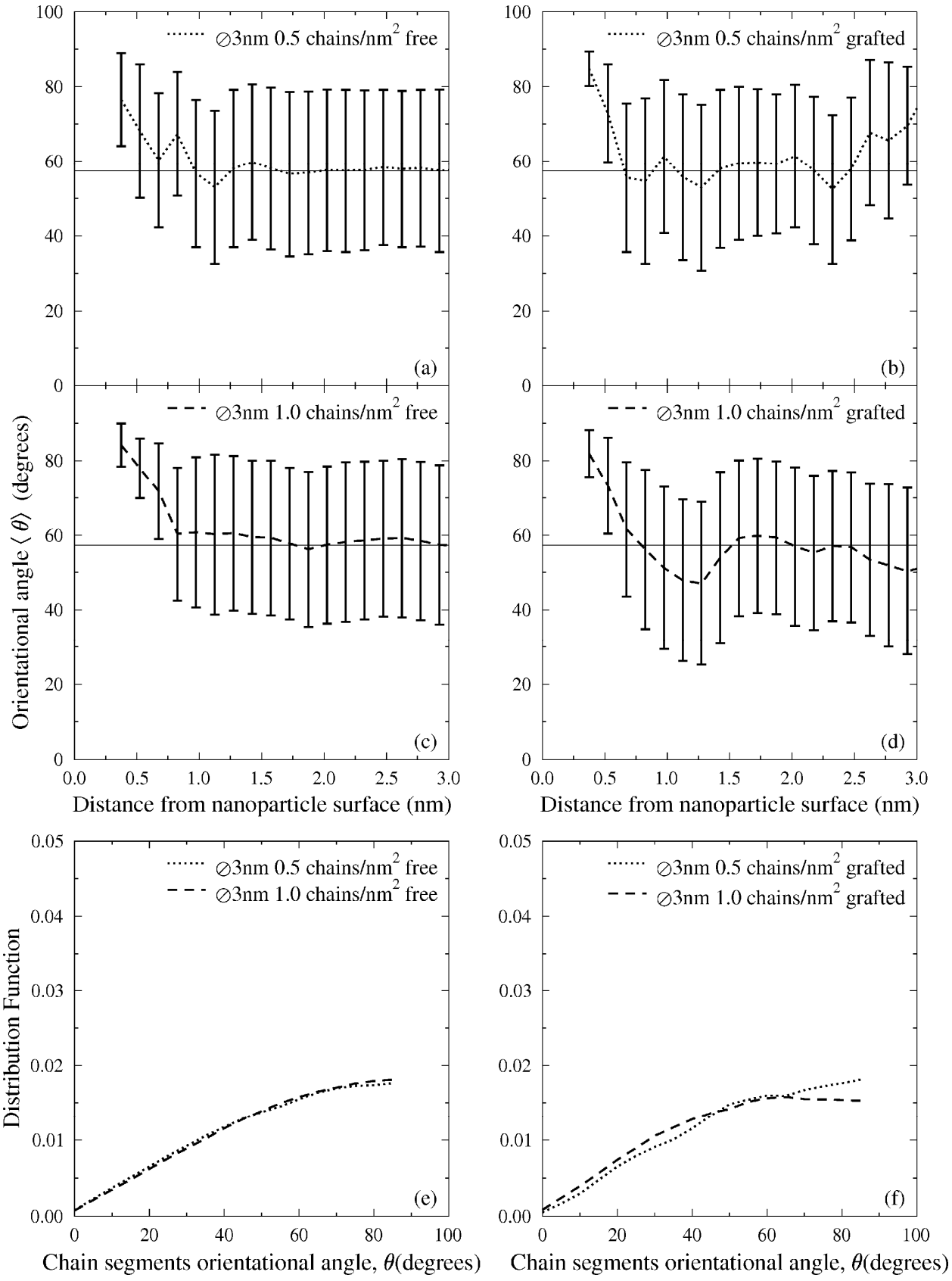

Figure A1.15. Orientational angle between the vectors connecting 3rd-neighbor monomers (*i* and *i*+3) of free and grafted polymer chains and the surface normal for systems with nanoparticles of diameter 3 nm and grafted densities 0.5 chains/nm^2 (panels (a) and (c) and 1.0 chains/nm^2 (panels (b) and (d)) at *T* = 590 K and *P* = 101.3 kPa.

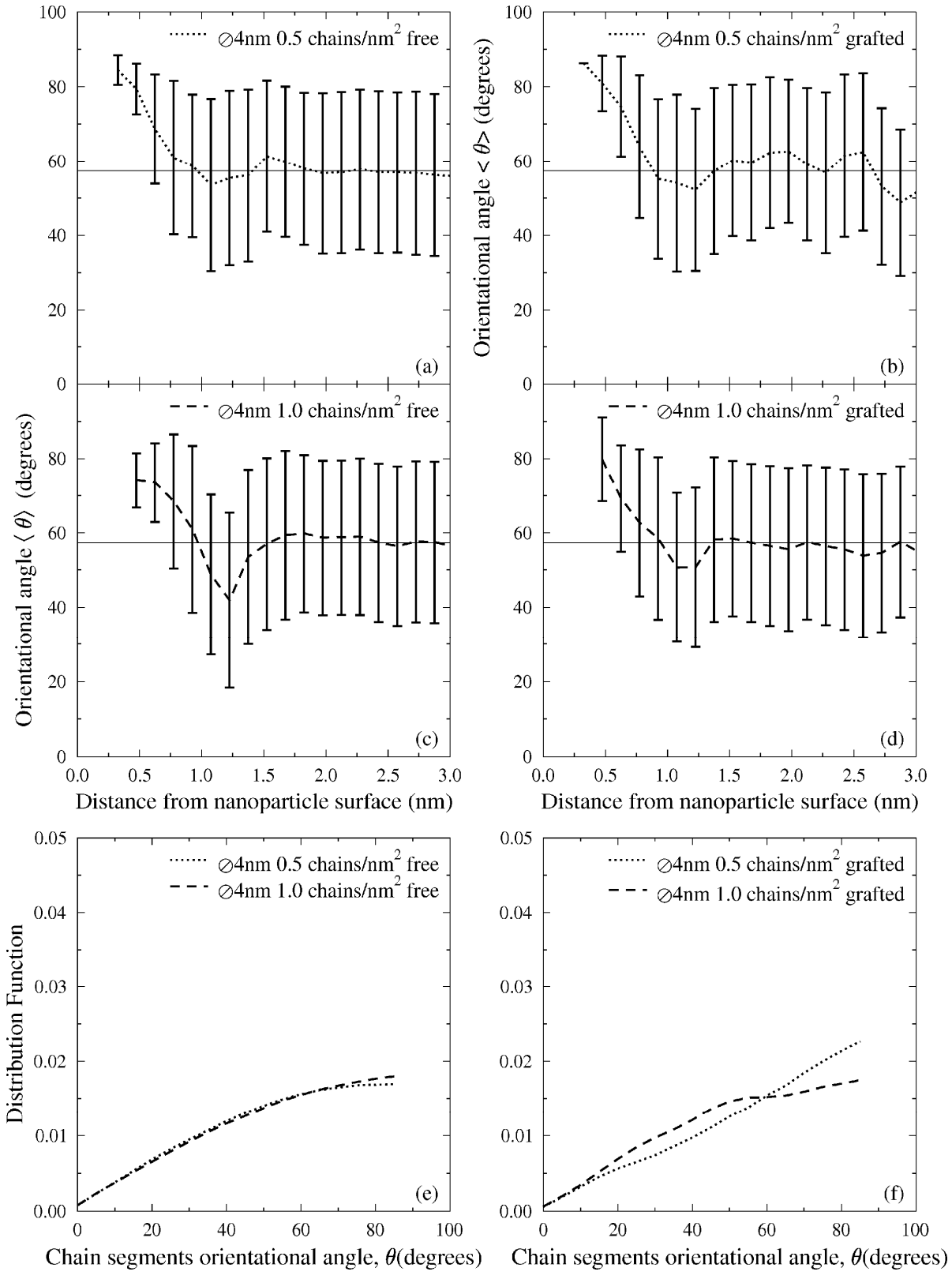

Figure A1.16. Orientational angle between the vectors connecting 3rd-neighbor monomers (*i* and *i*+3) of free and grafted polymer chains and the surface normal for systems with nanoparticles of diameter 4 nm and grafted densities 0.5 chains/nm^2 (panels (a) and (c) and 1.0 chains/nm^2 (panels (b) and (d)) at *T* = 590 K and *P* = 101.3 kPa.

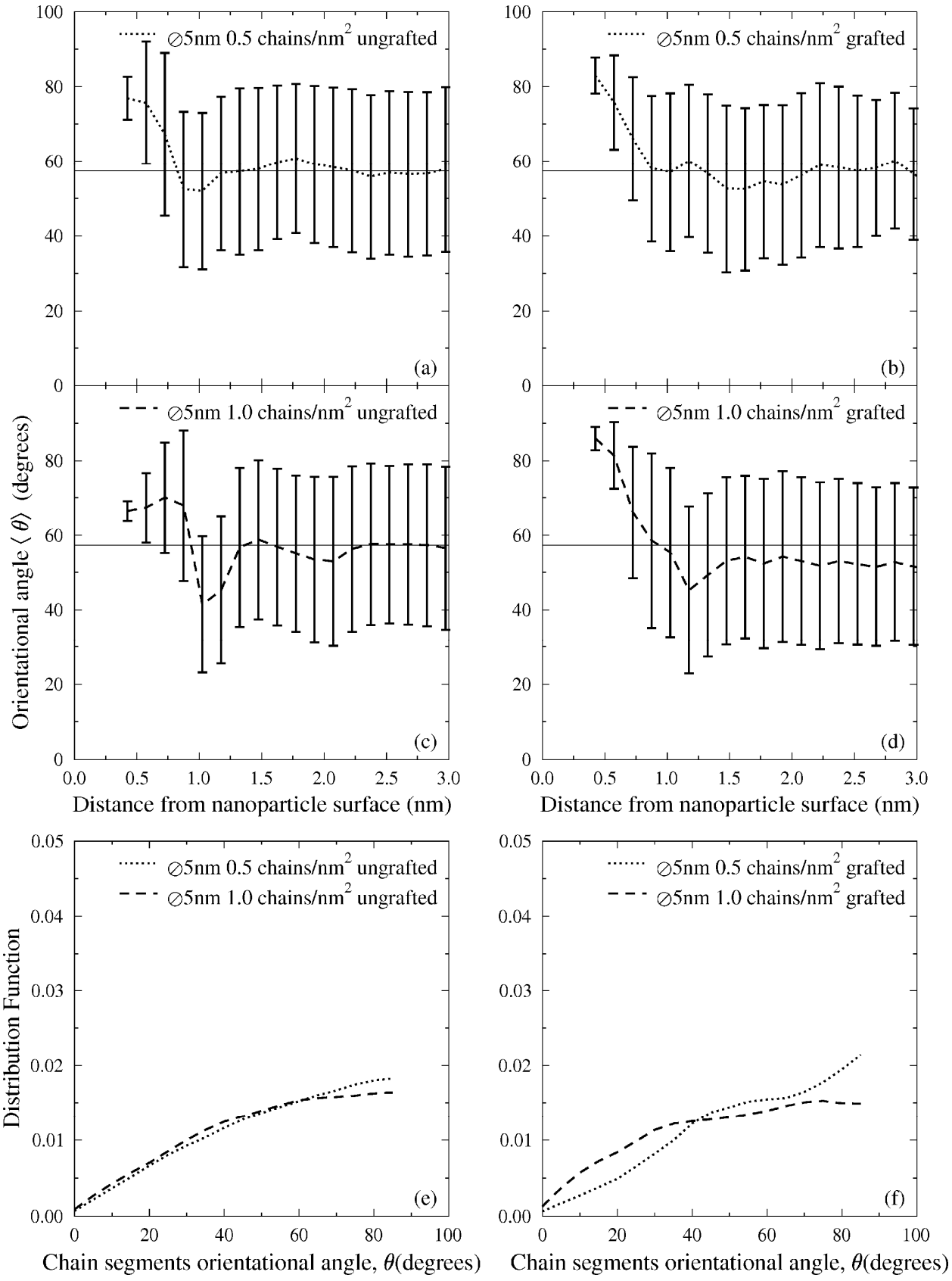

Figure A1.17. Orientational angle between the vectors connecting 3rd-neighbor monomers (*i* and *i*+3) of free and grafted polymer chains and the surface normal for systems with nanoparticles of diameter 5 nm and grafted densities 0.5 chains/nm^2 (panels (a) and (c) and 1.0 chains/nm^2 (panels (b) and (d)) at T = 590 K and P = 101.3 kPa.

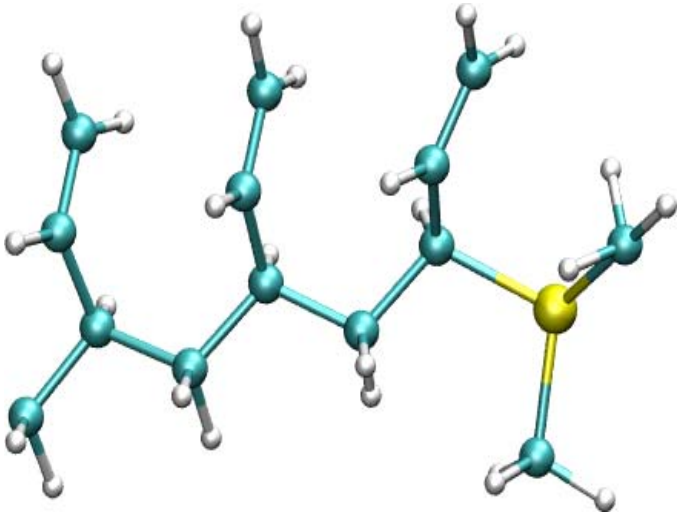

Figure A1.18. Anionic linker molecule (carbon, hydrogen, and silicon atoms are symbolized by cyan, grey, and gold, respectively).

Appendix 2

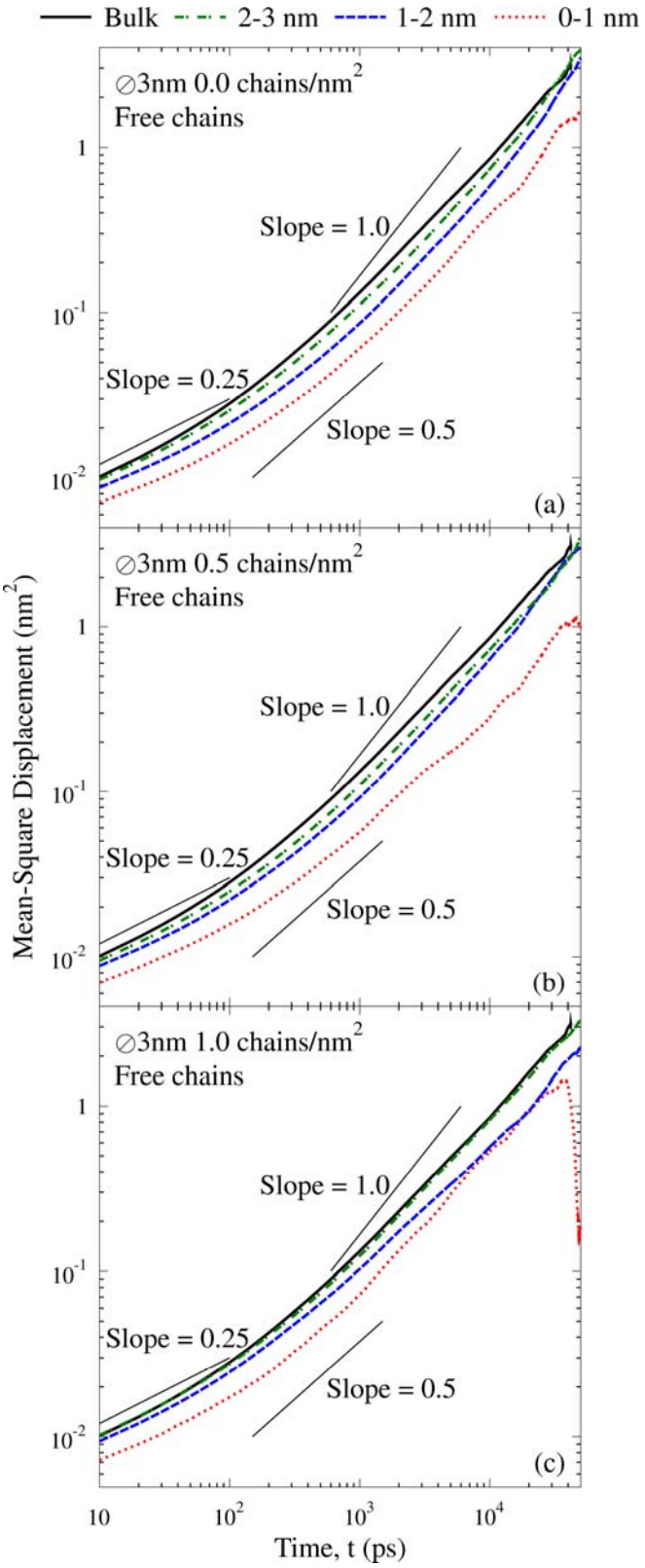

Figure A2.1. Center of mass mean-square displacement (MSD) plots of free 20 monomer polystyrene chains which reside the most in one of the 3 shells surrounding spherical particles of diameter = 3 nm at T = 590 K and P = 101.3 kPa. Each of the shells has a width of 1 nm.

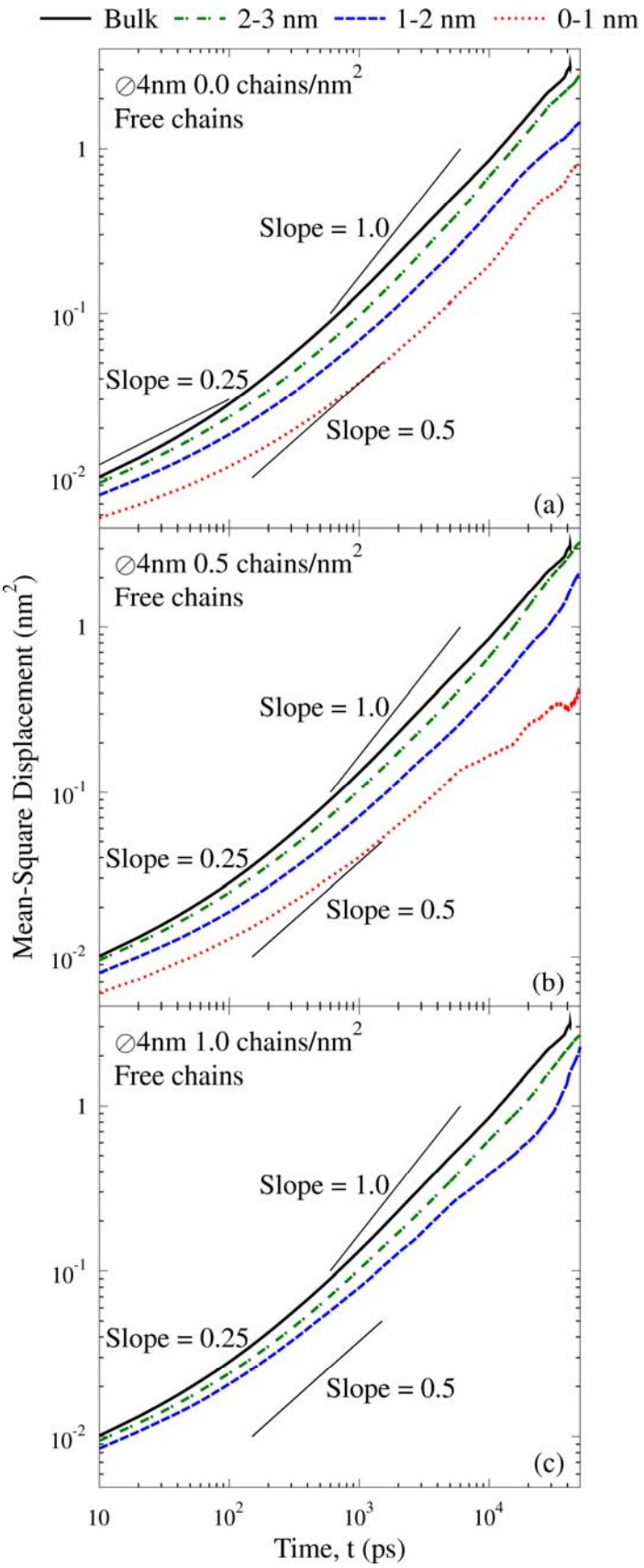

Figure A2.2. Center of mass mean-square displacement (MSD) plots of free 20 monomer polystyrene chains which reside the most in one of the 3 shells surrounding spherical particles of diameter = 4 nm at T = 590 K and P = 101.3 kPa. Each of the shells has a width of 1 nm.

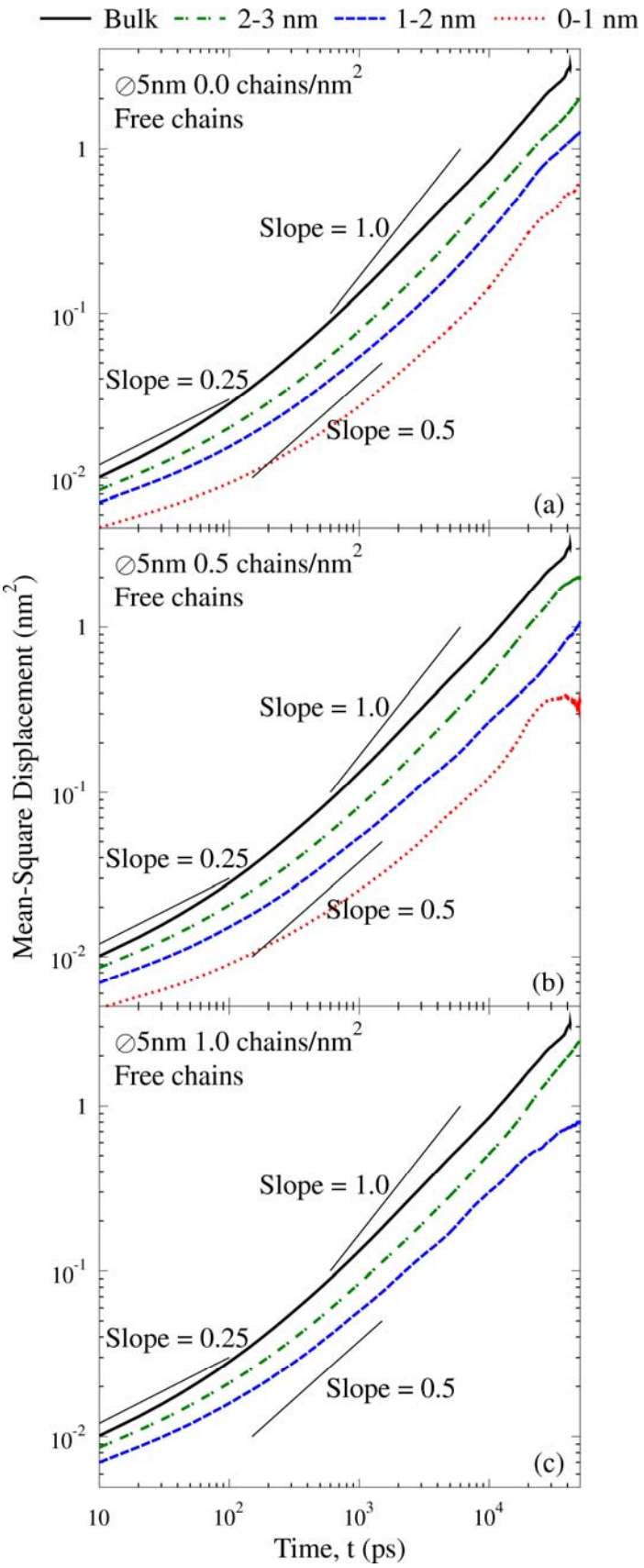

Figure A2.3. Center of mass mean-square displacement (MSD) plots of free 20 monomer polystyrene chains which reside the most in one of the 3 shells surrounding spherical particles of diameter = 5 nm at T = 590 K and P = 101.3 kPa. Each of the shells has a width of 1 nm.

Simulation Tools

The molecular dynamics simulations reported in this PhD thesis were carried out on the DFG project computer cluster in the Theoretical Physical Chemistry group of Prof. Florian Müller-Plathe at the Technische Universitat Darmstadt. The cluster was supplied by the company RAID MEDIA.

All the atomistic molecular dynamics simulations were performed using the molecular dynamics simulation tool called YASP. This tool was originally developed by Prof. Florian Müller-Plathe and later parallelized by Dr. Konstantin B. Tarmyshov.

Publications

Publications based on the present dissertation

1. Tinashe V. M. Ndoro, Michael C. Böhm, Florian Müller-Plathe. “Interface and Interphase Dynamics of Polystyrene Chains near Grafted and Ungrafted Silica Nanoparticles”, Macromolecules **2011**, http://pubs.acs.org/doi/abs/10.1021/ma2020613.

2*. Azadeh Ghanbari**,** Tinashe V. M. Ndoro**,** Frédéric Leroy, Mohammad Rahimi, Michael C. Böhm, Florian Müller-Plathe. “Interphase Structure in Silica-Polystyrene Nanocomposites: A Coarse-Grained Molecular Dynamics Study”, Macromolecules **2011**, http://pubs.acs.org/doi/abs/10.1021/ma202044e.

3. Tinashe V. M. Ndoro, Evangelos Voyiatzis, Azadeh Ghanbari, Doros N. Theodorou, Michael C. Böhm, Florian Müller-Plathe. “Interface of Grafted and Ungrafted Silica Nanoparticles with a Polystyrene Matrix: Atomistic Molecular Dynamics Simulations”, Macromolecules **2011**, 44, 2316-2327.

* Not presented in this dissertation.

Curriculum Vitae

Personal Information

Name:	Tinashe Victor Mandishonha Ndoro
Place of Birth:	Harare, Zimbabwe
Date of Birth:	17. November 1981
Nationality:	Zimbabwean

Education

2008 – 2011	Ph.D. (Chemistry), *Technische Universität Darmstadt,* Germany
2004 – 2007	M.Sc. (Chemical Engineering), *Rose-Hulman Institute of Technology,* USA
2001 – 2004	B.Sc. (Biochemical Engineering), *Jacobs University Bremen,* Germany

Work Experience

2007 – 2008	Engineer, *Haley and Aldrich Inc.*, New York, USA
2004	Student Intern**,** *Merck KGaA*, Darmstadt, Germany
2003	Student Intern, *Zimmer AG*, Frankfurt am Main, Germany

Publications

- Tinashe V. M. Ndoro, Michael C. Böhm, Florian Müller-Plathe. *Interface and Interphase Dynamics of Polystyrene Chains near Grafted and Ungrafted Silica Nanoparticles*, Macromolecules **2011**, http://pubs.acs.org/doi/abs/10.1021/ma2020613.
- Azadeh Ghanbari, Tinashe V. M. Ndoro, Frédéric Leroy, Mohammad Rahimi, Michael C. Böhm, Florian Müller-Plathe. *Interphase Structure in Silica-Polystyrene Nanocomposites: A Coarse-Grained Molecular Dynamics Study*, Macromolecules **2011**, http://pubs.acs.org/doi/abs/10.1021/ma202044e.
- Tinashe V. M. Ndoro, Evangelos Voyiatzis, Azadeh Ghanbari, Doros N. Theodorou, Michael C. Böhm, Florian Müller-Plathe. *Interface of Grafted and Ungrafted Silica Nanoparticles with a Polystyrene Matrix: Atomistic Molecular Dynamics Simulations*, Macromolecules **2011**, 44, 2316-2327.
- Andreas Kolmer, Nicole Anderl, Tinashe V. M. Ndoro**,** Karim Farah, Frédéric Leroy, Florian Müller-Plathe. *Review of Several Books on Polymer Science*, Soft Materials, **2009**, 7, 366-370.

(Tinashe Victor Mandishonha Ndoro) Darmstadt, 12. September, 2011

Tinashe Victor Mandishonha Ndoro
Schloßstraße 12
64297 Darmstadt - Eberstadt
Germany

Darmstadt, 12. September, 2011

Erklärung

Ich erkläre hiermit, noch keinen Promotionsversuch unternommen zu haben.

_____
(Tinashe Victor Mandishonha Ndoro)

Tinashe Victor Mandishonha Ndoro
Schloßstraße 12
64297 Darmstadt - Eberstadt
Germany

Darmstadt, 12. September, 2011

Eidesstattliche Erklärung

Ich erkläre hiermit an Eides Statt, dass ich meine Dissertation selbständig und nur mit den angegebenen Hilfsmitteln angefertigt habe.

_____

(Tinashe Victor Mandishonha Ndoro)